Nano Research

ISSN 1998-0124 CN 11-5974/O4
https://doi.org/10.26599/NR.2026.94908874

Review Article

Mechanistic insights into tunable copper valence states as photocatalytic active sites

Shihe Wu[1], Hui Liu[1], Wei He[1], Youyu Duan[2,3](✉), Yuhan Li[1](✉)

[1] Institute for Frontier Interdisciplinary Research in Intelligence and Environment, School of Big Data, Chongqing Technology and Business University, Chongqing 400067, China

[2] School of Materials Science and Engineering, Chongqing Jiaotong University, Chongqing 400074, China

[3] Chongqing Institute of New Energy Storage Materials and Equipment, Chongqing 401120, China

Nano Res., **Just Accepted Manuscript** • https://doi.org/10.26599/NR.2026.94908874

https://www.sciopen.com/journal/1998-0124 on May. 25, 2026

Just Accepted

TABLE OF CONTENTS (TOC)

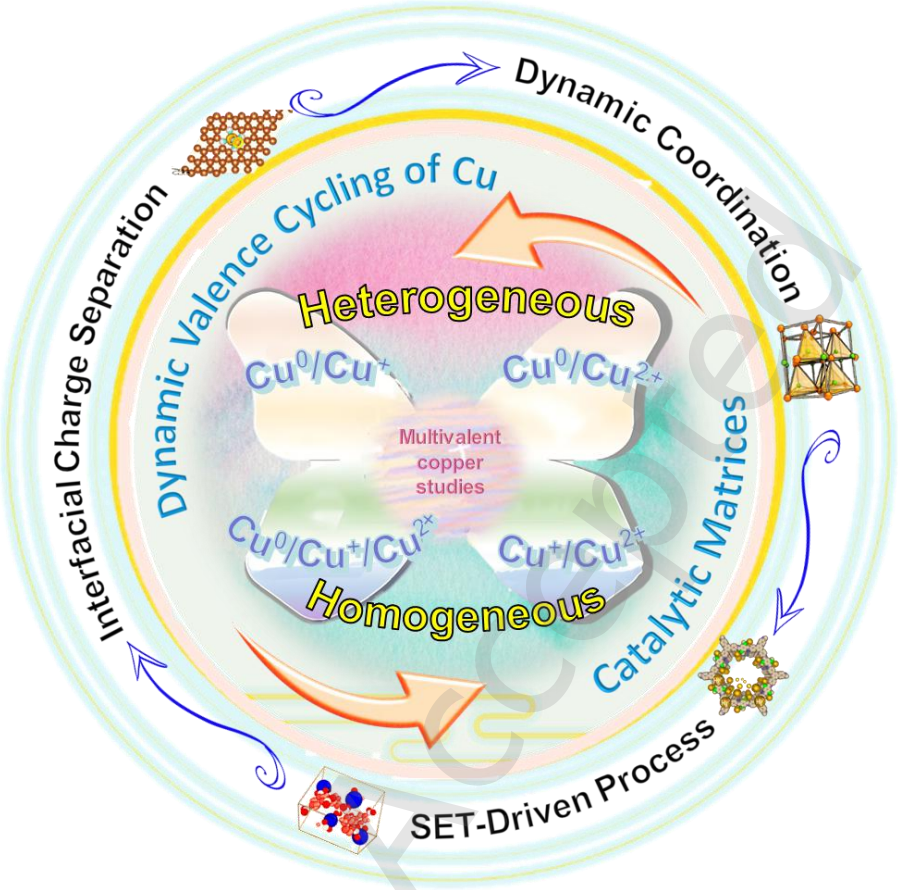

This review systematically elucidates the roles and synergistic valence dynamics of $Cu^0/Cu^+/Cu^{2+}$ species across homogeneous and heterogeneous photocatalytic systems, establishing a three-dimensional analytical framework that highlights their structure-activity relationships, regulation strategies, and prospects for light-driven synthesis, energy conversion, and environmental remediation.

Nano Research

Open Access

Review Article

Mechanistic insights into tunable copper valence states as photocatalytic active sites

Shihe Wu[1], Hui Liu[1], Wei He[1], Youyu Duan[2,3], and Yuhan Li[1]

[1] *Institute for Frontier Interdisciplinary Research in Intelligence and Environment, School of Big Data, Chongqing Technology and Business University, Chongqing 400067, China*
[2] *School of Materials Science and Engineering, Chongqing Jiaotong University, Chongqing 400074, China*
[3] *Chongqing Institute of New Energy Storage Materials and Equipment, Chongqing 401120, China*

Received: 16 April 2026; **Revised:** 8 May 2026; **Accepted:** 25 May 2026

Address correspondence to Yuhan Li, liyh@ctbu.edu.cn; Youyu Duan, youyuduan@cqjtu.edu.cn

Cite this article: *Nano Research*, 2026, 19, 94908874 https://doi.org/10.26599/NR.2026.94908874

ABSTRACT: Copper-based photocatalysts, featuring low cost, versatile valence states (Cu^0, Cu^+, Cu^{2+}), and outstanding photophysical and photochemical properties, hold great promise for organic synthesis, environmental remediation, and energy conversion. This review systematically examines the pivotal role of variable-valence copper species in photocatalysis, establishing a dual-dimensional framework that spans valence evolution and catalytic systems. It highlights advances in Cu^0 active sites, photoexcited Cu^+ and Cu^{2+} species, and heterogeneous platforms such as polymer ligands, metal-organic frameworks, and single-atom catalysts. In homogeneous systems, Cu^+ complexes achieve long-lived metal-to-ligand charge transfer states that drive single-electron transfer for C–C/C–X bond formation and alkene/alkyne bifunctionalization. Cu^{2+} participates in oxidation and radical cycles via ligand-to-metal charge transfer. In heterogeneous systems, Cu^0 nanostructures enhance light absorption via localized surface plasmon resonance, while Cu^+/Cu^{2+} semiconductors form Z/S-scheme heterojunctions to improve charge separation. Key strategies, including ligand engineering, defect control, interface design, and single-atom anchoring, are discussed to enhance carrier dynamics and stability. Despite challenges in *in-situ* characterization, mechanistic elucidation, and scalable synthesis, copper-based photocatalysts offer strong potential for light-driven synthesis, CO_2 valorization, and pollutant mineralization. Future efforts should focus on operando spectroscopy and theory-guided design of robust, selective catalysts to bridge fundamental research and industrial application.

KEYWORDS: copper-based photocatalyst; variable valence state; photocatalytic mechanism; homogeneous catalysis; heterogeneous catalysis.

1 Introduction

Photocatalysis offers a promising route for converting solar energy into chemical energy, with applications in organic synthesis, environmental remediation, and energy conversion. Traditional photocatalysts often rely on precious metal complexes (e.g., Ru, Ir), which achieve long-lived excited states upon visible light excitation [1–9]. However, their high cost and resource scarcity limit large-scale application [10,11]. Consequently, 3d transition metals have emerged as attractive alternatives due to their flexible coordination, tunable electronic structures [12,13], and diverse oxidation states [14–16]. Among these, Cu-based catalysts exhibit unique advantages owing to their multiple valence states (Cu^0, Cu^+, Cu^{2+}) [17–21]. This valence variability enables participation in diverse reactions via single or two electron pathways, including C–C coupling, CO_2 reduction, and pollutant degradation [22–26]. Compared to other 3d metals [27–29], Cu offers more accessible valence states, a superior light-response range, and longer excited-state lifetimes [30–32].

The inherent variable valence nature of Cu presents certain challenges, which initially constrained its practical application prospects [33,34]. However, further research indicates that precisely this dynamic equilibrium and synergistic interplay among multiple valence states constitutes the unique advantage of Cu-based catalysts, distinguishing them from other systems [35–39]. Under photoexcitation, Cu^0 nanoparticles generate hot electrons that are injected into the semiconductor conduction band via the LSPR effect, while the simultaneously formed Cu^+ species act as electron trap sites, promoting charge carrier separation. Cu^+ complexes are reported to form long-lived MLCT states, which are proposed to reduce substrates to radicals while being oxidized to Cu^{2+} via an SET process [40–42]. The generated Cu^{2+} is proposed to activate molecular oxygen or capture radicals via LMCT, potentially forming Cu^{3+} intermediates, which according to the cited studies ultimately regenerate Cu^+ via reductive elimination to complete the catalytic cycle [43–46]. This dynamic multivalent conversion mechanism is particularly prominent in CO_2 reduction [47–50]. Constructing a Cu^0-Cu^+-Cu^{2+} gradient heterostructure (e.g., $Cu@Cu_2O/CuO$) can further optimize interfacial charge migration pathways, improve the apparent quantum efficiency [51,52], and simultaneously mitigate photocorrosion issues [53,54]. Furthermore, heterojunctions formed at multivalent interfaces (e.g., Cu/Cu_2O) can suppress charge carrier recombination, enhance light absorption, and activate substrate molecules through surface plasmon effects (Cu^0) or defect sites (Cu^+) [55].

Despite these mechanistic insights, the existing literature on Cu-based photocatalysts often remains fragmented, with individual studies focusing on isolated valence states or specific catalytic systems rather than constructing a unified conceptual framework [56,57]. To address this limitation and move beyond a superficial juxtaposition of cases, this review constructs an integrated three-dimensional analytical framework. As illustrated in Figure 1, this framework is organized along two intersecting dimensions: (i) the vertical dimension of valence state evolution ($Cu^0 \rightarrow Cu^+ \rightarrow Cu^{2+}$), tracing the dynamic interconversion and synergistic mechanisms among these species; and (ii) the horizontal dimension of catalytic system diversity, spanning from homogeneous catalysis (e.g., molecular Cu^+/Cu^{2+} complexes) to heterogeneous catalysis (e.g., Cu^0 nanostructures, Cu_2O/CuO semiconductors, and MOF- or single-atom-based systems) [58]. Applications such as C–C coupling, CO_2 reduction, and pollutant degradation are discussed within the relevant mechanistic subsections as case studies that illustrate the principles of each valence state or catalytic system, rather than as an isolated catalog [59]. This integrated framework enables a systematic structure–activity analysis across different valence states and reaction environments. Where quantitative data are available, optimal valence ratios have been identified for certain systems. In Cu-doped photocatalysts, the optimal Cu^{2+} doping concentration typically falls within 1–5 mol%; higher loadings cause Cu sites to become recombination centers rather than active sites. In CO_2 reduction, a Cu^0-Cu^+-Cu^{2+} gradient heterostructure (e.g., Cu@Cu_2O/CuO) achieves CH_3OH selectivity exceeding 90%, demonstrating the benefit of controlled multivalent integration [59].

However, such quantitative design rules remain the exception rather than the norm; systematic structure-activity relationships across different valence state combinations are largely absent [60]. Where such data are unavailable, this review explicitly notes the gap to guide future investigation. Based on the nature of the involved variable-valence Cu species, this review systematically categorizes Cu-based photocatalysts into Cu^0 active sites, self-induced excited-state Cu^+, and visible-light-induced excited-state Cu^{2+}, and further extends the scope to heterogeneous catalytic systems such as polymer ligands, metal-organic frameworks, and single-atom Cu catalysts. These materials have been optimized through a series of performance enhancement strategies, including ligand design [61,62], doping and defect engineering [63–67], heterojunction construction [68–73], morphology and interface control, surface modification and MOF encapsulation, single-atom catalytic site design, bimetallic/multimetallic synergy, and antioxidant and stability strategies. In application areas, Cu-based photocatalysts demonstrate excellent catalytic activity [74–76] and selectivity [77–79] in reactions such as C–C coupling [80,81], C–N coupling [82,83], C–heteroatom coupling, alkene/alkyne bifunctionalization [84], asymmetric synthesis, CO_2 reduction, organic pollutant degradation [85,86], hydrogen production [87–90], water splitting, antibacterial applications [91], nitrogen reduction, reductive polymerization, and energy conversion and storage. This review focuses on elucidating the photocatalytic reaction mechanisms of Cu in the aforementioned systems, highlighting key processes such as SET, EnT, dynamic valence state conversion, and multivalent synergistic catalysis. It systematically clarifies the mechanistic roles of variable-valence Cu in photocatalysis, providing a multidimensional theoretical foundation and practical guidance for future research in this field.

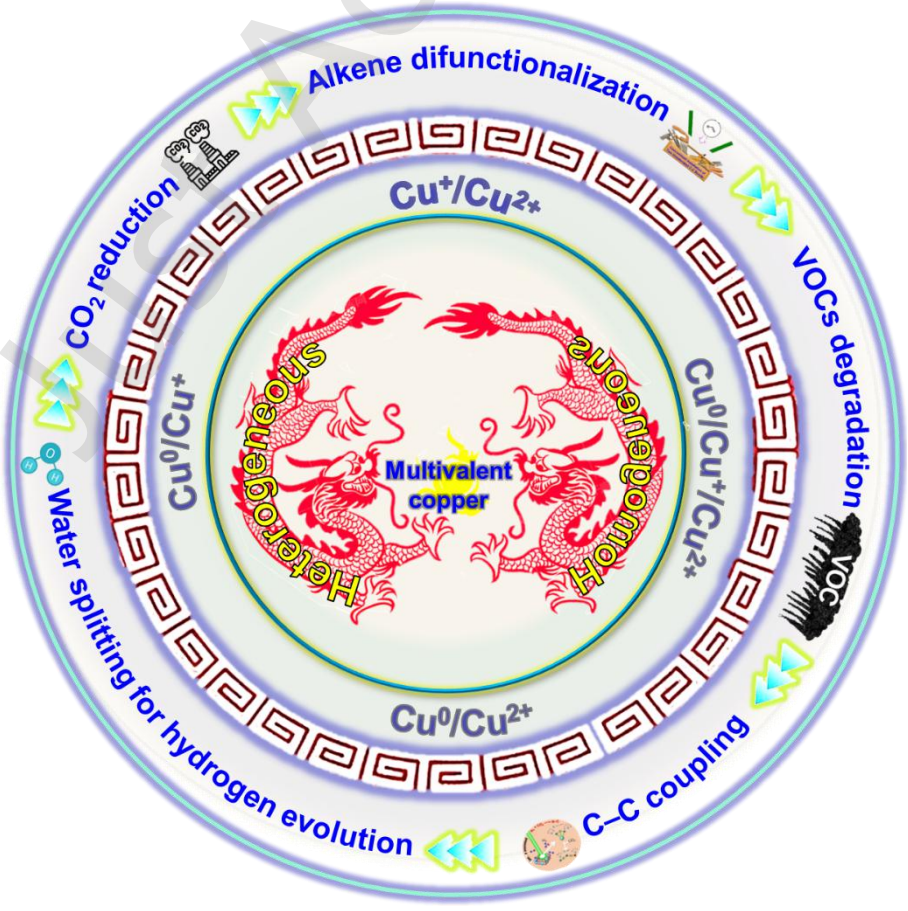

Figure 1 Classification, mechanisms of action, and application domains of Cu's variable valence states.

2 Cu^0 active sites

Cu predominantly exists in three valence states: Cu^0, Cu^+, Cu^{2+}, during photocatalytic processes. Cu^0, owing to its LSPR effect, can efficiently absorb visible and near-infrared light, and the generated hot electrons can be rapidly transferred to reactants, significantly enhancing photocatalytic efficiency, particularly excelling in CO_2 reduction and organic pollutant degradation [92]. Cu^+ complexes form long-lived MLCT states upon photoexcitation, generating radical intermediates via the SET mechanism, which are widely applied in reactions such as C-C coupling and alkene bifunctionalization [93] The flexibility in ligand design can further modulate reaction selectivity and efficiency [94]. Cu^{2+} tends toward LMCT, acting as an electron acceptor in photocatalytic oxidation reactions and collaborating with Cu^+ to complete the catalytic cycle [95], for instance, by stabilizing high-valent intermediates in ATRA reactions. Compared to the reducing capability of Cu^0 and the coordination diversity of Cu^+, Cu^{2+} in heterogeneous catalysis optimizes charge carrier separation efficiency and reduces electron-hole recombination through doping or heterojunction construction (e.g., CuO/TiO_2) [96]. The dynamic interconversion among the three valence states (e.g., the $Cu^0/Cu^+/Cu^{2+}$ cycle) constitutes the multifunctionality and high efficiency of Cu-based photocatalysts, enabling efficient utilization of photogenerated charges through synergistic effects [97]. Studies indicate that the mutual transformation between Cu^0 and Cu^+ can significantly influence the activity and stability of photocatalysts [98]. For example, Cu^0 possesses a high reducing ability, effectively promoting the transfer of photogenerated e^- and thereby enhancing photocatalytic efficiency. In contrast, Cu^+, due to its smaller ionic radius and higher charge density, can boost light harvesting ability and selectivity of photocatalysts. Furthermore, the presence of Cu^{2+} can accelerate transfer of photogenerated carriers and reduce electron-hole pair recombination, thereby improving photocatalytic performance [99].

2.1 Cu^0 species in homogeneous catalysis

In homogeneous photocatalytic systems, Cu^0 active sites typically exist as atoms or clusters within specific coordination environments, exhibiting unique molecular-level catalytic characteristics. Unlike conventional Cu complexes, Cu^0 in homogeneous systems often acts as an electron-deficient center, forming stable catalytically active sites through coordination with organic ligands. For example, in photoinduced C-C coupling reactions [100], Cu^0 atoms can participate in radical formation and capture via SET processes, and their unique electronic structure enables them to serve both as electron donors to promote reduction and as electron acceptors in oxidation processes. The dynamic interconversion among different Cu oxidation states, modulated by their coordination environments, often represents a deeper mechanism governing catalytic pathways and product selectivity. Especially in transformations involving radical intermediates, the initial oxidation state of Cu and its evolution during the photocycle can fundamentally alter the reaction trajectory [101]. A recent study by Sardana et al. provides a compelling example, systematically comparing the roles of Cu species in the photocatalytic reaction of nitroalkanes with alkenes/alkynes and revealing the precise regulatory function of Cu oxidation states as a "molecular switch" over the reaction pathway [102]. The initial oxidation state of the catalyst, the ligand structure, and their mutual interconversion during the photocycle collectively form a dynamic network that not only controls the generation mode of key radical intermediates but also governs subsequent interactions between the metal species and radicals [103]. This demonstrates that fine-tuning of Cu^0 active sites enables high-level editing of reaction selectivity, further expanding our understanding of the molecular-level photochemical behavior of Cu species. Complexes containing Cu^0 can form long-lived MLCT states under visible light excitation, a feature that makes it possible to drive diverse organic transformation reactions under mild conditions. Furthermore, through rational ligand design, the electron density and spatial configuration of Cu^0 active sites can be precisely modulated, thereby achieving fine control over reaction selectivity.

It is worth noting that the stability of Cu^0 species in homogeneous systems has consistently been a research challenge. Recent studies have shown that employing chelating structures with hard-base ligands such as nitrogen- or phosphorus-containing donors can effectively stabilize Cu^0 atoms, preventing their oxidation or agglomeration. This strategy not only enhances catalyst longevity but also expands its applicability in complex reaction systems. In the field of asymmetric synthesis, chiral ligand-modified Cu^0 centers have been successfully employed in constructing various chiral molecules, demonstrating good enantioselectivity and chemoselectivity. These advances indicate that, although research on Cu^0 in homogeneous systems is relatively limited, its unique electronic properties offer novel perspectives for developing new photocatalytic systems. In the light-driven radical Cu catalytic system reported by Luo et al., although the process primarily involves multivalent redox cycling, the ligand strategy employed aligns closely with the concept of Cu^0 stabilization [104]. This study utilized pyridine-N-heterocyclic carbene ligands, which not only improved the stability and halogen atom transfer efficiency of Cu^+ species under photoexcitation but also provided coordinative protection for potential low-valent Cu intermediates such as Cu^0. Consequently, high activity and selectivity were achieved in complex amination reactions. This work provides an important reference for future designs of photocatalytic systems based on Cu^0 or other low-valent metal states. In summary, Cu^0 species in homogeneous systems exhibit unique molecular-level catalytic behavior, acting as electron-deficient centers that can participate in both radical generation and capture via SET processes. The key design principle emerging from these studies is the critical role of chelating ligands (e.g., N- or P-containing donors) in stabilizing Cu^0 atoms against oxidation and agglomeration, thereby enabling their application in asymmetric synthesis and complex organic transformations. However, several unresolved challenges remain: (i) the transient nature of Cu^0 intermediates makes their direct spectroscopic characterization difficult; (ii) the factors governing the balance between Cu^0 stability and reactivity are not yet fully understood; and (iii) strategies for extending Cu^0-based photocatalysis to a broader range of substrates require further development. Future efforts should

focus on developing *in-situ* characterization techniques to capture the dynamic evolution of Cu^0 species during photocatalysis and on designing more robust ligand environments that can stabilize Cu^0 while maintaining high catalytic activity.

2.2 Cu^0 species in heterogeneous catalysis

Cu^0, as an important form of Cu, plays a critical role in heterogeneous catalytic systems, where its unique electronic structure and surface effects enable efficient absorption of visible and near-infrared light, significantly enhancing photocatalytic efficiency. The LSPR effect of Cu^0 (Fig. 2(a)) allows Cu nanocrystals to efficiently absorb photons across the visible to near-infrared spectrum, generating intense near-field electromagnetic enhancement, high-energy hot carriers, and localized photothermal effects, thereby markedly boosting photocatalytic reaction efficiency [105,106]. This effect not only promotes the interfacial adsorption and activation of reactants but also drives charge separation and transfer via nonradiative decay pathways, effectively lowering the energy barrier of key reaction steps [107]. Concurrently, within heterogeneous catalysis, Cu^0 is commonly loaded as nanoparticles onto various semiconductor supports, where it effectively suppresses photogenerated electron-hole recombination through the formation of Schottky junctions while serving as an electron trapping and transport center to enhance catalytic efficiency [108]. Furthermore, Cu^0 exhibits excellent co-catalytic performance in reactions such as photocatalytic hydrogen evolution, CO_2 reduction, and organic pollutant degradation,

Further research reveals that the core role of Cu^0 in photocatalytic reactions lies primarily in the capture and transport of photogenerated e-. Specifically, Cu^0 nanoparticles can generate hot electrons via their LSPR effect, which can be rapidly transferred to reactant molecules, thereby facilitating photocatalytic reactions. Additionally, surface defects and low-coordination atomic sites on Cu NPs can effectively adsorb reactant molecules, further enhancing catalytic efficiency. Cu NPs also exhibit excellent performance in the photocatalytic hydrogen evolution reaction (HER), where Cu^0 effectively reduces the reaction activation energy and accelerates electron transfer and hydrogen generation. For example, by compositing Cu nanoparticles with ZnS [115], an efficient Schottky junction can be constructed, significantly improving the efficiency of photocatalytic hydrogen evolution. These studies not only elucidate the important role of Cu^0 in photocatalysis but also provide new insights and a theoretical foundation for designing and developing efficient photocatalytic materials. Cu^0 nanoparticles can serve not only as co-catalysts but also further optimize performance through combination with other materials. For instance, loading Cu^0 onto the surface of semiconductor materials such as TiO_2 or ZnO forms a Schottky junction, promoting the transfer and separation of photogenerated e-, thereby suppressing electron-hole recombination and enhancing photocatalytic efficiency. Moreover, Cu^0 can act as an electron trapping center, promoting the interfacial adsorption and activation of reactants.

In addition, Cu single atoms (CuSAs), as a novel type of single-atom catalyst (SAC), exhibit unique advantages and promising application prospects in photocatalysis due to their distinctive electronic structure and maximized atom utilization efficiency. with its catalytic activity and stability being significantly enhanced through synergistic effects when forming heterojunctions with supports.

Driven by the cost-effectiveness and decent photoelectrochemical characteristics, Cu nanocrystals have emerged as attractive alternatives to precious metals, including gold and silver [109]. Nevertheless, challenges in preparation and practical uses arise from the tendency to oxidize in air. For the issue of Cu^0 oxidation under environmental conditions, recent research has focused on enhancing its stability through surface engineering and morphology control. For example, controlled synthesis methods are employed to fabricate Cu nanocrystals with specific morphologies (e.g., nanowires, nanoplates), and strategies such as coating, alloying, or surface ligand modification are applied to suppress oxidation, thereby preserving catalytic activity [110]. On this issue, Chen et al. systematically discussed controllable synthesis strategies, morphology modulation methods, and the multifunctional applications of Cu nanocrystals in fields such as photocatalysis and electrocatalysis, with a particular emphasis on various anti-oxidation surface engineering strategies (Fig. 2(b)) [111]. For instance, through rational design of the synthesis system, Cu nanocrystals with specific morphologies (e.g., nanoparticles, nanowires, nanoplates) can be prepared, thereby tuning their light absorption, charge transport, and exposure of catalytic active sites to further enhance photocatalytic performance. This demonstrates broad application prospects in areas such as biological antibacterial activity [112] and environmental organic pollutant degradation [113,114].

They display remarkable catalytic activity, particularly in the photocatalytic carbon dioxide reduction reaction (CO_2 RR), with outstanding performance in the selective production of methanol (CH_3OH). For example, Liu et al. achieved efficient photocatalytic conversion of CO_2 to CH_3OH via the confined synthesis of CuSAs anchored in polymeric carbon nitride (CuSAs@PCN) within crystalline UiO-66-NH_2 (Fig. 2(c)) [116]. The study reveals the introduction of CuSAs and the production of a type-II heterojunction structure are key factors enabling efficient CH_3OH generation. The introduction of Cu^0 not only optimizes the band structure but also promotes the separation and transfer of photogenerated charges through strong interactions with polymeric carbon nitride, thereby significantly enhancing photocatalytic performance (Fig. 2(d)). Importantly, Liu et al. employed *in-situ* diffuse reflectance infrared Fourier transform spectroscopy (DRIFTS) to monitor the photocatalytic CO_2 reduction reaction under visible-light irradiation. Key intermediates including *OCHO, *OCH_2, and *OCH_3 were detected, providing direct evidence of the reaction pathway toward CH_3OH generation. Additionally, XANES and EXAFS confirmed the mixed Cu^+/Cu^{2+} valence state and the Cu–N_4 coordination environment, while the absence of Cu–Cu scattering verified the atomic dispersion of Cu single atoms. Similarly, Woldu et al. reported that Cu-based SACs can achieve a Faradaic efficiency for CH_4 as high as 81% in electrocatalytic CO_2 reduction, emphasizing that tuning the coordination environment of Cu sites and synergistic effects among neighboring atoms can further promote C-C coupling to generate C^{2+} products such as C_2H_4 and C_2H_5OH [117]. Furthermore, the mechanistic role of Cu^0 in photocatalysis has been intensively studied (Fig. 2(e)). Theoretical calculations

have further elucidated the underlying mechanism of Cu^0 in photocatalysis. Doping with Cu^0 can significantly alter the density of states distribution of polymeric carbon nitride, narrowing its bandgap and introducing spin-polarized characteristics. This spin polarization endows Cu^0 with higher reactivity during CO_2 activation and reduction, thereby facilitating the conversion of CO_2 to CH_3OH (Fig. 2(f)). For instance, in the CuSAs@PCN system, the presence of Cu^0 significantly reduces the Gibbs free energy change (ΔG) for the initial step of CO_2 reduction (formation of the *OCHO intermediate), thus lowering the reaction barrier.

Moreover, the synergistic effect of Cu^0 within heterojunction structures is also crucial to consider. By integrating Cu^0 with MOFs or other semiconductor materials, highly efficient heterojunctions can be formed, leading to further enhancement in photocatalytic performance. For instance, the CuSAs@PCN@UiO system, where a composite formed by Cu^0 and polymeric carbon nitride is encapsulated within the crystalline framework of UiO-66-NH_2. This core-shell configuration boosts the separation efficiency of photogenerated charges, whilst leverages the MOF's strong CO_2 adsorption capacity to create a favorable, high-concentration local environment for the reaction. At the same time, the presence of Cu^0 within the heterojunction can fine-tune the charge transfer pathways, thereby further optimizing the efficiency of the photocatalytic reaction.

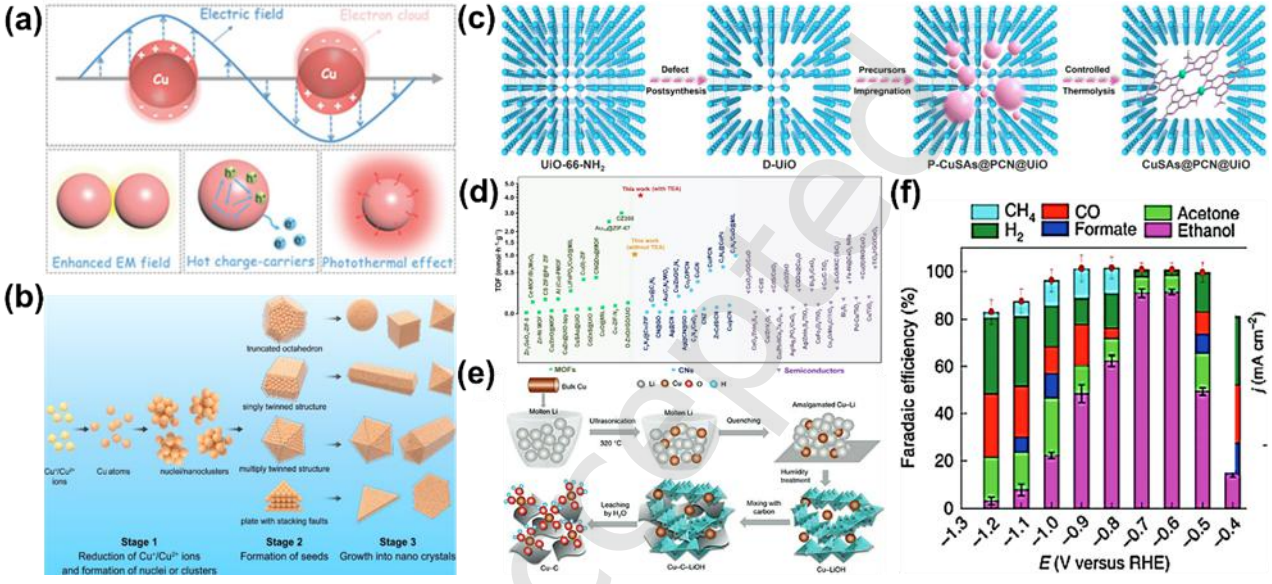

Figure 2 (a) Fundamental principles and key characteristics of localized surface plasmon resonance. (b) Developmental stages in the evolution of copper nanocrystals. Reproduced with permission from Ref. [111], © Elsevier B.V. 2025. (c) Synthetic pathway for CuSAs@PCN@UiO with pink spheres denoting PCN and CuSA precursors. (d) Catalytic performance in photocatalytic CO_2 reduction to CH_3OH: a TOF comparison of MOFs, carbon nitrides, and semiconductors. Reproduced with permission from Ref. [116], © Wiley-VCH GmbH 2024. (e) Reaction pathways for CO_2RR to high-value products, depicting SACs, DACs, tandem SAC-nanocatalysts(SACNCs), and sub-nanocluster catalysts (SNCCs). (f) Fabrication of single-atom Cu on a carbon support and evaluation of its performance in electrocatalytic CO_2 reduction. Reproduced with permission from Ref. [117], © Wiley‐VCH GmbH 2024.

Collectively, the studies reviewed in this section demonstrate that Cu^0 in heterogeneous systems functions through three primary mechanisms: (i) LSPR-driven hot electron generation and injection, (ii) Schottky junction formation with semiconductor supports to suppress charge recombination, and (iii) single-atom Cu sites that maximize atom utilization and enable unique catalytic pathways. These mechanisms share a common design principle: the precise control of Cu^0 size, morphology, and coordination environment is essential for optimizing light absorption, charge transfer, and surface reactivity. Despite significant progress, key challenges persist. First, the *in-situ* tracking of Cu^0 oxidation states during photocatalysis remains technically demanding. Second, the long-term stability of Cu^0 nanostructures under operational conditions requires further improvement through advanced anti-oxidation strategies. Third, the scalability of single-atom Cu catalysts with high loading densities (>1 wt%) without agglomeration is still a synthetic challenge. Future research should prioritize the development of operando spectroscopic methods to monitor Cu^0 evolution and the design of protective surface coatings that preserve Cu^0 activity without compromising light absorption.

3 Self-induced excited-state Cu^+ species

In contrast to the plasmon-dominated behavior of Cu^0, Cu^+ features a d^{10} electronic configuration that enables the formation of long-lived metal-to-ligand charge transfer states upon visible light excitation, making it particularly effective for single-electron transfer processes in homogeneous catalysis. The multivalent nature of Cu-based photocatalysts thus opens up a multidimensional space for tuning their performance, and among these valence states, Cu^+, characterized by its d^{10} configuration, flexible coordination ability, and controllable excited-state dynamics, exhibits outstanding catalytic potential in photocatalysis [118,119]. In homogeneous catalytic systems, Cu^+ complexes can form long-lived (microsecond-scale) MLCT states under visible light excitation. This feature, which is quite distinct from traditional organic photosensitizers (nanosecond-scale) and precious metal catalysts, offers an ideal platform for efficiently driving both SET and EnT processes [120]. Cu^+ demonstrates excellent coordination flexibility [121], enabling it to dynamically coordinate with nucleophilic substrates containing nitrogen, oxygen, or phosphorus to form highly reactive intermediates. Through photoinduction, these generate Cu^{2+} and radical species (e.g., alkyl/aryl radicals), facilitating diverse organic transformations such as C-C coupling and alkene bifunctionalization [122,123]. Furthermore, the

selectivity and efficiency of these reactions can be precisely tuned through ligand design [124]. It's worth noting that the *in-situ* coordination property of Cu^+ allows for the construction of an active catalytic system directly from Cu salts and substrates through dynamic coordination, without the need for pre-synthesizing stable complexes. This significantly broadens the scope of compatible substrates [125]. In the realm of heterogeneous catalysis, Cu_2O (bandgap ~2.17 eV) acts as a p-type semiconductor. When combined with n-type materials (e.g., TiO_2) to form a Z-scheme heterojunction, it greatly impedes charge carrier recombination. Simultaneously, the Cu^+/ Cu^{2+} redox couple (E° = +0.15 V *vs.* SHE) facilitates interfacial charge separation through valence cycling, markedly boosting the efficiency of reactions like CO_2 reduction and water splitting. While stability challenges such as photodecomposition and disproportionation exist, durability can be effectively improved through strategies like chelation with tetradentate ligands or encapsulation within MOFs. These attributes position Cu^+ as a bridge connecting homogeneous and heterogeneous photocatalytic systems. With its controllable excited-state dynamics, flexible coordination, and excellent cost-effectiveness, it emerges as an ideal candidate to replace precious metals for efficient photocatalytic conversions [126]. The following sections will systematically elaborate on the photoexcitation mechanisms of Cu^+ complexes and their pivotal roles in organic synthesis and energy conversion.

3.1 Photoexcitation of Cu^+ complexes

The research on the application of Cu^+ complexes in photocatalysis has evolved through several distinct phases, gradually unveiling their significant potential in organic synthesis. Early foundational work dates back to 1977, when McMillin et al. designed and synthesized the Cu^+ complex $[Cu(dmp)_2]BF_4$ (dmp = 2,9-dimethyl^{-1},10-phenanthroline) and investigated its photochemical properties [127]. They discovered that its MLCT excited state, generated upon excitation with 454 nm visible light, possessed both a long lifetime and a strong reducing power. This excited state was capable of reducing Co^{3+} to Cu^{2+} in K[*cis*-$Co(IDA)_2$]·$1.5H_2O$, providing key theoretical support for the utilization of Cu^+ complexes in photocatalysis and establishing a crucial link between the photoexcited kinetics of Cu complexes and their photocatalytic efficiency. In 1987, Kern and Sauvage reported on the use of the Cu^+ complex $Cu(dap)_2^+$ (dap = 2,9-di(p-methoxyphenyl)$^{-1}$,10-phenanthroline) (Fig. 3(a)) in photocatalysis [128]. Their work demonstrated the complex's catalytic ability to facilitate the reductive coupling of benzylic halides via photoinduced electron transfer. These pioneering studies not only showcased the fundamental photophysical properties of Cu^+ complexes but also laid a solid foundation for their subsequent applications in photocatalysis.

Moving into the 21st century, research on Cu^+-based photocatalysis progressively expanded to encompass a wider range of organic reactions. A pivotal moment came in 2012 when Sagadevan and Hwang reported that Cu^+ chloride (CuCl) could construct C-C bonds via an ATRA mechanism under visible light irradiation [129]. This work was a breakthrough, demonstrating that simple Cu^+ salts could efficiently catalyze C-C bond formation under mild conditions (Fig. 3(b)) without the need for expensive palladium catalysts or specialized ligands. Subsequently, Collins and colleagues further extended the utility of Cu^+ photocatalysis to the synthesis of heterocyclic compounds [130]. They developed a Cu-catalyzed system leveraging visible-light excitation and continuous-flow technology (Fig. 3(c)), successfully converting triarylamines and diarylamines into structurally diverse carbazole derivatives in good to excellent yields, while also demonstrating intriguing regioselectivity (Fig. 3(d)). This work provided a fresh perspective on photocatalytic heterocycle synthesis. Following these advances, research focus shifted towards the strategic design of ligands for Cu^+ complexes and the optimization of their photocatalytic performance. In 2018, Hu et al. reported a Cu^+ photocatalyst based on a 4,6-disubstituted 2,2'-bipyridine ligand (Fig. 3(e)), which was successfully applied to the chlorotrifluoromethylation of alkenes (Fig. 3(f)) [131]. Through this deliberate ligand design, they managed to prolong the photoexcited dynamics of the Cu^+ species and enhance its catalytic efficacy, thereby furnishing a more efficient and selective tool for Cu^+-based photocatalytic organic synthesis.

As mechanistic understanding deepened and synthetic ambitions grew, the field progressed to a more sophisticated stage focused on advanced stereoselective control and mechanistic innovation, as illustrated in the timeline (Fig. 4). In 2021, Zhu et al. reported a Cu-catalyzed asymmetric radical carboesterification reaction, achieving the enantioselective construction of a C-O bond at an acyclic alkyl radical center [132]. This work utilized alkyl diacyl peroxides as both carbon and oxygen sources to accomplish the 1,4-carboesterification of dienes under Cu catalysis, delivering good regioselectivity and high enantioselectivity. In 2023, Song et al. achieved an efficient carbon-oxygen coupling between $C(sp^3)$-H bonds and carboxylic acids to generate chiral esters via Cu^+-catalyzed asymmetric oxidative coupling, overcoming the limitations of traditional methods that relied on linear alkenes and peroxyesters [133]. In 2024, Chen et al. developed a Cu/Rh bimetallic synergistic catalytic system that enabled a ternary reaction among terminal alkynes, diazo esters, and allylic carbonates, successfully constructing a 1,5-enyne scaffold featuring an all-carbon quaternary center [134]. In 2025, Mandal et al. employed a heteroleptic Cu^+ complex, $[Cu(dmp)(BINAP)]BF_4$, to achieve highly regio- and stereoselective β-chloroacylation of alkenes and alkynes via a photocatalytic ATRA reaction. The dual-ligand environment in their design was tailored to optimize the functions of Cu^+ and Cu^{2+}, respectively [135]. That same year marked a major mechanistic breakthrough in the field: Luo et al. reported a light-driven radical Cu-catalyzed allylic amination. This work represented the first instance of generating an electrophilic allyl-Cu^{3+} intermediate via a radical pathway, which then efficiently formed a C-N bond through an outer-sphere nucleophilic substitution mechanism [104]. This work not only opened up an entirely new reaction paradigm for Cu catalysis but also signaled a paradigm shift for Cu^+ photocatalysis, moving from the traditional "radical generation/inner-sphere reductive elimination" model to a novel "radical generation/outer-sphere nucleophilic substitution" stage.

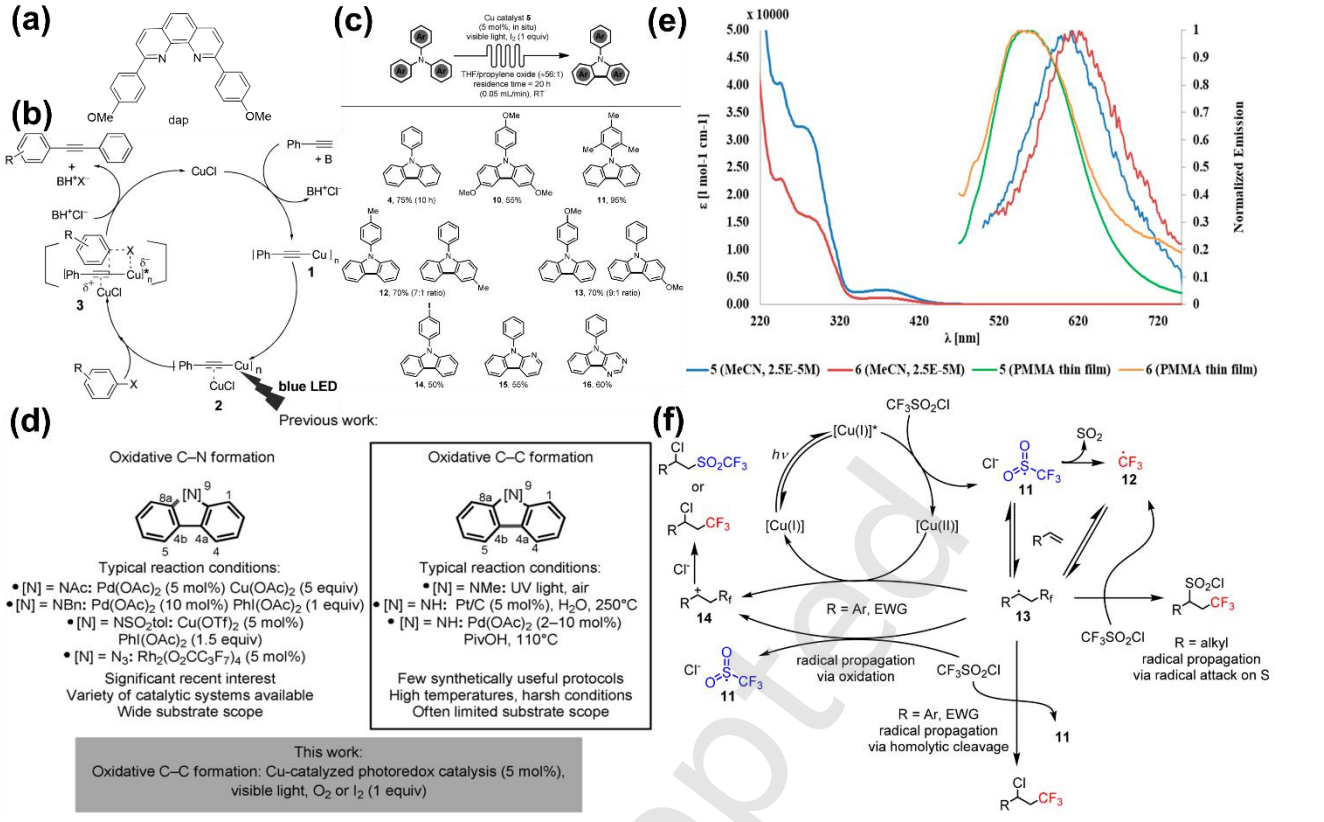

Figure 3 (a) Chemical structure of the DAP Ligand. Reproduced with permission from Ref. [128], © RSC Publishing 1987. (b) Proposed mechanism for the Cu^+ chloride-catalyzed Sonogashira coupling under visible-light irradiation. Reproduced with permission from Ref. [129], © Wiley-VCH GmbH & Co. KGaA, Weinheim 2012. (c) Synthetic challenges and contemporary strategic approaches to carbazole derivatives. (d) Synthetic route for constructing carbazoles from triarylamine precursors. Reproduced with permission from Ref. [130], © Wiley-VCH GmbH & Co. KGaA, Weinheim 2013. (e) Molecular architecture of the Cu^+ photocatalyst based on a 4,6-disubstituted 2,2'-bipyridine ligand. (f) Mechanistic pathway for the trifluoromethylation and trifluorosulfonylation-enabled functionalization of alkenes. Reproduced with permission from Ref. [131], © American Chemical Society 2018.

As research has progressed, Cu^+ complexes have demonstrated ideal visible-light photocatalytic activity across a wide range of chemical transformations. These include alkene bifunctionalization [136], C-C, C-O, C-N, and C-S coupling, as well as cyclization reactions and oxidation reactions. Cu^+L_n complexes can act as independent photocatalysts. Upon excitation by visible light, a Cu^+L_n complex is capable of transferring a single electron to an electron acceptor (such as an alkyl halide, R-X), generating a radical species R$\backsim$ and a transient $Cu^{2+}L_n$ intermediate. This radical R$\backsim$ can subsequently be captured by an alkene or alkyne, leading to a new radical species R'$\backsim$, thereby propagating the radical chain. The subsequent pathway for the $Cu^{2+}Ln$ intermediate primarily follows one of two mechanistic routes [137]. In the ligand transfer mechanism, $Cu^{2+}Ln$ undergoes ligand exchange with a nucleophile (Nu), which is then transferred to the radical R$\backsim$ to form the coupled product R-Nu, simultaneously regenerating the initial Cu^+L_n catalyst to close the catalytic cycle. In the radical rebound mechanism, $Cu^{2+}L_n$ is proposed to combine with the primary radical R•, potentially forming a high-valent R-Cu^{3+}-L_n intermediate according to the cited studies. This intermediate then undergoes ligand exchange with the nucleophile Nu, forming an R-$Cu^{3+}L(n^{-1})$-Nu species. Finally, a coupling product R-Nu is generated via β-hydride elimination or another elimination process, concurrently regenerating the Cu^+L_n catalyst and completing the cycle.

The utility of Cu^+ complexes in photocatalysis stems not only from their diverse accessible oxidation states and adaptable ligand architectures but also from their notable ability to stabilize radical intermediates. Once coordinated with appropriate ligands, these Cu^+ complexes can function as photocatalysts under visible light irradiation, facilitating either SET or EnT processes. This capability enables them to drive a broad spectrum of organic transformations, such as the bifunctionalization of alkenes and alkynes, as well as cross-coupling reactions for forming C-C and C-N bonds. Across these studies, common design principles emerge: ligand rigidity, electronic properties, and steric bulk profoundly influence excited-state lifetimes, redox potentials, and reaction selectivity. Nevertheless, several unresolved questions remain. First, the precise factors governing the partitioning between inner-sphere and outer-sphere pathways are not yet fully predictable. Second, the role of solvent and counterions in modulating Cu^+ excited-state dynamics is underexplored. Third, the extension of Cu^+ photocatalysis to energy-related transformations (e.g., water splitting, CO_2 reduction) remains limited compared to its success in organic synthesis. Future efforts should focus on developing predictive structure–activity relationships through combined computational and experimental approaches, and on expanding the scope of Cu^+ photocatalysis to solar fuel generation

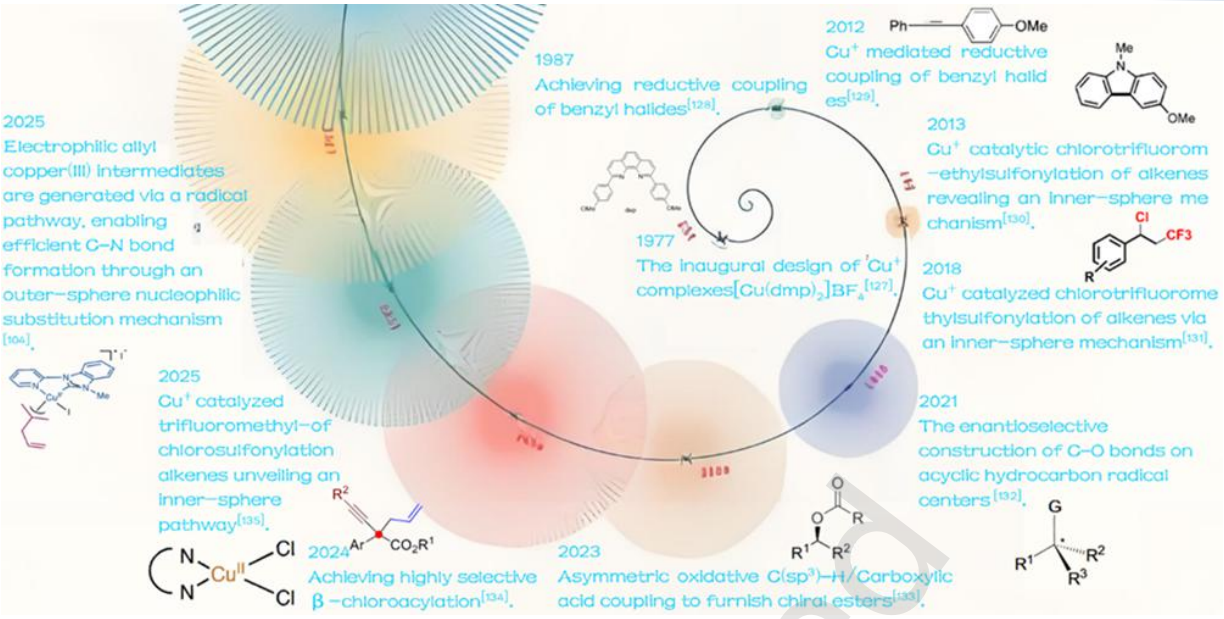

Figure 4 Timeline of key developments. (a) 1977: McMillin et al. pioneered the design of a Cu^+ complex, $[Cu(dmp)_2]BF_4$. Reproduced with permission from Ref. [127], © American Chemical Society 1977. (b) 1987: Kern and Sauvage achieved the reductive coupling of benzylic halides. Reproduced with permission from Ref. [128], © RSC Publishing 1987. (c) 2012: Sagadevan and Hwang demonstrated Cu^+-mediated reductive coupling of benzylic halides. Reproduced with permission from Ref. [129], © Wiley-VCH GmbH & Co. KGaA, Weinheim 2012. (d) 2013: Collins et al. accomplished the Cu^+-catalyzed trifluoromethylchlorosulfonylation of alkenes. Reproduced with permission from Ref. [130], © Wiley-VCH GmbH & Co. KGaA, Weinheim 2013. (e) 2018: Hu et al. reported Cu^+-catalyzed alkene trifluoromethylchlorosulfonylation, providing evidence for an inner-sphere mechanism. Reproduced with permission from Ref. [131], © American Chemical Society 2018. (f) 2021: Zhu et al. achieved enantioselective C-O bond formation at an acyclic alkyl radical center. Reproduced with permission from Ref. [132], © Springer Nature 2021. (g) 2023: Song et al. realized asymmetric oxidative coupling between a $C(sp^3)$-H bond and a carboxylic acid to form a chiral ester. Reproduced with permission from Ref. [133], © American Chemical Society 2024. (h) 2024: Chen et al. achieved highly selective β-chloroacylation. Reproduced with permission from Ref. [134], © American Chemical Society 2024. (i) 2025: Mandal et al. elucidated the inner-sphere mechanism of alkene trifluoromethylchlorosulfonylation. Reproduced with permission from Ref. [135], © Springer Nature 2025. (j) 2025: Luo et al. reported the generation of an electrophilic allyl-Cu^{3+} intermediate via a radical pathway, enabling efficient C-N bond construction through an outer-sphere nucleophilic substitution mechanism. Reproduced with permission from Ref. [104], © Springer Nature 2025.

3.1.1 Carbon-Heteroatom coupling

Photochemistry has played a pivotal role in enabling a wide range of organic transformations that were previously unattainable. Broadly speaking, photochemical mechanisms, such as SET and EnT processes, provide pathways for converting photon energy into usable chemical energy [138-140]. As a result, a versatile strategy with photoredox catalysis promptly evolving and being widely employed in organic chemistry [141,142]. Within this mechanistic framework, a light-absorbing photocatalyst, upon excitation, can act as an electron acceptor or donor toward organic or organometallic substrates. This SET process is powerful because it facilitates the generation of highly reactive radical species under remarkably mild conditions, and it can also effectively activate other catalysts that would otherwise be inert in the absence of both a photocatalyst and visible light [143].

In traditional organic photochemistry, reactions primarily relied on ultraviolet (UV) light excitation (200-400 nm) because the electronic transitions (such as $\pi\rightarrow\pi^*$ or $n\rightarrow\pi^*$) of most organic compounds occur mainly in the UV region [144]. However, over the past two decades, the field has undergone significant technological innovation, with researchers progressively developing new photocatalysts capable of efficiently absorbing photons in the visible light region (400-700 nm) [145,146]. It is worth noting that early visible-light photocatalysts were predominantly based on precious metal complexes. While these exhibited excellent photophysical properties, their high cost and limited resource availability constrained large-scale applications. This technological bottleneck was overcome by the groundbreaking work of Kainz et al., who first reported a reaction system that efficiently constructs C-N bonds using Earth-abundant Cu as the catalyst under blue light (450-495 nm) irradiation [147]. Cu-based catalysts not only display photocatalytic activity comparable to that of precious metals, but their unique d^{10} electronic configuration also offers distinct advantages, including a highly tunable ligand field and favorable excited-state lifetimes, particularly beneficial for visible-light-driven organic reactions.

Cu displays a notable carbophilicity, allowing it to form a variety of Cu-carbon species including Cu-aryl and Cu-alkyl intermediates. Coupling reactions developed based on this property can be used to construct diverse chemical bonds, including $C(sp^2)$-$C(sp^3)$, $C(sp^2)$-$C(sp^2)$, $C(sp^3)$-$N(sp^2)$, $C(sp^3)$-$N(sp^3)$, $C(sp^3)$-O, $C(sp^3)$-C(sp) and $C(sp^3)$-$C(sp^3)$. Coupling reactions play a vital role in organic synthesis, offering straightforward strategies for the yield of C-X bonds (where X = C, N, O, B, etc.) [148]. Cu-catalyzed coupling reactions have been studied for decades, ever since the initial development of Ullmann-type coupling in 1901. This section will be organized according to the different types of C-X bond formations, covering reactions such as Suzuki-Miyaura coupling, Glaser coupling, Sonogashira coupling, and Ullmann coupling.

Liu et al. achieved an efficient carbon-oxygen coupling between $C(sp^3)$-H bonds and carboxylic acids to produce chiral esters via

a Cu-catalyzed asymmetric oxidative coupling (Fig. 5(a)) [133]. This method broke through the limitations of the traditional Kharasch reaction, which required linear alkenes and peroxyesters. The key to their success was the synergistic employment of a cationic Cu catalyst and blue-light excitation to enable the stereoselective capture of radical intermediates. This approach not only avoids the reliance on unstable reagents like peroxyesters used in traditional methods but also accomplishes efficient oxidative coupling through visible-light excitation and a Cu^+ catalyst, significantly simplifying the synthesis of chiral esters. Furthermore, through a combination of DFT calculations and experimental verification, the researchers elucidated the mechanistic role of the Cu^+ complex in the reaction, which involves hydrogen atom abstraction, radical formation, and the generation of a Cu^{3+} intermediate (Fig. 5(b)). These findings are mechanistically coherent, as the reductive elimination step formally represents the oxidation of the side-chain substituent by the Cu metal center. Bunescu et al. further expanded the multicomponent coupling strategy by developing an anion-mediated dual-catalytic system for the multicomponent azidoarylation of alkenes (Fig. 5(c)) [149]. This method employs a visible-light-driven Cu^+ complex as the catalyst to achieve a three-component coupling reaction involving an alkene, an aryl electrophile, and a nitrogen nucleophile (Fig. 5(d)). The innovative aspect lies in the azide anion-mediated redox-neutral dual catalytic cycle, which elegantly addresses the challenge of nitrogen-centered capture following the addition of an aryl radical to the alkene.

The azide anion acts not only as a nitrogen source but also mediates the redox balance between Cu catalysts through an inner-sphere electron transfer mechanism. This process not only accommodates a broad range of alkene and aryl components but also provides an efficient route for synthesizing biologically active β-arylethylamine scaffolds. Cai et al. extended this logic to the late-stage functionalization of complex molecules by developing a photoinduced, Cu-catalyzed $C(sp^3)$-P bond-forming reaction [150]. Using N-(acyloxy)phthalimides as radical precursors, they achieved efficient coupling with secondary phosphines (Fig. 5(e)). The strategy utilizes Cu^+ complexes, which, upon photoexcitation, generate alkyl radicals via a SET process. These radicals then form an intermediate with a Cu^{2+} species, ultimately leading to $C(sp^3)$-P bond formation through reductive elimination. They also accomplished the azidoarylation of alkenes using arylthianthrenium salts and a single Cu photocatalyst (rac-BINAP-Cu^+-N_3). Photoexcitation of this Cu complex simultaneously controls both aryl radical generation and azide transfer, significantly enhancing the reaction's compatibility with complex arene substrates and multiply substituted alkenes. This work highlights the dual role of variable-valence Cu (Cu^+/Cu^{2+}) in photocatalysis, serving both as a photosensitizer and a redox catalyst. UV-vis absorption spectroscopy and crystal structure analysis (Fig. 5(f)) confirmed that the *in-situ* generated rac-BINAP-Cu^+-azide complex is the photoactive species, capable of single-electron reducing arylthianthrenium salts under blue light to generate aryl radicals and a Cu^{2+} intermediate. The aryl radical subsequently adds to the alkene to form an alkyl radical, which then undergoes nitrogen group transfer from the Cu^{2+}-azide species to complete the C-N bond construction. This mechanism avoids the need for an external photosensitizer, thereby simplifying the reaction system. Furthermore, the reaction exhibits broad substrate scope, accommodating various substituted alkenes and complex arylthianthrenium salts, offering a new strategy for the efficient synthesis of β-arylethylamines.

The aforementioned studies systematically construct a developmental framework for carbon-heteroatom coupling, reflecting a coherent logical progression from mechanistic elucidation to synthetic application. The journey began with using visible-light-excited Cu^+ for selective C-H activation and C-O bond construction, then evolved into multicomponent cooperative catalysis strategies to tackle radical capture challenges, and ultimately expanded to the late-stage precise functionalization of complex molecules. In terms of catalytic materials, the research evolved from simple Cu salts to *in-situ* generated, well-defined, and functionally integrated ligand-Cu complexes (e.g., rac-BINAP-Cu^+-N_3), achieving synergistic optimization of photosensitizing and catalytic properties. This progression demonstrates the field's advancement from mechanistic exploration to synthetic utility, offering modular solutions for constructing important scaffolds like carbon-heteroatom bonds.

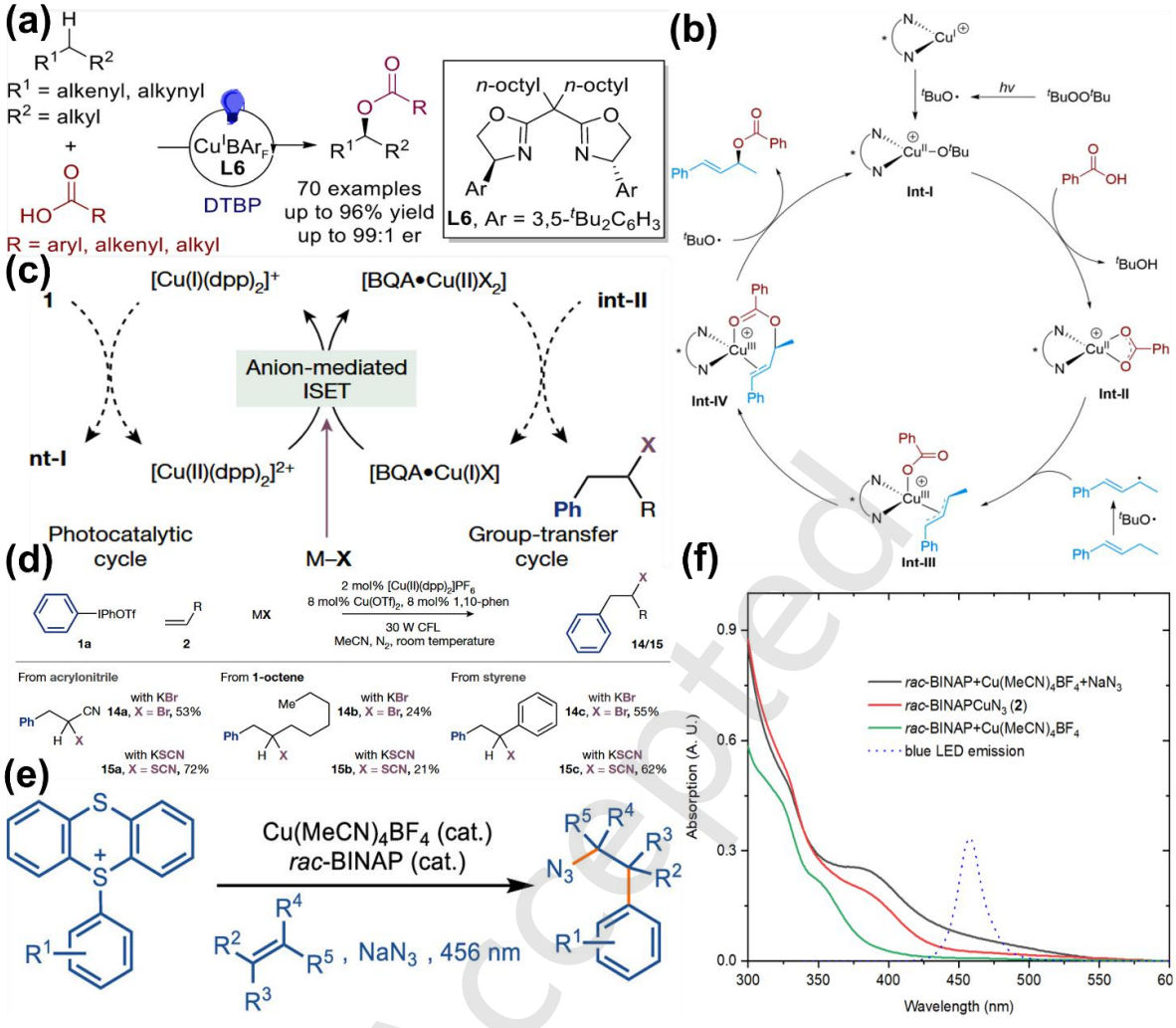

Figure 5 (a) Synthesis of racemic melphalan employing N,N-Bis(2-chloroethyl)aniline as a precursor. (b) Proposed mechanism. Reproduced with permission from Ref. [133], © American Chemical Society 2025. (c) Mechanistic pathway for the photocatalytic aryl functionalization of alkenes via ISET. (d) Initial experimental outcomes of aryl bromination and aryl thiocyanation of alkenes. Reproduced with permission from Ref. [149], © Springer Nature Limited 2021. (e) Attaining elevated enantioselectivity in the oxidative coupling of C(sp^3)-H bonds and carboxylic acids. (f) Analysis performed by UV-vis absorption spectroscopy. Reproduced with permission from Ref. [150], © American Chemical Society 2023.

3.1.2 Bifunctionalization of alkenes/alkynes

The role of Cu complexes in the bifunctionalization reactions of alkenes and alkynes has garnered significant attention in recent years, with their unique catalytic properties offering novel strategies and methodologies for synthetic chemistry. The Cu^{2+} intermediate, generated from photoexcited Cu^{+}* via SET, can cooperate with various functional groups, thereby accelerating the transfer of ligands to intermediate radicals in diverse ATRA reactions [151,152]. Consequently, Cu^{+} complexes are highly effective in promoting the photocatalytic bifunctionalization of alkenes and alkynes, leading to the formation of complex, high-value organic molecules.

In the context of ATRA reactions, Cu complexes serve not only as cost-effective alternatives, replacing traditional ruthenium (Ru) and iridium (Ir) photocatalysts, but also demonstrate distinct advantages in alkene and alkyne bifunctionalization due to their unique dynamic coordination ability and inner-sphere reaction mechanisms [153]. A pioneering example was reported in 2015, focusing on the vicinal trifluoromethylation/chlorosulfonylation of alkenes. Bagal et al. employed $[Cu(dap)_2]Cl$ as the catalyst to investigate a visible-light-mediated trifluoromethylchlorosulfonylation reaction, achieving efficient conversion of unactivated alkenes (Fig. 6(a)) [154]. This study not only showcased the high efficiency of Cu complexes in photocatalysis but also, through comparison with other photocatalysts (e.g., $[Ru(bpy)_3]Cl_2$ and $[Ir(ppy)_2(dtbbpy)]PF_6$), revealed the unique mechanistic role of Cu complexes in the reaction. Unlike traditional outer-sphere mechanisms, Cu complexes likely operate via an inner-sphere mechanism, where coordination stabilizes reaction intermediates, enabling distinct reaction pathways. When using sterically hindered substrates (e.g., 1s) or bulkier Cu complexes, the reaction favors the formation of chlorinated products (Fig. 6(b)). This indicates that the coordination of SO_2Cl to Cu is relatively weak and susceptible to steric or ligand effects, further supporting the dynamic nature of ligand transfer in the inner-sphere mechanism. Furthermore, Cu complexes exhibit broad substrate compatibility, including unactivated alkenes and alkynes. Their use significantly enhances the efficiency and selectivity of alkene and alkyne bifunctionalization reactions, providing new tools and methods for constructing complex molecular architectures and thereby expanding their application scope in organic synthesis.

Chen and colleagues have made significant contributions to the

field of homogeneous terminal C-H functionalization [155]. As they have outlined (Fig. 6(c)), the role of Cu complexes in alkene bifunctionalization extends well beyond mere electron transfer. Typically, Cu catalysts activate the carbon-carbon double bond through coordination with the alkene, which in turn facilitates nucleophilic attack to achieve alkene bifunctionalization. Leveraging this activation by the Cu catalyst, alkenes can react with various carbon electrophiles to produce multifunctionalized alkene products. Conversely, Cu catalysts are also widely applied in the bifunctionalization of alkynes. Cu-catalyzed hydrofunctionalization of alkynes, for instance their semi-hydrogenation, efficiently converts alkynes to alkenes, providing key intermediates for synthesizing multifunctionalized alkenes. Activated by the Cu catalyst, alkynes can react with various carbon nucleophiles or electrophiles to yield multifunctionalized alkyne products. These reactions exhibit broad substrate scope and can proceed under mild conditions, minimizing environmental impact.

Bimetallic cooperative catalysis is a powerful strategy for developing efficient and novel organic reactions, enabling challenging transformations that are often difficult to achieve with a single metal catalyst. In 2025, Chen et al. developed a Cu/Rh bimetallic cooperative catalytic system that enabled a ternary reaction among terminal alkynes, diazo esters, and allylic carbonates [134]. This successfully constructed a 1,5-enyne scaffold featuring an all-carbon quaternary center and accomplished acylation-allylation of the carbene via a Meyer-Schuster rearrangement. This successfully constructed a 1,5-enyne scaffold featuring an all-carbon quaternary center and accomplished acylation-allylation of the carbene via a Meyer-Schuster rearrangement. The key to this reaction lies in the synergistic interplay between Cu nanoparticles and the Rh/Xantphos complex, which are responsible for the alkynylation and allylic alkylation of the carbene, respectively. Furthermore, concerning the evolution of the two metal catalyst precursors, the reaction between Cu acetylide and the bisphosphine ligand generated a tetranuclear Cu cluster, suggesting potential aggregation of the Cu species. During the pronounced induction period of the reaction, mercury poisoning tests and experiments substituting commercially available Cu nanoparticles (Fig. 6(d)) both indicated that the precatalyst, Cu^+ chloride, might undergo *in-situ* aggregation within the reaction system to form Cu nanoparticles, which then catalyze the reaction between the carbene and the terminal alkyne. The study proposes that the catalytic process likely involves the synergy between the carbene insertion catalyzed by the *in-situ* aggregated Cu nanoparticles and the allylic substitution catalyzed by the rhodium complex (Fig. 6(e)). Also in 2025, Mandal et al. employed a heteroleptic Cu^+ complex, $[Cu(dmp)(BINAP)]BF_4$, to achieve β-chloroacylation of alkenes and alkynes via a photocatalytic ATRA reaction [135]. This catalyst features a unique dual-ligand environment design: in the Cu^+ state, BINAP provides a long excited-state lifetime (2,188 ns) and sufficient reducing potential ($^{-1}$.64 V *vs.* SCE) to enable single-electron reduction of acid chlorides, generating acyl radicals. In the Cu^{2+} state, the diamine ligand preferentially coordinates, facilitating efficient chlorine atom transfer to the carbon-centered radical, forming a stable C-Cl bond. This mechanism overcomes the efficiency limitations of traditional homoleptic Cu catalysts (e.g., $[Cu(dmp)_2]Cl$), which suffer from short excited-state lifetimes (90 ns). The studies, which covered a broad substrate scope, jointly underscore the pivotal role of transition metal catalysis in alkene and alkyne bifunctionalization. On one hand, bimetallic cooperative catalysis enables multi-bond formation through stepwise activation of different substrates (e.g., the Cu/Rh system). On the other hand, photocatalytic ATRA reactions achieve highly selective transformations via precise capture of radical intermediates (e.g., the Cu^+/Cu^{2+} cycle). Both studies, through their mechanistic investigations, reveal the decisive impact of the dynamic evolution of metal species (such as Cu nanoparticles or the Cu^{2+}-Cl intermediate) on reaction efficiency, providing important paradigms for designing novel bifunctionalization reactions.

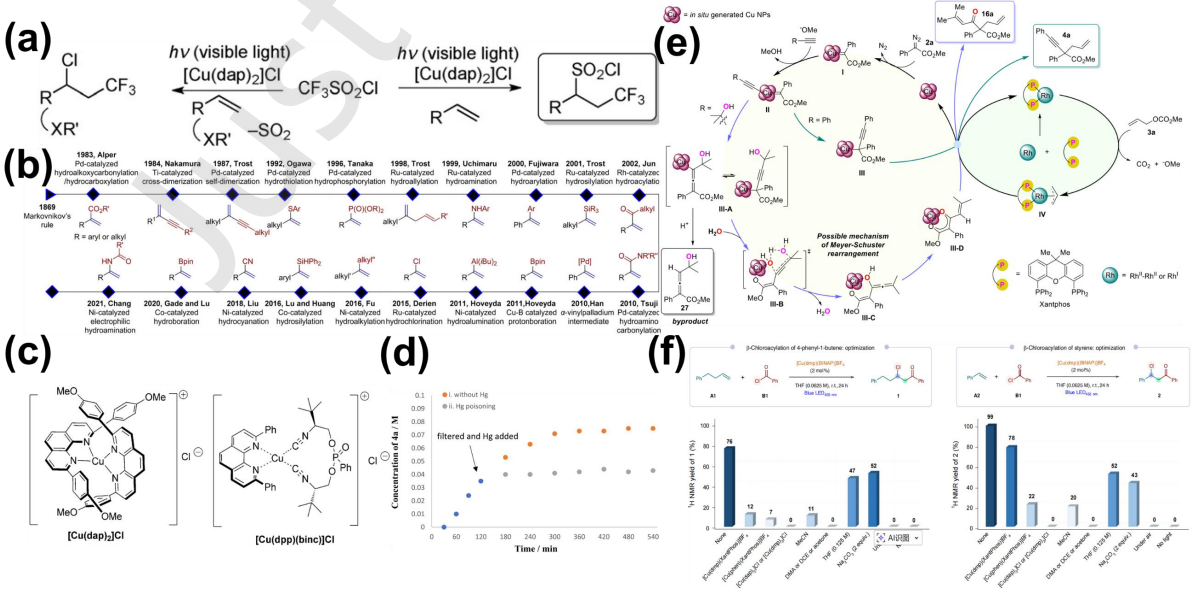

Figure 6 (a) Trifluoromethylation of alkenes via visible-light-driven photocatalysis. (b) Steric effects of substrates and catalysts on the trifluoromethylchlorosulfonylation *vs.* chlorination of alkenes. Reproduced with permission from Ref. [154], © Wiley-VCH GmbH & Co. KGaA, Weinheim 2015. (c) Markovnikov-selective hydrofunctionalization of terminal alkynes catalyzed by transition metals. Reproduced with permission from Ref. [155], © RSC Publishing 2024. (d) Mercury poisoning test validating the catalytic role of Cu nanoparticles. (e) A plausible reaction mechanism for Rh/Cu bimetallic catalysis. Reproduced with permission from Ref. [134], © American Chemical Society 2024. (f) Comparative efficacy of heteroleptic *vs.* homoleptic Cu^+

complexes in ATRA-type chloroacylation. Reproduced with permission from Ref. [135], ©Springer Nature 2025.

3.1.3 Structure and function

Efficient photocatalytic reactions can be achieved by rationally designing the structure of Cu complexes and optimizing reaction conditions. By carefully designing the ligand environment of Cu complexes, it is possible to modulate the oxidation state and electron transfer capability of Cu, thereby enabling selective control over reaction pathways [156]. For instance, in some photocatalytic reduction reactions, altering the electronic properties of the ligand can facilitate efficient electron transfer from Cu^{+} to Cu^{2+}, thereby driving the reaction forward. Take, for example, the Cu-catalyzed photocatalytic reaction between iodoalkanes and alkenes. Modifying the ligand's electronic properties enables efficient Cu^{+} to Cu^{2+} electron transfer, promoting the reaction. This type of reaction not only exhibits high selectivity and yield but also allows toward effective and versatile iodoalkane conversion.

Within Cu catalytic systems, coordination with different ligands can impart distinct chemical properties and redox capabilities to the Cu center. Ligand design has long been recognized as a powerful tool, as coordinating ligands can significantly alter the reactivity of metal complexes [157]. In the Cu-catalyzed photocatalytic reaction between bromonitroalkanes and alkenes, Cu^{+} complexes efficiently reduce the bromonitroalkane to a radical upon photoexcitation, which then adds to the alkene to form the desired product. Similarly, in the Cu-catalyzed photocatalytic reaction of iodoform with alkenes, Cu^{+} complexes efficiently reduce iodoform to a radical under light, leading to an addition reaction with the alkene to yield the target product. Cu^{+} generates radical intermediates via SET after photoexcitation. Subsequently, Cu^{2+} stabilizes these intermediates through ligand transfer or rebound mechanisms, enabling an efficient reaction pathway [158]. Furthermore, Cu^{+} complexes are also employed in the photocatalytic reduction of aryl iodides, where they efficiently reduce the aryl iodide to a radical under light, allowing it to react with nucleophiles to form the desired product. Tang and Tsui reported a Cu-catalyzed pentafluoroethylation reaction using $Et_3SiCF_2CF_3$ as the pentafluoroethyl source, successfully achieving the pentafluoroethylation of aryl and alkenyl iodides [159]. This reaction demonstrates the high efficiency of Cu in introducing the CF_2CF_3 group, highlighting its crucial role in C-C bond formation and also revealing a selective photocatalytic defluorination process. Angus et al. provided an in-depth exploration of how tetradentate phenanthroline ligands affect the performance of Cu^{+} photoredox catalysts. Their work revealed how ligand rigidity and steric bulk modulate catalyst stability and photophysical properties, thereby optimizing catalytic efficiency [160]. By designing a series of Cu^{+} complexes featuring tetradentate ligands, they investigated the impact of ligand structure on catalyst performance. They found that the ligand's rigidity, electronic properties, and the coordination angle with the Cu center significantly influence the catalyst's stability and photocatalytic performance. For example, ligands with larger coordination angles and appropriate flexibility can enhance the photocatalytic efficiency of Cu^{+} complexes while maintaining good reaction selectivity, providing crucial theoretical guidance for designing high-performance Cu^{+} photocatalysts. In the realm of asymmetric alkyne bifunctionalization, the work of Wang et al. further expands the ability to control reaction selectivity through ligand environment, achieving regiodivergent asymmetric bifunctionalization of alkynes via ligand modulation [161]. This control over regioselectivity is particularly valuable for synthesizing high-value chiral molecules, as it allows access to multiple isomers from the same starting materials. Cu-based photocatalysts demonstrate excellent functional group tolerance and broad substrate compatibility in reactions. This versatility enables Cu-catalyzed photoreactions to not only process conventional organic substrates but also to be effectively applied to the late-stage functionalization of complex bioactive molecules, thereby significantly streamlining the synthetic routes to valuable intermediates. This study not only demonstrates the unique capability of Cu complexes in controlling reaction regioselectivity but also uses DFT calculations to uncover the origin of the ligand-based control mechanism. Collectively, these studies show that the ligand environment not only stabilizes Cu complexes but also, through a synergy of electronic effects and steric hindrance, governs both the regioselectivity and stereoselectivity of reactions.

3.2 Photogeneration of Cu^{+} complexes *in situ*

Nucleophilic substrates can react or coordinate directly with Cu^{+} salts to form visible-light-absorbing Cu^{+} complexes without exogenous ligands. Consequently, these *in-situ* generated, photoactive Cu^{+} catalysts exhibit a broad application scope [162,163]. Unlike many transition metals, Cu^{+} can directly coordinate with substrates containing nitrogen, oxygen, or phosphorus to form visible-light-responsive complexes. Upon excitation, these undergo SET to generate high-valent Cu^{2+} species, which then participate in synthetic reactions, such as coupling reactions, functionalizations, and dynamic kinetic resolution [164]. The *in-situ* generation of the photoactive Cu^{+} catalyst avoids potential contamination or losses during handling and transfer. This ensures precise control over reaction conditions, thereby enhancing both reaction efficiency and selectivity [165]. The excited-state Cu^{+}-substrate complex reduces electrophiles via a SET process. The resulting Cu^{2+}-substrate complex then engages in diverse synthetic transformations, including cross-coupling reactions and functional group modifications [166]. Based on this concept, the following discussion is presented.

3.2.1 Cross-Coupling reactions induced by nucleophiles

In cross-coupling reactions, the excited-state Cu^{+}-nucleophile species can act as a reductant for various Y-Z precursors, generating carbon or heteroatom (N, O, P) radicals. These radicals then react with a Cu^{2+}-nucleophile complex to achieve various types of coupling processes, such as forming C-C, C-N, C-O, and C-P bonds. This mechanism not only broadens the application scope of Cu^{+} complexes in light-driven organic transformations but also offers a versatile tool for constructing diverse chemical bonds under mild and environmentally benign conditions. Building on the multifunctional nature of Cu^{+} complexes in photo-mediated conversions, the following section reviews some innovative coupling reactions.

A survey of the literature reveals that modulating the metal oxidation number can accelerate several fundamental steps in coupling schemes. For example, in stoichiometric settings, Hillhouse and others have demonstrated that oxidation of the

metal center can dramatically increase the rate of reductive elimination, thereby enabling rapid formation of C-N and C-O bonds [167–169]. These concepts have been translated into catalytic variants, such as the Chan-Evans-Lam reaction, where oxidation of a Cu species facilitates a fast product-release pathway to form aryl-heteroatom bonds [170–172]. While this pathway from Cu^{2+} itself is slow, elimination from a Cu^{3+} intermediate is facile. The Cu^{3+} state is readily attainable through the use of mild oxidants, including molecular oxygen.

Moreover, the formation of Cu^{+} complexes often relies on the *in-situ* coordination of Cu salts with ligands, generating photoactive intermediates that enable efficient photoinduced electron transfer processes. This is particularly evident in cross-coupling reactions involving Cu^{+} complexes and nucleophiles, where they exhibit unique catalytic prowess. For instance, two research groups reported notable advances in 2023. In the work by Wang's group, the *in-situ* coordination of Cu^{+} with a BINAP ligand generated a highly efficient photocatalytic species for C(sp^3)-P bond formation (Fig. 7(a)) [173]. In the study by Shi's group, they developed a Cu-catalyzed N-alkylation reaction (Fig. 7(b)) [174]. The Cu^{+} complex was generated *in situ* via a Cu salt (CuBr) upon ligation (e.g., 1,10-phenanthroline). Upon excitation by visible light, this complex effectively promoted a SET process, generating alkyl radical intermediates. Utilizing visible-light-induced photoredox catalysis, they accomplished the coupling of NH-sulfoximines with alkyl diacyl peroxides. This reaction proceeded at room temperature without added base, exhibited good functional group tolerance, and delivered product yields ranging from 45% to 91%. Roland et al. employed the Cu-based photocatalyst Cu(dmp)(DPEPhos)BF_4 to achieve the efficient synthesis of borabicyclobutane and 2-oxabicyclo[2.1.1]hexane (Fig. 7(c)) [175]. In 2024, Abderrazak et al. utilized benzyl thiocyanate as an ATRA reagent to accomplish highly selective thiocyanation and isothiocyanation of alkenes [176].Their study found that the Cu^{+} complex could not only generate radicals via reductive C-S bond cleavage but also interact with the radical intermediates through inner- or outer-sphere mechanisms, enabling selective synthesis of different products (Fig. 7(d)). These studies not only reveal the versatility of Cu^{+} complexes in photocatalytic reactions but also provide new ideas for developing more efficient and greener organic synthesis methods. Through rational design of ligands and reaction conditions, researchers can efficiently construct various chemical bonds under mild conditions, further advancing the field of photocatalysis.

In the production of fine chemicals and materials, the transition metal-catalyzed cross-coupling between aryl halide electrophiles and heteroatom nucleophiles is one of the most widely used reactions. Cu-catalyzed coupling reactions date back to the early 20th century, but their early applications were not widespread, limited by harsh reaction conditions and high catalyst loadings [177,178]. Palladium catalysts, which enabled the first mild couplings over 80 years later, came to dominate the field of cross-coupling reactions [179,180]. It wasn't until the late 20th century, with breakthroughs in ligand design and the advent of new ligands, that coupling reactions based on the more abundant and lower-cost metal Cu began to show potential comparable to palladium catalysis [181]. However, mechanistic studies of Cu-catalyzed couplings have lagged behind those of palladium, partly because Cu complexes are often paramagnetic, making them more difficult to characterize spectroscopically. Additionally, ligand exchange processes are often faster than the fundamental steps of the catalytic cycle, complicating the identification of active species and key steps [182].Consequently, most Cu catalysts were historically identified through trial and error. Furthermore, the potential interconversion of Cu's multiple oxidation states (e.g., Cu^{+} and Cu^{2+}) during catalysis adds another layer of complexity to unraveling its mechanism. The oxidation state of the active catalyst and its consistency throughout the catalytic cycle has long been a subject of speculation [183]. Within the classic Ullmann coupling, Cu-catalyzed C-O bond formation has been a major focus of research. Early work focused primarily on the formation and transformation of Cu^{+} and Cu^{3+} intermediates, believed to play crucial roles in key steps like oxidative addition and reductive elimination [184,185]. The traditional view held that Cu-catalyzed Ullmann coupling proceeds via Cu^{+}/Cu^{3+} intermediates. However, in 2023, Delaney's group challenged this through combined experimental and computational studies, revealing a non-classical mechanism where an oxamide ligand-stabilized Cu^{2+} complex acts as the catalyst [186]. Their research showed that this highly active catalyst activates aryl halides via a unique pathway: the Cu^{2+} resting state directly participates in a concerted oxidative addition process, inserting the C-X bond into the Cu center to form a high-valent intermediate. Notably, the stability of this intermediate stems from the redox non-innocence of the oxamide ligand. Its ligand-radical character effectively delocalizes electron density from the metal center, circumventing the high energy barrier associated with traditional Cu^{3+} intermediates. Using integrated characterization approaches, encompassing electron paramagnetic resonance (EPR), X-ray single-crystal diffraction, and kinetic experiments (Fig. 7(e)), the researchers confirmed the Cu^{2+} species as the catalytically active center. Particularly noteworthy is the excellent air stability of the pre-assembled Cu^{2+} catalyst, which achieved a turnover number (TON) exceeding 1000 in the coupling of aryl chlorides, a performance that significantly surpasses traditional Cu^{+}/Cu^{3+} catalytic systems. This study not only provides a new theoretical paradigm for Cu catalysis but also opens a new avenue, the "ligand-stabilized high-valent state" strategy, for designing efficient and stable first-row transition metal catalysts (Fig. 7(f)), offering crucial guidance for developing green catalytic systems as alternatives to precious metals.

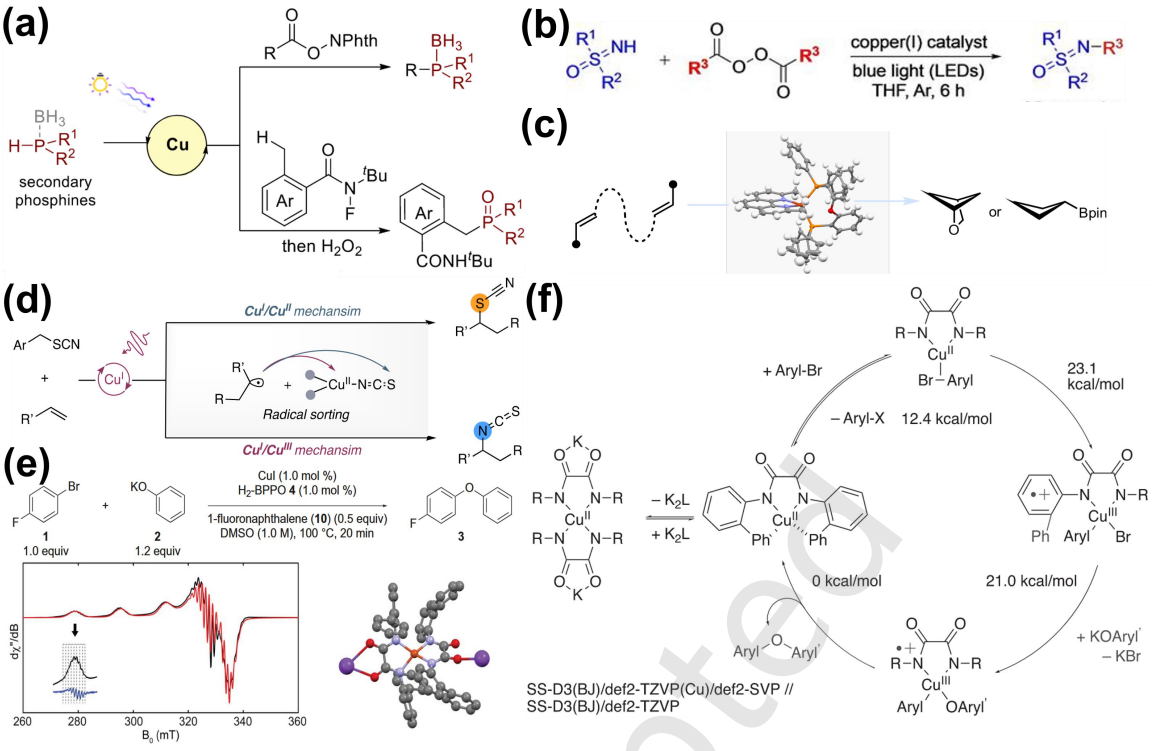

Figure 7 (a) *in situ* generation of a Cu^{+}-BINAP catalyst enabling C(sp^3)-P bond construction. Reproduced with permission from Ref. [173], © American Chemical Society 2023. (b) Schematic workflow of the Cu-catalyzed N-alkylation of NH-sulfoximines with alkyl diacyl peroxides. Reproduced with permission from Ref. [174], © Wiley-VCH GmbH 2023. (c) Synthetic routes toward borabicyclobutane and 2-oxabicyclo[2.1.1]hexane. (d) Regioselective preparation of organyl sulfonyl chlorides and isothiocyanates using Benzyl sulfate as an ATRA reagent. Reproduced with permission from Ref. [175], © American Chemical Society 2024. (e) Structural characterization of a Cu^{2+} complex mixture utilizing X-band EPR and single-crystal XRD. (f) Mechanism and synthetic utility of the cross-coupling transformation. Reproduced with permission from Ref. [186], © The American Association for the Advancement of Science 2023.

3.2.2 Substrate-Induced asymmetric reactions

The application of Cu complexes in asymmetric synthesis has emerged as a prominent research focus in organic chemistry in recent years. Cu, a transition metal with rich oxidation states (Cu^0, Cu^+, Cu^{2+}) and diverse coordination geometries, demonstrates immense potential in asymmetric catalysis due to its unique electronic properties and catalytic capabilities. Particularly in photocatalysis, Cu complexes can not only act as SET reagents to initiate radical reactions but also, through interaction with visible light, form excited states that enable precise control over reaction pathways [187,188]. The coordination environment created by chiral ligands around the Cu center determines the stereochemical outcome of reactions [189]. By tailoring the steric bulk and electronic features of these groups, precise control over the reaction's enantioselectivity can be achieved [190].

Cu complexes also play a significant role in photoinduced asymmetric coupling reactions. In 2023, Song et al. reviewed the latest advances in Cu-catalyzed, photoinduced enantioselective coupling reactions (Fig. 8(a)), highlighting the unique advantages of Cu complexes in constructing C(sp^3)-C(sp^2) and C(sp^3)-N bonds [191]. By combining with chiral ligands, Cu complexes can effectively promote both radical generation and capture, leading to highly enantioselective cross-coupling reactions.

In asymmetric radical cross-coupling reactions, Cu complexes, in synergy with chiral ligands, efficiently enable the establishment of C(sp^3)-C(sp^2), C(sp^3)-C(sp^3), as well C(sp^3)-X (where X = O, N, etc.) bonds. For example, in 2024, Wang et al. successfully achieved the efficient conversion of various radical precursors (such as N-hydroxyphthalimide esters and malonimidates) via a photoinduced Cu-catalyzed strategy, synthesizing optically active compounds with high enantioselectivity (Fig. 8(b)) [192]. In this catalytic system, the Cu catalyst not only acts as a radical trap to stabilize highly reactive radical intermediates but also facilitates cascade multicomponent reactions through a photoinduced dual-functional catalytic mechanism. This innovative strategy significantly broadened the substrate scope of the reaction and successfully achieved efficient asymmetric functionalization of unsaturated systems such as alkenes, 1,3-dienes, and 1,3-enynes, offering a new method for the stereoselective synthesis of complex chiral molecules. Of particular importance, this study was the first to reveal the application of radical anions, generated via single-electron reduction of aromatic alkenes, in asymmetric cyanation reactions, further enriching the repertoire of synergistic photocatalytic and Cu-catalyzed reaction modes. The breakthrough contribution of this work lies in its use of a photocatalytic cooperative mechanism involving variable-valence Cu, which effectively addresses the long-standing challenges of controlling chemoselectivity and stereoselectivity in traditional radical reactions. These research achievements have not only significantly expanded the substrate scope for radical reactions but have also markedly improved reaction regioselectivity and stereoselectivity through the mild conditions enabled by photocatalysis.

Additionally, in the construction of C(sp^3)-N bonds, Cu-catalyzed radical coupling reactions offer a new pathway for

synthesizing chiral amines. Radical coupling reactions using Cu-based materials have been recognized for their mild reaction conditions, broad substrate scope, and excellent stereoselectivity. However, achieving high enantioselectivity and regioselectivity in such radical couplings remains a challenge, particularly when dealing with inactivated C(sp^3)-H bonds. Traditional Cu-catalyzed radical couplings often require pre-activated substrates or specific directing groups, which limits their application in the synthesis of complex molecules. Furthermore, the high reactivity of radical intermediates can lead to various side reactions, thereby reducing both selectivity and yield. Liu et al. achieved the efficient synthesis of various chiral amines via a Cu-based catalytic radical process. These reactions not only exhibit broad substrate compatibility but also leverage a photoinduced strategy to enable milder and greener reaction conditions (Fig. 8(c)) [193]. The core of this strategy lies in using visible light to excite the Cu catalyst, which promotes radical generation and chiral control, thereby efficiently constructing C(sp^3)-N bonds. Building on this, Yang et al. utilized a carefully designed Cu^+ catalyst and chiral ligands to efficiently synthesize products with divergent regioselectivities from the same set of starting materials, simply by adjusting reaction conditions such as ligand choice or solvent (Fig. 8(d)) [194]. For example, when a sterically bulky chiral bisphosphine ligand was used, the reaction predominantly yielded C(sp^3)-C(sp^3) coupled products (Fig. 8(e)). Conversely, employing a less hindered anionic cyanobisoxazoline ligand shifted the outcome primarily to C(sp^3)-N coupled products (Fig. 8(f)). This strategy of steering reaction pathways through ligand selection provides a novel conceptual framework for Cu^+-catalyzed radical coupling reactions. Taken together, the studies on *in-situ* generated Cu^+ complexes reveal a powerful and operationally simple strategy for photocatalysis: the direct coordination of Cu^+ salts with nucleophilic substrates or simple ligands to form photoactive species without pre-synthesis of stable complexes. The key advantage of this approach is its exceptional substrate compatibility and ease of use, enabling rapid screening of reaction conditions and expanding the accessible chemical space. Mechanistically, these systems operate through a common $Cu^+/Cu^{2+}/Cu^{3+}$ redox cycle, where the *in-situ* formed Cu^+-substrate complex acts as both the photosensitizer and the catalytic center. However, the very flexibility that enables this approach also presents challenges. The speciation of Cu complexes under reaction conditions is often poorly defined, complicating mechanistic studies and the rational optimization of catalysts. Furthermore, the stability of *in-situ* formed species varies widely depending on substrate and ligand choice, and catalyst decomposition or agglomeration remains a concern. Key design principles emerging from this body of work include: (i) the use of chelating ligands (e.g., BINAP, phenanthroline) to stabilize Cu intermediates even when added in situ; (ii) the importance of matching ligand electronics to the redox potential of the targeted transformation; and (iii) the potential of dual catalytic systems (e.g., Cu/photoredox) to overcome the limitations of single-catalyst approaches. Future research should focus on developing high-throughput screening methods to identify optimal *in-situ* catalyst formulations and on advancing spectroscopic techniques capable of characterizing transient Cu species under turnover conditions.

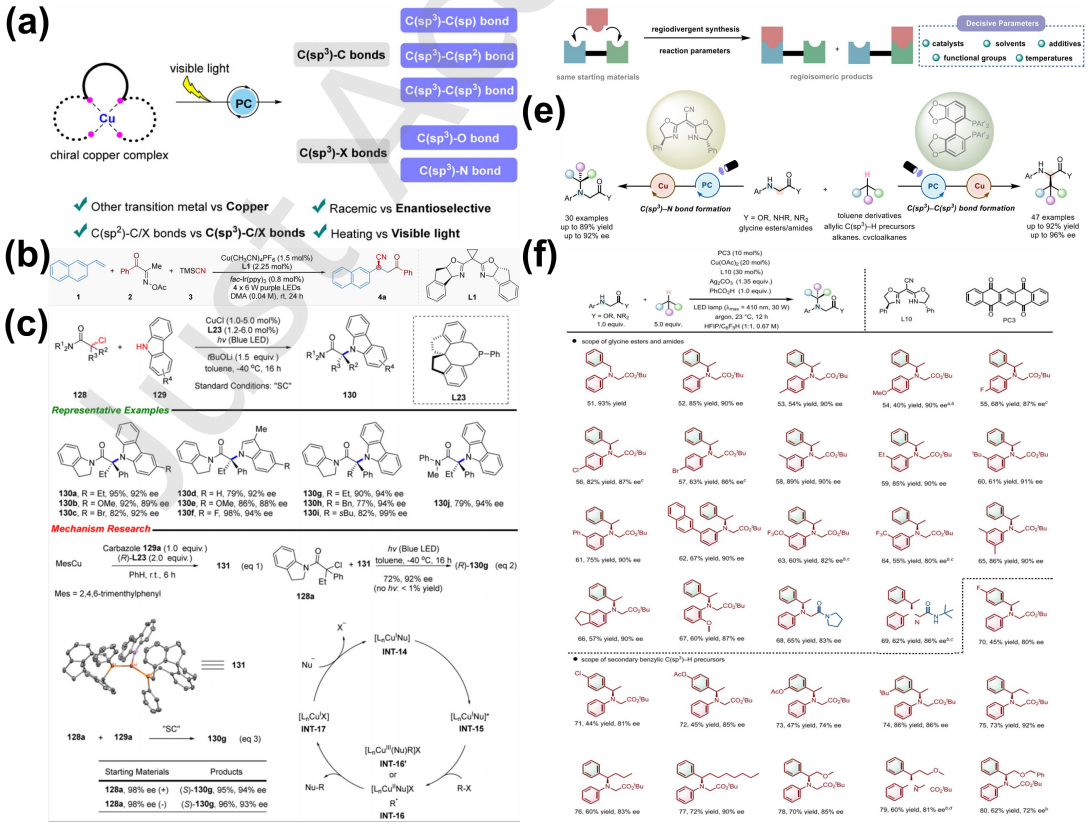

Figure 8 (a) Photocatalytic copper-catalyzed enantioselective coupling transformations. Reproduced with permission from Ref. [191], © RSC Publishing 2023. (b) Asymmetric three-component acylcyanation of alkenes enabled by dual photoredox and copper catalysis. Reproduced with permission from Ref. [192], © American Chemical Society 2024. (c) Efficient enantioselective C-N bond formation promoted by blue-light irradiation. Reproduced with permission from Ref. [193], © RSC Publishing 2024. (d) Influence of reaction parameters on steering regiodivergent synthetic outcomes. (e) Regiodivergent and enantioselective

transformations exhibiting regiodivergence and enantioselectivity. (f) Cu-catalyzed, light-mediated C(sp^3)-N coupling between glycine derivatives and benzylic C(sp^3)-H sources via photocatalytic conditions. Reproduced with permission from Ref. [194], © American Chemical Society 2025.

3.3 Heterogeneous catalysis by Cu^+

Photocatalysts are primarily classified into two categories based on their physicochemical properties and reaction system characteristics: homogeneous and heterogeneous photocatalysts. Homogeneous photocatalysts are typically dissolved in the reaction medium, ensuring excellent contact with reactants. They often exhibit high activity, selectivity, good reaction rates, and straightforward control. However, they suffer from drawbacks like poor stability and challenges in recovery [195,196]. For instance, some homogeneous photocatalysts based on precious metal complexes show outstanding catalytic efficiency in visible-light-driven organic synthesis. Yet, their tendency to undergo photodegradation or solvent-induced structural changes under light limits their feasibility for large-scale industrial use. Furthermore, the recovery process for homogeneous catalysts is often complex, requiring additional separation steps, which increases both cost and energy consumption.

In contrast, heterogeneous photocatalysts exist as solids, immobilized on supports by physical or chemical means, offering good stability and easy recyclability. Heterogeneous photocatalysts such as metal oxides (CuO, Cu_2O), metal sulfides (CuS), and covalent organic frameworks (COFs) are research hotspots in photocatalysis due to their advantages in visible optical harvesting and the effective carrier transfer and migration [197]. For example, incorporating a Cu-Xantphos complex (featuring a tetracoordinated Cu^+ geometry) into a crystalline porous COF yielded an efficient photocatalyst (Xant-Cu-BP_y). This material exhibits excellent activity, leveraging its high crystallinity, π-conjugated framework, and tunable pore structure to provide outstanding light absorption and efficient charge separation via concurrent energy and electron transfer [198]. Moreover, their immobilized nature allows for easy recovery post-reaction through simple filtration or centrifugation, reducing costs and enhancing process sustainability.

However, heterogeneous photocatalysts also have limitations. For example, some traditional semiconductor photocatalysts (like TiO_2) experience rapid carrier recombination and weak absorption in the visible light region. To overcome these shortcomings, researchers employ strategies such as constructing heterojunctions, doping, and surface modification to boost the behavior of heterogeneous photocatalysts.

Cu^+ has drawn widespread interest in heterogeneous catalysis because of its unique electronic structure and light absorption characteristics. Cu^+ compounds, such as Cu_2O and CuCl, have been extensively studied as photocatalysts for reactions such as water splitting, CO_2 reduction, and contaminant treatment [199]. Research indicates that the photoactivity of Cu^+ compounds depends on their surface properties, crystal structure, and electronic structure. For example, surface defects and oxygen vacancies can serve as active sites, promoting the adsorption and activation of reactants. Furthermore, by controlling the morphology and size of Cu^+ compounds, their light absorption capability and charge carrier transport efficiency can be optimized, leading to enhanced photocatalytic performance. For achieving better photoactivity of Cu^+, researchers have developed various modification strategies, including doping, surface modification, and constructing heterojunctions For instance, compositing Cu^+ compounds with semiconductor materials like TiO_2 or ZnO can effectively promote the separation and transfer of photogenerated charge carriers, suppress electron-hole recombination, and thereby increase photocatalytic activity [200]. Additionally, loading with noble metals can enhance both the light absorption capacity and electron transport efficiency of Cu^+. Given the unique electronic and photo-responsive nature of variable-valence Cu species (like Cu^0, Cu_2O, and CuO), which enables them to act as electron transfer mediators boosting carriers' have delved into the roles of different Cu valence states by constructing various heterojunctions (such as Z-scheme, S-scheme, and type-II heterojunctions).

For example, Cu_2O exhibits p-type material with narrow bandgap of approximately 2.2 eV, allowing it to efficiently absorb visible light. However, its photocatalytic activity in pure form is limited [201]. By forming a heterojunction, particularly a Z-scheme heterojunction, with an n-type semiconductor (like TiO_2), Cu_2O can significantly extend charges lifetimes and broaden the light-responsive range of the photocatalytic material [202]. In a study by Chen et al., researchers fabricated a three-dimensional monolithic TiO_2/Cu_2O foam photocatalyst using sacrificial templating and *in-situ* growth methods, constructing a Z-scheme heterojunction (Fig. 9(a)) [203]. The incorporation of Cu_2O not only broadened the catalyst's light response into the visible region but also, through its p-type semiconductor nature, formed an efficient Z-scheme heterojunction with n-type TiO_2, markedly promoting the separation and migration of photogenerated carriers. XPS analysis (Fig. 9(b)) confirmed the presence of Cu^+ in Cu_2O, which participates in redox reactions through valence state changes (Cu^+/Cu^{2+}) under illumination, effectively suppressing electron-hole recombination and thereby boosting catalytic activity. Additionally, the narrow bandgap of Cu_2O (~2.35 eV) enhances visible light absorption, while the three-dimensional porous structure of the Cu foam further optimizes gas-solid mass transfer efficiency. Under simulated sunlight and UV irradiation, the catalyst achieved toluene degradation rates of 90.2% and 58.6%, respectively, and retained 88% of its activity after four cycles, demonstrating excellent stability. ESR and radical trapping experiments identified ·OH and $·O_2^-$ as the primary active species for toluene degradation and elucidated the synergistic mechanism where Cu_2O acts as an electron transport mediator within the Z-scheme heterojunction. On another front, the form of Cu present (Cu^0, Cu^+, Cu^{2+}) significantly influences photocatalyst performance. Cu^+ promotes charge transfer dynamics by modulating the electronic structure. Studies show there is a dynamic equilibrium among the different Cu valence states, and this balance is continuously adjusted during photocatalysis to meet the demands of the reaction. As exemplified by Yan et al., they successfully prepared a cruciform-like mesoporous structure of Cu_2O/Cu/N-C (Fig. 9(c)) by etching a $HKUST^{-1}$ precursor [204]. The main contribution of this work lies in the construction of a Cu_2O/Cu/N-C heterojunction interface, which enabled efficient charge dynamics, leading to highly efficient photocatalysis for the homocoupling reaction of terminal alkynes. Through theoretical calculations and experimental

validation, the study demonstrated that the Cu_2O/Cu/N-C interface effectively separates photogenerated electron-hole pairs and promotes the formation of key intermediates and internal charge rearrangement. Specifically, the different work functions among Cu_2O, Cu, and the N-doped carbon layer (Fig. 9(d)) cause band bending downward at the interface, creating a built-in electric field. This built-in electric field not only drives the migration of photogenerated e^- from Cu_2O to the N-doped carbon layer but also significantly prolongs charge dynamics, thereby increasing photocatalytic efficiency. The Ebri's group successfully prepared a Cu_2O/Cu^0 composite photocatalyst via non-aqueous flow synthesis and optimized the synthesis conditions using design of experiments and response surface methodology [205]. They found that introducing Cu^0 effectively suppresses carriers recombination, while the formation of a Cu_2O/Cu^0 interface enhances charge separation efficiency, leading to a notable enhancement of photoactivity. Furthermore, the flow synthesis method not only enabled efficient continuous production of the catalyst but also allowed precise control over reaction parameters (like temperature, residence time, and precursor concentration) to tune the ratio of Cu_2O to Cu^0 (Fig. 9(e)-(f)), further optimizing the material's light absorption properties and stability. In summary, Cu^+-based heterogeneous photocatalysts, particularly Cu_2O and Cu^+-doped systems, offer distinct advantages in visible-light-driven reactions due to their narrow bandgap (~2.2 eV for Cu_2O) and p-type semiconducting properties. The central mechanistic insight across these studies is that the photocatalytic performance of Cu^+ is critically dependent on: (i) the formation of heterojunctions (Z-scheme, S-scheme, or type-II) with n-type semiconductors (e.g., TiO_2, ZnO, g-C_3N_4) to achieve efficient charge separation; (ii) the creation of internal electric fields at Cu^+/support interfaces that drive directional charge migration; and (iii) the dynamic Cu^+/Cu^{2+} redox cycling, which serves as a self-regulating electron-transfer mechanism. A key design principle emerging from this literature is that the spatial arrangement of Cu^+ sites and the engineering of interface defects are at least as important as the intrinsic electronic properties of Cu^+ itself. However, significant challenges remain. Cu^+ is inherently prone to oxidation and photocorrosion, leading to gradual deactivation under prolonged illumination. The trade-off between high Cu^+ loading (for enhanced light absorption) and charge recombination (at defect sites) is not well understood. Moreover, most studies focus on model reactions under idealized conditions; the performance of Cu^+-based heterojunctions in real-world applications (e.g., wastewater treatment, flue gas CO_2 reduction) remains largely unexplored. Future research should prioritize the development of protective strategies (e.g., coating with carbon layers or MOFs) that stabilize Cu^+ without blocking active sites, and the systematic evaluation of catalyst durability under continuous-flow, realistic operating conditions.

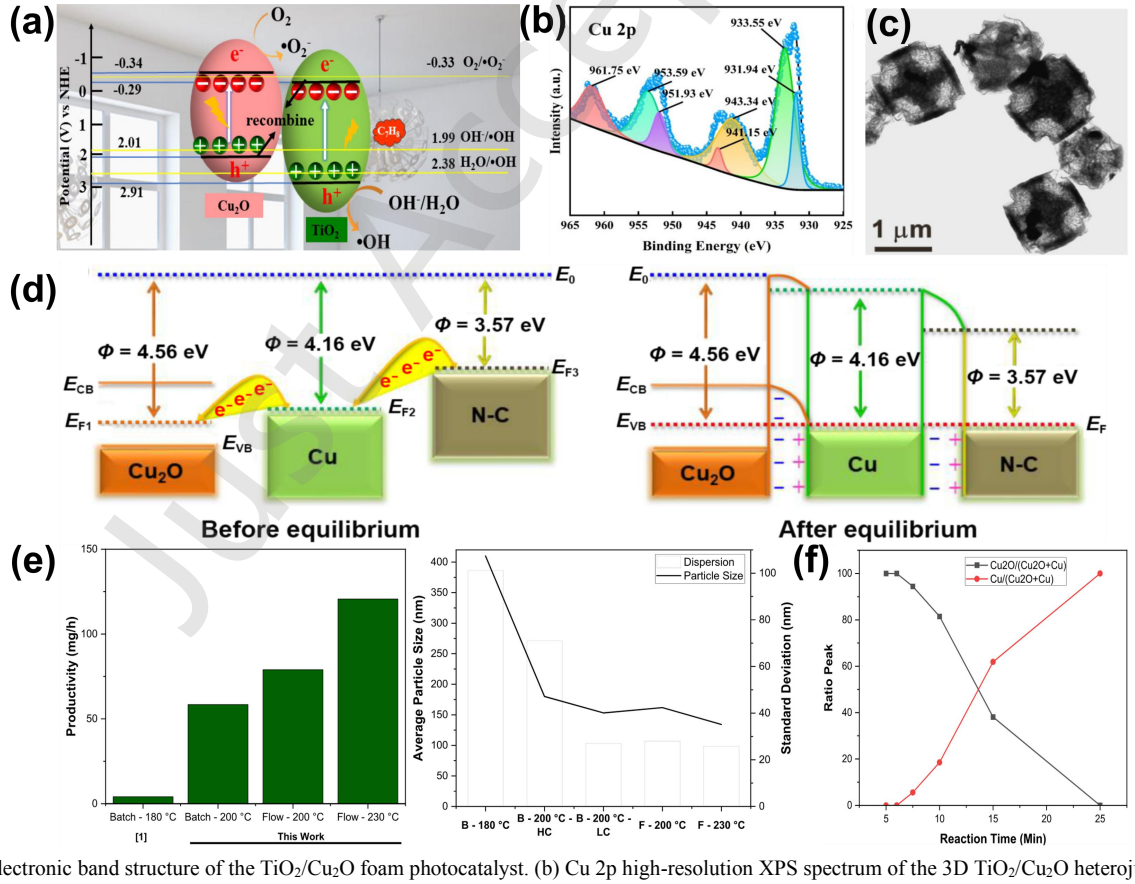

Figure 9 (a) Electronic band structure of the TiO_2/Cu_2O foam photocatalyst. (b) Cu 2p high-resolution XPS spectrum of the 3D TiO_2/Cu_2O heterojunction foam. Reproduced with permission from Ref. [203], © Springer Nature 2024. (c) Microstructure of cruciform-like mesoporous Cu_2O/Cu/NC revealed by SEM. (d) Energy band alignment diagrams of Cu_2O, Cu and N-doped carbon contacts. E_{CB} and E_{VB} represent conduction band minimum (CBM) and valence band maximum(VBM), respectively. Reproduced with permission from Ref. [204], © Tsinghua University Press 2024. (e) Comparative productivity in g/h for the batch process done at 180℃ done by Staniuk et al. [205] and batch and flow processes presented in this work. Average particle size and standard deviation of the particle size obtained for batch (B) and flow (F) syntheses done at different temperatures and different concentrations (HC = High concentration, LC = Low concentration). (f) Temporal evolution of the diffraction peaks corresponding to Cu_2O (36.4°) and Cu^0 (43.3°) at 202 ℃. Reproduced with permission from Ref. [206], © Elsevier B.V. 2024.

4 Visible-light excited Cu^{2+}

Beyond the MLCT-dominant photochemistry of Cu^{+} complexes discussed above, further investigations have explored the excited-state dynamics of Cu^{2+} species. Although studies on Cu^{2+} photocatalysis started relatively early, their excited-state mechanisms differ fundamentally from those of Cu^{+}. With a d^9 electron configuration, the excited state of Cu^{2+} typically involves LMCT, in contrast to the more common MLCT process observed for Cu^{+} [207]. This LMCT mechanism enables Cu^{2+} complexes to generate strongly oxidizing species under light, making them suitable for oxidation reactions and radical generation, thereby offering complementary reactivity to the SET-driven transformations favored by Cu^{+}. In recent years, as understanding of Cu^{2+} photochemistry has deepened, its application has gradually expanded across both homogeneous and heterogeneous catalytic systems, demonstrating unique advantages particularly in organic synthesis, environmental catalysis, and energy conversion [208–211].

Next, we will systematically elaborate on the research progress and application mechanisms of visible-light-excited Cu^{2+} from the perspectives of homogeneous and heterogeneous catalysis, respectively.

4.1 Homogeneous catalysis by photoexcited Cu^{2+}

In 1962, Kochi first discovered that $Cu^{2+}Cl_2$, under UV light, produces $Cu^{+}Cl$ and chlorine radicals (Cl ↺), marking the beginning of photocatalytic studies on Cu^{2+} compounds [212]. Generally, Cu^{+} complexes are prone to form MLCT states upon photoexcitation, whereas Cu^{2+} complexes, due to the lower-energy vacant orbitals of the Cu^{2+} center, tend to undergo LMCT states, which can oxidize electron-rich compounds. Cu^{2+} halides, $Cu^{2+}X_2$, can also be photoexcited to form an excited $[Cu^{2+}X_2]^*$ state, which can generate radicals via the LMCT process. Building on this concept, Wang and colleagues reported in 2024 a Keggin-structure-based Cu^{2+} complex, $(SiMo_{12}O_{40})[Cu(2,2'\text{-bipy})_2]_2 \cdot 2H_2O$. Their study demonstrated that the complex formed between Cu^{2+} ions and 2,2'-bipyridine ligands effectively absorbs light energy and degrades organic dyes through the extraction and migration of photoexcited carriers. This complex displayed decent behavior towards both photocatalytic treatment of methylene blue and electrocatalytic reduction of nitrite [213].

The photocatalytic reactions of Cu^{2+} complexes typically involve two mechanisms: SET and EnT. Under photoexcitation, Cu^{2+} complexes can generate highly reducing Cu^{+} species, which promote the activation and conversion of substrates. For instance, in Cu-catalyzed ATRA reactions, Cu^{2+} complexes generate radical intermediates by reducing the substrate, which then undergo addition to alkenes to yield the desired product. Additionally, Cu^{2+} complexes can facilitate reactions via an EnT mechanism, where the energy from their excited state is transferred to the substrate. In 2023, Reichle et al. prepared the photochemical assisted Cu-catalyzed bromonitroalkylation of alkenes, highlighting the crucial role of Cu^{2+} complexes in stabilizing and modulating radical intermediates [214]. Their study showed that Cu^{+} complexes like $[Cu(dap)_2]Cl$, upon photoexcitation, efficiently mediate the addition of bromonitroalkanes to alkenes, producing high-value 1,3-bifunctionalized products. EPR spectroscopy further revealed that the Cu complex interacts with the radical intermediates via an inner-sphere mechanism, suppressing the radical cyclization pathway and thereby enabling a highly selective ATRA reaction. This transformation is driven by the efficient interaction between Cu^{2+} and the radical intermediates, which can even outcompete the highly favorable cyclization from a transient to a persistent radical. EPR studies indicated that the reaction pathway under Cu catalysis is distinct from that under iridium catalysis; the Cu-catalyzed system effectively inhibits the radical cyclization process, leading to high product selectivity. In 2024, Zhou et al. investigated the role of silicon-doped carbon dots (SiCDs) in Cu-catalyzed atom transfer radical polymerization (photoATRP), uncovering the key function of Cu^{2+} complexes in photocatalytic polymerization [215]. Their research showed that e^- generated from photoexcited SiCDs can reduce Cu^{2+} to Cu^{+}, thereby initiating the ATRP reaction. This photocatalytic system not only exhibits a fast reaction rate but also demonstrates tolerance to oxygen, making it suitable for efficient polymerization in aqueous systems.

Cu^{+} complexes exhibit outstanding catalytic performance in photocatalytic organic synthesis. Their excited-state dynamics, ligand-tuning mechanisms, and reaction selectivity have been systematically studied across various systems. To further elucidate the structure-performance relationships of different Cu^{+} catalysts, this review summarizes representative homogeneous Cu^{+} photocatalyst systems from recent years (Table 1). This table includes their ligand types, preparation methods, photocatalytic conditions, reaction types, and performance metrics, offering a multi-dimensional reference for catalyst design and optimization.

Table 1 Summary of the properties and applications of homogeneous photocatalysts

Time	Catalysts	Preparation	Typology	Light	Purpose	Valence effect	Function	Synergy	performance	Ref.
2023	rac-BINAP-CuI-azide	Mixing rac- BINAP, $Cu(MeCN)_4BF_4$, and NaN_3 at room temperature.	Photoinduced three- component radical coupling.	450 nm blue LED.	Access to functionalized arylethylamines.	The Cu^{+}/Cu^{2+} cycle drives radical generation and C-N_3 coupling	Cu^{2+}- azide serves as an "electron sink" that suppresses charge recombination and enhances reaction efficiency	Ligands stabilize Cu^{+} and Cu^{2+} intermediates, preventing Cu aggregation or deactivation.	Synthesis of β- aryl ethylamine precursors in high yields (40-71%).	[150]
2021	Cu^{+}(dpp)	Cu+ salt	Photoind	30 W	Providing	Cu^{+}/Cu^{2+}	Cu^{2+}- BQA acts	Dual-Cu system	The yield	[149]

	$_2$ PF_6(dpp=2,9-diphenyl-^{1},10-phenanthroline)	coordinated with dpp ligand under inert conditions.	uced multicomponent radical coupling reaction.	CFL (visible light).	single-step access to β-arylethylamines	catalytic cycle.	as a nitrogen- group - transfer catalyst, capturing alkyl radicals to form C-N bonds.	synergistically separates radical generation and N-group transfer, avoiding side reactions.	of β- phenyl azides reached 81%.	
2025	CuCl/NaBArF	Mixed *in situ*.	Photoinduced Cu- catalyzed asymmetric C(sp^3)-H coupling.	12 W blue LED (395 nm).	The synthesis of alkenes and alkynes	Cu^{3+} eliminates to give product, returning to Cu^+ catalyst.	Cu^{3+} serves as a key intermediate, participating in C(sp^3)-H bond activation and carboxylic acid coupling.	Enhanced Cu electrophilicity promotes acid binding and radical capture.	Yields of 40-88% with high enantioselectivity (91:9-99: 1 er).	[133]
2025	Cu(dmp)(BINAP)]BF_4	Prepared by reacting Cu salts with ligands under an inert atmosphere.	ATRA reaction	Blue LED (λ_{max} = 455 nm).	Developing an efficient and selective β- chloroacylation method	The reaction involves a Cu^+/Cu^{2+} catalytic cycle.	Cu^+ is responsible for photoactivation and electron transfer, while Cu^{2+} handles chlorine transfer.	the dual- ligand environment (BINAP and dmp) separately optimizes the functions of Cu^+ and Cu^{2+}	Yields 37–99% with excellent regio- and stereocontrol.	[135]
2024	1- Naph - PTH (1- naphthylphenothiazine).	-	Transition- metal - catalyzed cross- coupling (perfluoroethylation).	Blue LED (450-470 nm typicall).	A photocatalytic hydrodefluorination of pentafluoroethylarenes	A Cu^+/Cu^{3+} catalytic cycle promotes the perfluoroethylation of C-I bonds.	Cu centers directly participate in C-CF_2CF_3 bond formation.	Releasing CF_2CF_3 groups to the Cu center.	Yield up to 92%.	[159]
2025	Cu^+ complexes of tetradentate phenanthroline ligands.	The complex was prepared by reacting the ligand with a Cu salt under an inert atmosphere.	ATRA reaction.	Blue LED (10 W, 467 nm).	Modifying ligand structure boosts photocatalytic performance.	Cu^+/Cu^{2+} redox via reductive quenching	Serves as an active site, participating in electron transfer processes.	Tetradentate ligands stabilize Cu and adapt to excited-state geometry changes.	Showed high selectivity in ATRA (17a:17b = 86:10).	[160]
2023	Cu(MeCN)$_4$PF$_6$	Cu(MeCN)$_4$PF$_6$ and BINAP were mixed in THF solvent.	Photoinduced Cu-catalyzed C(sp^3)-P bond formation reaction	20 W blue LED lamp (460 nm).	Photoinduced Cu- catalyzed C(sp^3)-P bond formation method	Cu^+/Cu^{2+} catalytic cycle to sustain catalyst activity in the cycle.	The Cu center acts as an active site in the reaction, participating in electron transfer processes.	BINAP enhances Cu photocatalysis and stabilizes intermediates by coordinating to Cu.	Efficient C(sp^3)-P bond formation capability with yields up to 80%.	[173]

2023	CuBr	Mixed *in situ*.	Photoinduced Cu- catalyzed N- alkylation reaction	Blue LED (460 nm).	Photoinduced Cu- catalyzed N- alkylation.	Cu^{+}/Cu^{2+} complete the catalytic cycle.	Serves as a charge transfer mediator, promoting radical generation.	Ligands synergistically stabilize intermediates and boost light absorption and electron transfer.	N- alkylation: 45–91% yields.	[174]
2024	Cu(dmp)(DPEPhos)BF_4	CuBr, dmp, and DPEPhos were mixed in solvent to form an active Cu- ligand complex.	Photoinduced Cu- catalyzed [2+2] cycloaddition reaction.	Blue LED (460 nm).	Photoinduced Cu- Catalyzed [2+2] Cycloaddition. method.	-	Charge transfer mediator.	-	Efficient [2+2] cycloaddition achieved with 38–90% yields.	[175]
2025	PC1: 2- Chloroanthraquinone, PC3: 5,7,12,14- pentacenetetrone.	-	Photoinduced asymmetric catalysis.	LED λ_{max} = 410/418 nm, 30/50 W.	Efficient regiodivergent, enantioselective C(sp^3)-H functionalization.	Cu catalysts ($Cu^{+}/Cu^{2+}/Cu^{3+}$) participate in redox cycles.	Complexes formed between Cu and chiral ligands are key to stereocontrol.	Cu catalysts control the stereoselective transformation of radicals.	C(sp^3)-C(sp^3): up to 92%; C(sp^3)-N: up to 93%.	[194]
2024	$(SiMo_{12}O_{40})[Cu(2,2'-bipy)_2]_2 \cdot 2H_2O$	Hydrothermal method.	-	100 W UV lamp (λ = 254 nm).	Degradation of organic dyes and electrocatalytic reduction of nitrite.	-	Cu^{2+}, whose d- d transitions enhance visible- light absorption.	Cu^{2+} catalyzes the decomposition of H_2O_2 to generate ·OH radicals.	Degradation of MB reached 99.2% within 36 min	[213]
2024	SiCDs	"Bottom- up" hydrothermal method.	Photocatalyzed atom- transfer radical polymerization (photoATRP).	Using blue (465 nm) or violet (405 nm) LED lamps.	Digital light processing (DLP) 3D printing.	-	Cu^{2+} serves as the active catalyst for ATRP.	SiCDs synergize with Cu catalysts ($CuBr_2$) to accelerate the $Cu^{2+} \rightarrow Cu^{+}$ conversion.	The reaction rate correlates with the bandgap width of SiCDs	[215]

In contrast to the MLCT-dominated photochemistry of Cu^{+}, Cu^{2+} complexes operate primarily through LMCT mechanisms under photoexcitation, generating strongly oxidizing radicals (e.g., Cl· from $CuCl_2$) or undergoing reduction to Cu^{+}. The key mechanistic insight across the reviewed studies is that Cu^{2+} photocatalysis is particularly well-suited for oxidative transformations and for reactions requiring the generation of high-energy radicals. A common design principle is the use of LMCT-active ligands (e.g., halides, carboxylates, or bipyridine derivatives) that facilitate efficient light absorption and radical formation. Compared to Cu^{+} systems, Cu^{2+} photocatalysis offers complementary reactivity, especially in ATRA reactions, polymerization, and pollutant degradation, where the oxidizing power of the LMCT state is advantageous. However, several challenges persist. The excited-state lifetimes of Cu^{2+} complexes are generally shorter than those of Cu^{+} analogues, limiting their efficiency in bimolecular quenching steps. The mechanisms of Cu^{2+} photocatalysis are often less well understood than those of Cu^{+}, in part due to the paramagnetic nature of Cu^{2+}, which complicates spectroscopic characterization. Furthermore, the tendency of Cu^{2+} to disproportionate or form insoluble species under reaction conditions can lead to catalyst deactivation. Key design principles emerging from recent work include: (i) the use of cooperative photoredox-copper dual catalysis to combine the strong oxidizing power of Cu^{2+} LMCT with the reducing power of conventional photocatalysts; (ii) the incorporation of Cu^{2+} into rigid ligand frameworks or solid supports to prevent deactivation; and (iii) the tuning of ligand field strength to modulate LMCT energies and redox potentials. Future research should focus on extending the temporal resolution of spectroscopic methods to capture Cu^{2+} LMCT dynamics and on developing Cu^{2+}-based systems for solar-driven oxidation

reactions, including water oxidation and organic pollutant mineralization.

4.2 Heterogeneous catalysis by photoexcited Cu^{2+}

In heterogeneous photocatalytic systems, changes in the valence state of Cu are not only closely tied to the transfer of photogenerated charge carriers and the reaction process but are also influenced by the catalyst's composition, structure, and reaction conditions. For instance, introducing other metal or non-metal elements into Cu-based photocatalysts can modulate the distribution of Cu valence states, thereby optimizing photocatalytic performance [216]. Studies have found that appropriate doping can promote the balanced interconversion between Cu^0 and Cu^+, enhancing both the activity and stability of the photocatalyst. Moreover, by controlling synthesis conditions such as temperature, pH, and reaction time, the ratio of Cu valence states can be tuned, enabling fine control over photocatalytic performance [217,218]. As a dopant, Cu can broaden the absorption threshold of photocatalysts into visible range through forming dopant states above the valence band, induced by its 3d orbitals.

In recent years, researchers have employed a combined experimental and theoretical approach to deeply investigate the interactions among different Cu valence states in photocatalysts and their impact on photocatalytic performance [219]. For example, using *in-situ* spectroscopic techniques like X-ray photoelectron spectroscopy and UV-vis absorption spectroscopy to monitor real-time changes in Cu valence states during photocatalysis has revealed the dynamic transformation mechanisms of these states [220]. Simultaneously, theoretical calculations, such as density functional theory, have provided crucial support for understanding how changes in Cu valence affect photocatalytic reaction pathways and energy barriers.

With respect to heterogeneous reaction, the doping of Cu and the influence of its different valence states on photocatalyst performance have become a major research focus. Cu possesses multiple valence states (e.g., Cu^0, Cu^+, Cu^{2+}) that play distinct roles in photocatalysis. Their complex interconversion relationships significantly affect the separation and migration of photogenerated charge carriers as well as catalytic activity. In a study published by She et al., an efficient photocatalytic CO_2 reduction catalyst was prepared by co-doping Cu and N into carbon-modified TiO_2 via high-temperature pyrolysis (Fig. 10(a)) [221]. They found that introducing Cu not only optimized the catalyst's electronic structure, promoting carrier dynamics, but also significantly enhanced CO_2 adsorption capacity. Density functional theory (DFT) calculations indicated that Cu and N co-doping lowered the ΔG for the CO_2 reduction reaction (Fig. 10(b)), thereby facilitating the reaction. Furthermore, the study found that the form of Cu present (e.g., Cu^0 and Cu^{2+}) significantly impacted catalyst performance. The presence of Cu^{2+}, likely due to the formation of Cu-N_x sites during pyrolysis, was found to aid in improving the catalyst's photogenerated charge carrier separation efficiency. Additionally, charge transfer between different metals can reduce the bandgap and enhance photocatalytic performance. In another study by Shi et al., researchers doped Cu^{2+} into $ZnIn_2S_4$ to construct a Si quantum dots (SiQDs)/Cu-doped $ZnIn_2S_4$ (Cu_xSZ) heterojunction photocatalyst for overall water splitting [222]. They found that doping with Cu^{2+} increased the electron density around S atoms in $ZnIn_2S_4$, thereby promoting the water reduction reaction. Moreover, by partially substituting Zn atoms, the introduction of Cu^{2+} altered the electronic structure of $ZnIn_2S_4$, lowering the energy barrier for the water oxidation reaction (OER) (Fig. 10(c)). Experimental results showed that Cu^{2+} doping significantly improved the overall water splitting performance of the photocatalyst, achieving efficient H_2 and O_2 production rates.

In the field of CO_2 RR, the valence changes in Cu-based catalysts (e.g., Cu^+/Cu^{2+}) play a key role in regulating reaction pathways and intermediate adsorption, demonstrating remarkable performance. Xu et al. reported a Cu-alkynyl coordination polymer (CA-CP) [223]. By constructing an amphiphilic heterojunction with iodine vacancy-rich $BiOCl_xBr_yI_{1-x-y}$(IV-BX) (Fig. 10(d)), they achieved efficient photocatalytic CO_2 reduction. Their study found that the Cu-alkynyl units (ADCAUs) in CA-CP serve as active sites for CO_2 adsorption and activation, exhibiting high selectivity. Furthermore, the amphiphilic structure not only promoted H_2O dissociation and proton supply but also improved photogenerated charge carrier separation efficiency via a Z-scheme charge transfer mechanism, leading to a significant boost in CO_2 photoreduction activity. The major contribution of this work lies in revealing the unique mechanistic role of Cu-based coordination polymers in CO_2 photoreduction and providing new insights for designing efficient CO_2 photoreduction catalysts (Fig. 10(e)). In another 2025 study, Xu et al. constructed a 3D Cu cluster covalent organic framework (COF), which stabilized Cu^+ cluster units through covalent linkages. This design significantly lowered the formation energy barrier for the *COOH intermediate, thereby enhancing CO_2 reduction efficiency (Fig. 10(f)) [224]. These studies not only highlight the central role of Cu's variable valence in photocatalysis but also, through precise control of Cu's coordination environment and electronic structure, provide new ideas for designing efficient and stable photocatalysts. Their key contribution lies in optimizing Cu active sites through atomic-level design and interface engineering, providing an important theoretical and experimental foundation for CO_2 resource utilization.

In heterogeneous systems, Cu^{2+} species function predominantly as dopants or as components of mixed-oxide semiconductors (e.g., CuO). The reviewed studies converge on several key mechanistic findings. First, Cu^{2+} doping introduces impurity energy levels within the bandgap of host semiconductors (e.g., TiO_2, $ZnIn_2S_4$, g-C_3N_4), thereby extending visible-light absorption. Second, the Cu^{2+}/Cu^+ redox couple acts as a charge-transfer mediator, facilitating electron–hole separation and migration to surface active sites. Third, the presence of Cu^{2+} can stabilize oxygen vacancies or create Lewis acid sites that enhance CO_2 adsorption and activation. Common design principles include: (i) optimal dopant concentrations typically lie in the range of 1–5 mol%, above which Cu^{2+} sites become recombination centers; (ii) the formation of Cu–N_x or Cu–C_x coordination environments (e.g., in Cu–N–C materials) enhances Cu^{2+} stability and electron transfer; and (iii) the combination of Cu^{2+} doping with heterojunction construction (e.g., Z-scheme or type-II interfaces) yields synergistic improvements in charge separation. Despite these advances, unresolved challenges remain. The dynamic behavior of Cu^{2+}

under photocatalytic conditions, particularly its potential reduction to Cu^{+} or Cu^{0}, is poorly understood, and *in-situ* tracking of Cu oxidation states during turnover is rarely performed. The long-term stability of Cu^{2+} dopants against leaching or segregation is a concern for practical applications. Furthermore, the structure–activity relationships for Cu^{2+}-catalyzed CO_2 reduction are less developed than those for Cu^{0} and Cu^{+} systems. Future research should prioritize operando X-ray absorption spectroscopy and electron paramagnetic resonance studies to correlate Cu^{2+} electronic structure with catalytic performance, and the development of durable Cu^{2+}-doped photocatalysts for continuous-flow CO_2 reduction and water treatment.

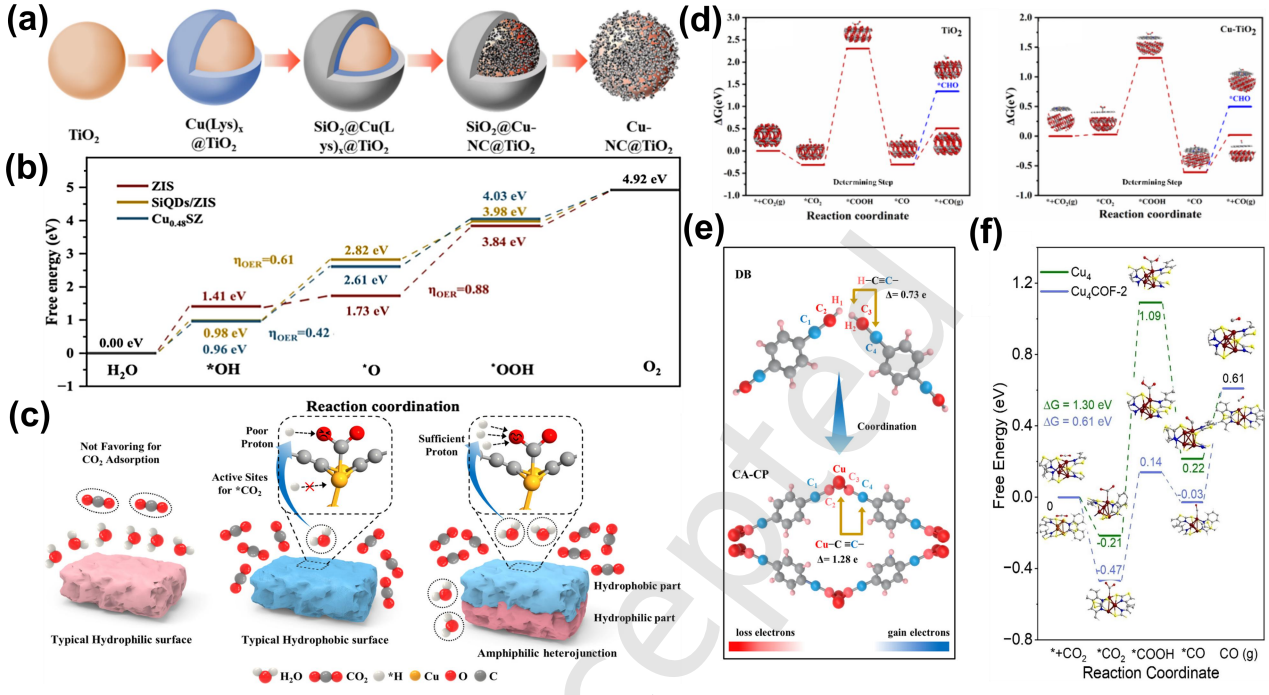

Figure 10 (a) Preparation pathway for the Cu-NC@TiO_2 composite photocatalyst. (b) Proposed mechanism of the photocatalytic CO_2-to-CO reduction by Cu-NC@TiO_2. Reproduced with permission from Ref. [221], © Elsevier B.V. 2024. (c) Comparative OER performance of ZIS, SiQDs/ZIS and $Cu_{0.48}SZ$. Reproduced with permission from Ref. [222], © Elsevier B.V. 2024. (d) Structural diagrams of representative hydrophilic, hydrophobic (CA-CP), and amphiphilic (CA-CP/IV-BX) heterojunction photocatalysts. (e) Atomic charge distribution analysis for DB and CA-CP interfaces, where positive and negative values indicate charge accumulation and depletion, respectively. Reproduced with permission from Ref. [223], © Elsevier B.V. 2024. (f) Free-energy profiles for the photoreduction of CO_2 to CO on Cu and CuCOF-2. Reproduced with permission from Ref. [224], © Wiley-VCH GmbH 2025.

4.3 Cooperative photoredox- Cu dual catalysis

Cu's multiple accessible oxidation states allow it to serve as an active center in diverse chemical catalytic reactions, which can proceed via either single-electron or two-electron pathways. Cu^{0} can function as an active site, directly participating in photocatalytic reactions, whereas Cu^{+} and Cu^{2+} promote carrier dynamics by modulating the electronic structure [225].

In a homogeneous environment, Cu^{+} complexes typically act as photosensitizers, efficiently transferring e^{-} to substrates upon photoexcitation to generate radical intermediates. These radical intermediates can then participate in further reactions, enabling the transformation of the substrate [226]. For example, in Cu-catalyzed ATRA reactions, Cu^{+} complexes can efficiently reduce alkyl halides to radicals upon photoexcitation; these radicals then add to alkenes to yield the desired product. This reaction mechanism not only avoids side reactions common in traditional thermally initiated radical chain processes but also significantly enhances both the selectivity and yield of the reaction. Cu^{2+} complexes, on the other hand, play a different role in photocatalysis. Due to its higher oxidation state, Cu^{2+} can act as an electron acceptor, working in synergy with Cu^{+} complexes to achieve radical regeneration and sustain the catalytic cycle. For instance, in some photocatalytic oxidation reactions, Cu^{2+} complexes can capture radical intermediates and convert them into the target product through a redox cycle. This synergistic interaction not only improves reaction efficiency but also minimizes the accumulation of radical intermediates, thereby reducing the likelihood of side reactions [227].

Furthermore, owing to Cu's favorable persistent radical effect, the radical intermediates generated during photoinduced catalysis are selectively captured at metal active sites. The as-obtained Cu intermediates possess significant reactivity potential. In recent years, many researchers have begun combining Cu^{+} or Cu^{2+} salts with traditional rhodium- or iridium-based photocatalysts to achieve cooperative catalysis. This synergistic catalytic mechanism not only enhances the efficiency and selectivity of photocatalytic reactions but also provides important theoretical guidance and practical direction for developing new photocatalytic systems. The proposed reaction mechanism involves the following key steps: (1) The electrophile undergoes single-electron reduction via an external photocatalyst (e.g., Rh- or Ir-based) to generate the primary radical R_1 ↻; (2) The high-valent external catalyst is proposed to oxidize the Cu^{+} complex to a Cu^{2+}complex, $Cu^{2+}L_n$; (3) $Cu^{2+}L_n$ undergoes ligand exchange with an anionic nucleophile to form a $Cu^{2+}L_{(n}{}^{-1)}Nu$ intermediate; (4) This $Cu^{2+}L_{(n}{}^{-1)}Nu$ species captures the primary radical R_1 ↻ to generate a high-valent transient intermediate, $Cu^{3+}R_1L_{(n}{}^{-1)}Nu$; (5) Finally, $Cu^{3+}R_1L_{(n}{}^{-1)}Nu$ undergoes reductive elimination to yield the coupled product and regenerate the initial Cu^{+} catalyst [228].

For example, Wang et al. prepared the visible-light-induced, Cu-catalyzed asymmetric three-component reaction. By employing a chiral bisoxazoline ligand, the Cu complex achieved high enantioselectivity in a radical coupling reaction [229]. The key to this stereoselective control lies in the formation of a Cu^{3+} complex (Fig. 11(a)). The synergistic action of Cu^{+} and Cu^{2+} allows the reaction to proceed under mild conditions with high enantioselectivity. In this process, photoexcited Cu^{+} generates Cu^{2+}, which then combines with a radical intermediate to form a stable Cu^{3+} complex. Subsequent reductive elimination yields the target product (Fig. 11(b)). This sequence showcases the cooperative catalysis of Cu complexes across different valence states, highlighting their crucial role in both radical generation and capture.

In heterogeneous environments, the variable valence nature of Cu also enables it to promote the production of reactive oxygen species (ROS), including ·OH and $·O_2^-$, through redox reactions (e.g., Cu^{+}/Cu^{2+}) during photocatalysis, thereby accelerating pollutant degradation. A major contribution of these studies is the rational design of Cu-based heterojunction photocatalysts, which addresses issues like low quantum efficiency and narrow spectral response in traditional photocatalysts, offering new strategies for the efficient degradation of volatile organic compounds (VOCs), among others. Zoric et al. investigated the contribution of Cu to unassisted CO_2 conversion [230]. They found that under reaction conditions, Cu primarily exists as oxides, hydroxides, and carbonates of Cu^{+} and Cu^{2+}, rather than as metallic Cu (Fig. 11(c)). Under operational photocatalytic conditions, Cu^{+} is further oxidized to Cu^{2+}, indicating the transfer of photogenerated h^{+} from Au to Cu (Fig. 11(d)). This finding suggests that within bias-free gas-phase environments, Cu exists in oxidized carbonates-enriched forms. Upon cooperating with plasmonic Au, it acts as an oxidative center, potentially enabling a new avenue towards water oxidation. The variable valence characteristic of Cu also allows it to facilitate to form ROSs (·OH and $·O_2^-$) via redox reactions (such as Cu^{+}/Cu^{2+}) during photocatalysis, speeding up the degradation of pollutants. The key contribution of these works lies in the rational design of Cu-based heterojunction photocatalysts, which tackles problems like low quantum efficiency and limited spectral response in conventional systems, offering novel approaches for efficient VOCs degradation and antibacterial applications. In the field of antibacterial photocatalysis, Cu-based materials have been intensively explored because of the excellent antimicrobial nature. For instance, Li et al. reported a composite coating based on 2D g-C_3N_4/Cu_2O/Cu [231]. By constructing an S-scheme heterojunction structure (Fig. 11(e)), they significantly enhanced the photocatalytic antibacterial performance. The presence of Cu improved the carrier dynamics, whilst promoted charge transfer through forming an intrinsic electric field, leading to highly effective antibacterial outcomes (Fig. 11(f)). Additionally, the antioxidant properties of Cu suppressed the photocorrosion of Cu_2O. The synergy among different Cu valence states further enhanced the coating's stability and long-term antibacterial durability, presenting a promising metallic option for protecting metal materials against microbial corrosion. These studies provide both theoretical support and experimental evidence for the application of Cu-based photocatalytic materials in environmental purification and antimicrobial fields.

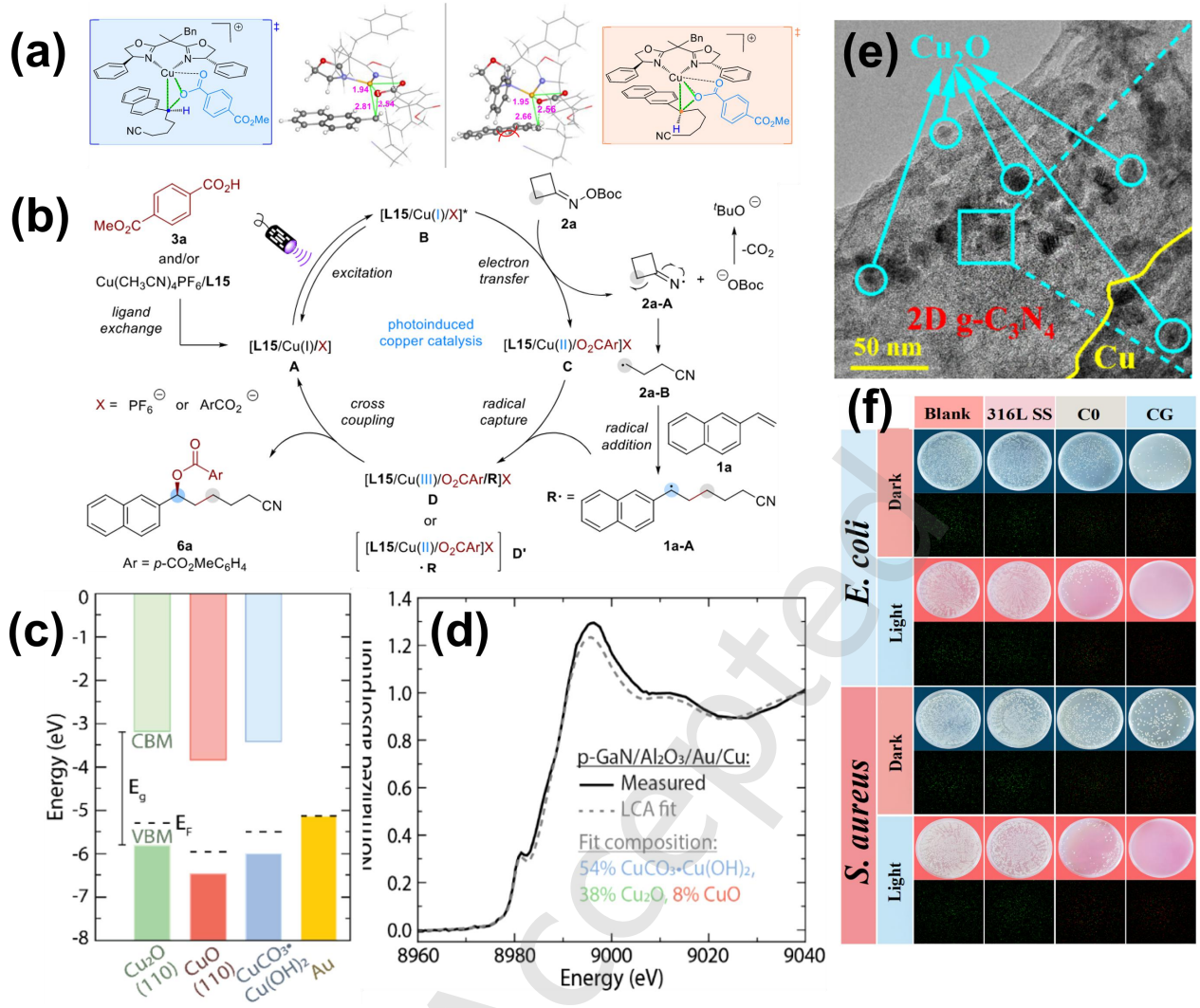

Figure 11 (a) Transition-state structures governing enantioselective carbon-oxygen bond formation. (b) Proposed catalytic cycle underlying the Cu-catalyzed photo-ATRA reaction. Reproduced with permission from Ref. [229], © American Chemical Society 2022. (c) Linear combination analysis (LCA) fitting of Cu K-edge XANES spectra for as-prepared p-GaN/Al_2O_3/Au/Cu. (d) DFT-calculated band alignments for various Cu oxide phases on Au. CBM, VBM and Fermi level (E_F) are indicated for Cu_2O, using literature values for bandgaps and ionization potentials. Reproduced with permission from Ref. [230], © American Chemical Society 2024. (e) Transmission electron microscopy (TEM) image of CG. (f) Antibacterial activity assessment of synthesized samples against planktonic E. coli and S. aureus. Reproduced with permission from Ref. [231], © Elsevier B.V. 2024.

5 Coordination-Environment-Engineered Cu-Based Photocatalysts

Building upon the fundamental understanding of Cu^0, Cu^+, and Cu^{2+} photocatalysis, researchers have in recent years developed a series of more structurally complex and functionally diverse heterogeneous Cu-based photocatalytic materials that extend beyond conventional single-valence-state systems. These emerging platforms integrate Cu species with supports such as polymer ligands, metal-organic frameworks [232], or single-atom carriers [233,234]. This integration not only preserves the variable valence characteristics and photocatalytic activity of Cu but also significantly enhances material stability, recyclability, and adaptability to specific reactions. Consequently, these architectures offer unique advantages in stability, recyclability, and active site engineering, representing a promising direction for the further development of Cu-based photocatalysis. These heterogeneous catalysts exhibit excellent performance in visible-light-driven organic synthesis, CO_2 RR, pollutant degradation, and HER, establishing themselves as an emerging direction in Cu-based photocatalysis research [235,236]. To comprehensively compare the performance characteristics of different heterogeneous systems, this review consolidates key parameters (Table 2) of representative heterogeneous Cu-based photocatalysts, encompassing band structure, synthesis methods, photocatalytic conditions, and performance metrics. This compilation provides systematic data support and design guidance for future research.

In the following sections, we will systematically introduce the design strategies, structural features, and application progress in photocatalysis of these novel heterogeneous Cu-based photocatalysts, covering three main categories: polymer ligand-based photocatalysts, MOF-based photocatalysts, and SACs.

Table 2 Summary of the properties and applications of heterogeneous photocatalysts

Time	Catalysts	Dopant	Band structure	Preparation	Typology	Light	Purpose	Synergy	Performance	Ref.
2024	Three-dimensional monolithic TiO_2/Cu_2O foam	-	TiO_2:3.20 eV;Cu_2O:2.35 eV	Sacrificial template method and *in situ* growth method.	Z-scheme heterojunction.	Xe lamp (500 W) / UV lamp (15 W).	VOC degradation.	Cu_2O and TiO_2 synergistically broaden the light absorption range of the photocatalyst.	3D TiO_2/Cu_2O heterojunction foam outperforms pure TiO_2 and Cu_2O in toluene degradation.	[203]
2024	Cu_2O/Cu(Cu_2O/Cu/N-C)	Nitrogen doping.	Different work functions of Cu_2O, Cu, and N-C cause band bending at their interface.	The precursor was prepared by solvothermal reaction, then etched and annealed.	Ternary heterojunction.	Blue light(λmax=400 nm)	Driving organic reactions: photocatalytic terminal alkyne coupling.	Built-in field and band bending help separate and move charges.	The yield of photocatalytic coupling of terminal alkynes over Cu_2O/Cu/N-C is nearly tenfold that of pure Cu_2O.	[204]
2024	Cu-NC@TiO_2	Co-doping with Cu and N.	Conduction band from Cu,N-C; valence band from TiO_2.	SiO_2 coating, high-temperature pyrolysis, and solution etching to remove SiO_2.	-	A 300 W xenon lamp.	Photocatalytic CO_2 reduction.	Cu/N co-doping enhances conductivity and optimizes electronic structure.	The CO production rate reached 46μmol$g^{-1}h^{-1}$, while the CH_4 production rate reached 2.9 μmol$g^{-1}h^{-1}$.	[221]
2024	Composite of SiQDs and Cu-doped $ZnIn_2S_4$	Cu doping and introduction of SiQDs.	The band gap of $Cu_{0.48}$SZ is 2.86 eV.	Sol-gel method.	Z-scheme heterojunction.	300 W Xe / 420 nm LP filter.	Photocatalytic overall water splitting.	-	The production rates of H_2 and O_2 were 210 μmol·$g^{-1}h^{-1}$ and 97 μmol$g^{-1}h^{-1}$, respectively.	[222]
2025	CA-CP	Iodine vacancies.	The optical band gap (Eg) of CA-CP is 1.89 eV.	300 °C makes I vacancies and heterostructure, then CH_3OH builds amphiphilic junction via charge..	Amphiphilic heterojunction.	300 W Xe (λ ≥ 420 nm).	Photocatalytic CO_2 reduction.	Z-scheme heterojunction with IVV-BX reduces e-/h^+ recombination.	A CO production rate of 157.6 μmol$g^{-1}h^{-1}$	[223]
2025	Cu_4COFs	-	Band gap of 1.92 eV.	Cu_4-NH_2 clusters were synthesized, then covalently linked with organic linkers to form Cu_4COFs stepwise.	-	Under a pure CO_2 atmosphere, using visible light (λ ≥ 420 nm).	Photocatalytic CO_2 reduction.	-	Cu_4COF-2 demonstrated a high CO production rate (23.8 μmol$g^{-1}h^{-1}$) with CO selectivity of 94.3%.	[224]
2024	Composite coating of 2D g-C_3N_4/Cu_2O/Cu	-	The band gap width is 1.86 eV.	-	S-scheme heterojunction.	300 W Xe (400 nm filter).	Photocatalytic antibacterial performance.	Forming an S-scheme heterojunction between Cu_2O and 2D g-C_3N_4.	An antibacterial rate of 100% was achieved.	[231]

2024	CuSAs@PCN@UiO	Single-atom Cu doping.	CuSAs@PCN: band gap of 2.37 eV.	Precursors loaded into D-UiO mesopores, followed by low-temperature pyrolysis to form a hollow structure.	II scheme heterojunction.	Visible light (λ ≥ 420 nm).	Photocatalytic conversion of CO_2 to CH_3OH.	Synergizing with the UiO-66-NH_2 shell, CuSAs@PCN provides catalytic sites.	A CH_3OH production rate of 4.15 $mmolg^{-1}h^{-1}$ surpass most MOF and carbon nitride benchmarks	[116]
2023	Cu@Xantphos@ASMNPs	Xantphos as dopant.	-	Co-precipitation followed by the sol-gel method to prepare DAFO@ASMNPs, stirred at room temperature.	-	A 20 × 2 W white LED lamp.	Visible-light-driven cross-dehydrogenative coupling reaction.	Synergistic interaction between Cu, Xantphos ligands, and DAFO ligands.	The target product was synthesized in up to 93% yield.	[239]
2023	PL-MOF-di-Cu	Diphenylphosphine coordination doping.	In the visible light region (400-470 nm).	Solvothermal synthesis followed by ligand exchange immobilizes Cu on MOF.	-	Blue LED lamp (427 nm).	Hofmann-Löffler-Freytag reaction and C(sp^3)-H amination reaction.	Synergistic interaction between Cu, binap ligands, and the MOF matrix.	The target product was synthesized in up to 99% yield.	[240]
2024	MIL-53(Fe);NH_2-MIL-53(Fe)	Ligand modification.	MIL-53(Fe):2.61 eV;NH_2-MIL-53(Fe):1.66 eV	Solvothermal synthesis.	Semiconductor-biomolecule heterojunction.	Visible light (λ > 420 nm) or simulated sunlight (λ > 290 nm), using LEDs or xenon lamps.	Photocatalytic tetracycline degradation.	MOF protects laccase from photodamage, while laccase enhances the charge separation efficiency of MOF.	The degradation rate of tetracycline (TC) reached 78.87% for NH_2-MIL-53(Fe)/Lac.	[243]
2025	Pt@NH_2-UiO-66@Cu-TCPP	Embedded doping with Pt nanoparticles.	The band gap of Pt@NH_2-UiO-66 (PU) is 2.73 eV; Cu-TCPP: band gap of 3.01 eV.	-	Cascade Z-scheme heterojunction.	A 300 W xenon lamp equipped with a 400 nm cut-off filter.	Photocatalytic CO_2 reduction.	Cu and Pt@NH_2-UiO-66 formed a Z-scheme heterojunction, enhancing the built-in electric field.	CO production rate under visible light (40.2 $\mu molg^{-1}h^{-1}$)is 11.6 and 7.0 times higher than pristine NH_2-UiO-66 and Cu-TCPP, respectively	[244]
2022	CuSA-TiO_2	Single-atom Cu doping.	The band structure primarily depends on the characteristics of TiO_2.	Cu@TiO_2 via MIL-125 calcination.	-	A 300 W xenon lamp equipped with a 400 nm cut-off filter.	Photocatalytic hydrogen production	The strong interaction between single-atom Cu and TiO_2 can enhance the stability of Cu.	The H_2 evolution rate (101.7 $mmolg^{-1}h^{-1}$) is 24 times that of pristine TiO_2.	[250]

2023	Cu-SAEB	Modification with CuSAs	-	Cu_1/MS was first prepared by photoreduction of MoS_2 with Cu species, then 15 wt% Cu_1/MS was coated onto MIL and hydrothermally treated to obtain Cu-SAEB.	Z-scheme charge transfer pathway.	Simulated sunlight irradiation.	Photocatalytic CO_2 reduction.	-	The CO production rate reached as high as 236.0 μmol$g^{-1}h^{-1}$	[251]
2023	Single-atom Cu-bridged carbon nitride(C_3N_4)sheets	Nitrogen vacancies.	-	Calcination (600–620 °C) of Cu/monomer co-assembled within C_3N_4 interlayers yields the target photocatalyst.	-	A 300 W xenon lamp with an average light intensity of 200 mW/cm^2	Photocatalytic hydrogen production.	Strong Cu–C_3N_4 interaction and nitrogen vacancies synergistically promote photogenerated charge separation and transport.	The H_2 evolution rate reached 11.23 mmol $g^{-1}h^{-1}$	[252]

5.1 Polymer ligand-based photocatalysts

The variable valence nature of Cu and the diversity of ligands not only enrich the structures of Cu-based catalysts but also allow for precise tuning of the redox potentials of photoexcited Cu complexes. This fine-tuning is critical to photoactivity of photoactive Cu complexes [237]. Consequently, frameworks based on polymer ligands have attracted widespread attention.

For example, Zhang's group reported a Cu^+-based photocatalyst fabricated by coordinating and polymerizing triphenylamine (TPA) [238]. By introducing bulky substituents at the ortho-position of the ligand, they distorted the conjugation between TPA and the Cu^{2+}-carboxylate node (Fig. 12(a)). This Cu^+ photocatalyst effectively suppressed the fluorescence quenching of the photosensitizer's excited state by Cu^{2+}, thereby improving photocatalytic efficiency. This demonstrates the critical role of the ligand microenvironment in stabilizing specific Cu oxidation states. Electrochemical impedance spectroscopy (EIS) showed that carrier migration resistance of the distorted catalyst (Cu-Twisted) was about three times greater than that of the planar analogue (Cu-Planar) (Fig. 12(b)). EPR spectra further confirmed that the Cu^{2+} signal in Cu-Twisted remained largely unchanged after illumination, whereas it decreased significantly in Cu-Planar (Fig. 12(c)), providing direct evidence that the distorted structure effectively inhibits Cu^{2+}-mediated fluorescence quenching. Building on this, Rana's group further explored the structure-performance relationship of Cu in photocatalysis [239]. They constructed a Cu-based heterojunction photocatalyst, Cu@Xantphos@ASMNPs, which enabled the photocatalytic conversion of aromatic tetrahydroisoquinolines to their corresponding iminium ion precursors (Fig. 12(d)). This catalyst significantly boosted photoactivity via expediting electron migration from Cu^+ to the substrate under visible light. This catalyst significantly enhanced photocatalytic efficiency by facilitating electron transfer from Cu^+ to the substrate under visible light.

Researchers from Ben's group constructed an efficient heterojunction photocatalyst (PL-MOF-di-Cu) by embedding Cu^+ dimers into a MOF [240]. X-ray photoelectron spectroscopy analysis confirmed that the supported Cu species remained in the monovalent state (Cu^+), which is key to its high photocatalytic activity (Fig. 12(f)). The successful construction of this catalyst benefited from a ligand exchange and post-synthetic metalation strategy based on a pillared-layer MOF. First, a bisphosphine ligand (binap) featuring a hydroxamic acid linker was anchored onto the MOF surface. Subsequent treatment with Cu salts yielded monomeric and dimeric Cu species, respectively (Fig. 12(g)). This architecture not only boosted the activity of the Cu photocatalyst but also significantly enhanced catalyst reusability by leveraging the inherent stability of the MOF. Compared to its homogeneous Cu^+ counterpart, PL-MOF-di-Cu exhibited a higher TON and broader substrate scope in photocatalytic reactions. Furthermore, the Cu^+-dimer-embedded MOF photocatalyst demonstrated excellent performance in various iminyl radical-mediated reactions, including both intramolecular and intermolecular radical cyclizations, as well as radical additions to alkenes. These reactions not only showcase the high efficiency of Cu-based photocatalysts in organic synthesis but also offer new ideas for greener chemical synthesis.

Polymer ligand-based Cu photocatalysts represent an emerging class of materials that combine the molecular-level tunability of homogeneous catalysts with the recoverability and stability of heterogeneous systems. The key mechanistic insight across the reviewed studies is that the polymer matrix plays multiple roles: (i) it provides a sterically constrained coordination environment that can stabilize specific Cu oxidation states (e.g., Cu^+ *vs.* Cu^{2+}); (ii) it prevents Cu aggregation and leaching through chelating or encapsulating effects; and (iii) it can participate in light absorption and energy transfer, particularly when conjugated polymers are employed. A common design principle is the use of bulky substituents or rigid polymer backbones to distort the Cu coordination geometry, thereby suppressing non-radiative decay pathways that would otherwise quench the excited state. The incorporation of Cu into polymers also enables magnetic or stimuli-responsive properties that facilitate catalyst recovery. However, several challenges remain. The synthesis of well-defined polymer–Cu complexes with controlled Cu loading and spatial distribution is non-trivial. The polymer matrix can also impede substrate diffusion to Cu active sites, leading to lower turnover frequencies compared to homogeneous analogues. The long-term stability of polymer-supported Cu under continuous

illumination and in the presence of reactive oxygen species is not well established. Future research should focus on developing modular polymer platforms that allow systematic variation of ligand density, linker length, and backbone flexibility, and on integrating Cu-polymer catalysts into continuous-flow reactors for scalable synthesis.

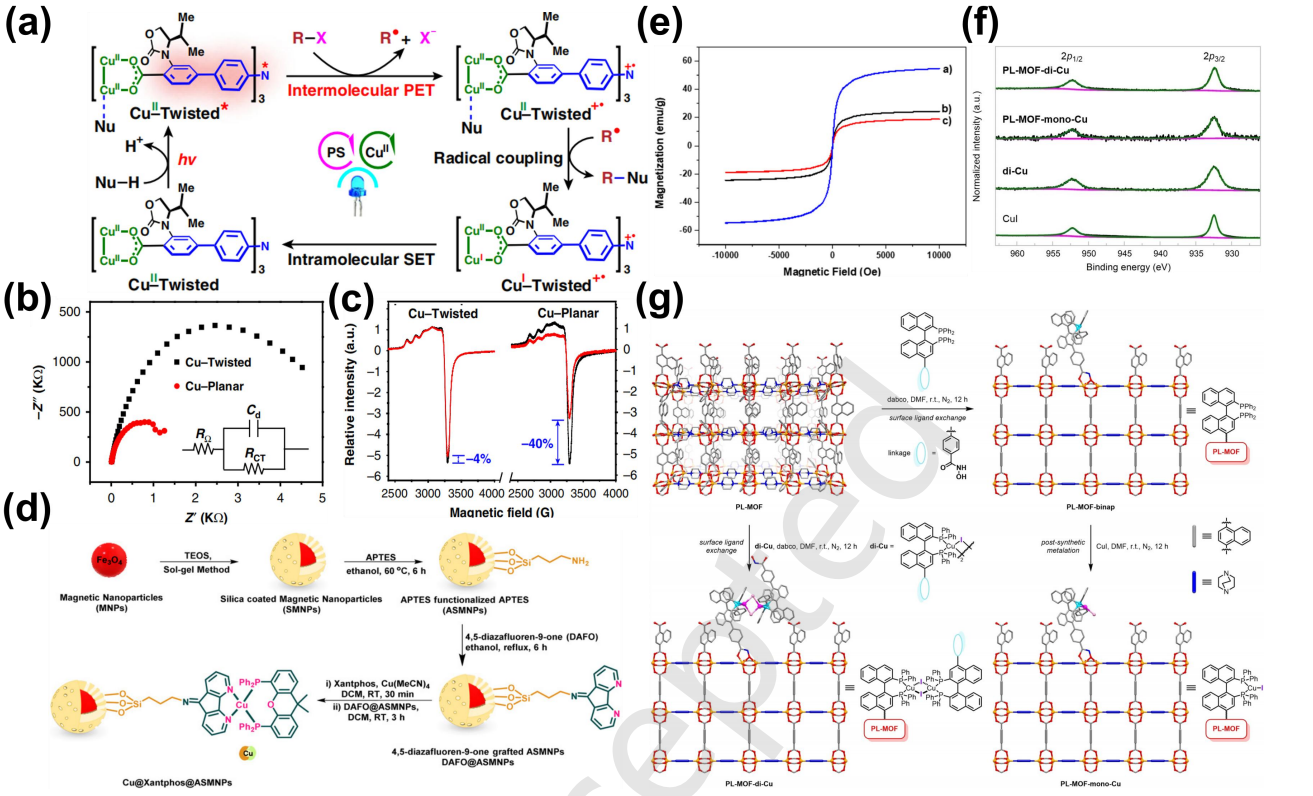

Figure 12 (a) Cooperative catalytic action in the Cu^{2+}-dye system. (b) Analysis of rectifying optoelectronic properties via EIS and photocurrent response measurements. (c) EPR spectra of Cu-twisted and Cu-planar. Reproduced with permission from Ref. [238], © Springer Nature 2020. (d) Synthesis of the Cu-based photoredox catalyst Cu@Xantphos@ASMNPs. (e) Magnetization hysteresis loops of the magnetic nanoparticle series: MNPs, SMNPs, and Cu@Xantphos@ASMNPs. Reproduced with permission from Ref. [239], © RSC Publishing 2023. (f) Cu 2p XPS Spectra of PL-MOF-Di-Cu and PL-MOF-Mono-Cu. (g) Preparation of binap-Cu photosensitizers immobilized on pillar-layered MOFs magenta, orange, gray, blue, red, cyan, pink: Cu, Zn, C, N, O, P, I. DMF=N,N-dimethylformamide. Reproduced with permission from Ref. [240], © Wiley-VCH GmbH 2023.

5.2 MOF-Based photocatalysts

Owing to their distinctive structural advantages, MOF materials have garnered significant attention in recent years, particularly for gas separation applications, and have also become an important subject of study in the field of photocatalysis [241,242]. MOFs, constructed via self-organization of metal ions or clusters with organic linkers, are a class of porous crystalline materials characterized by high specific surface area, tunable pore sizes, and tailorable surface chemistry. Their porous structure can significantly shorten the transport distance of photogenerated charge carriers, suppressing bulk recombination and thereby enhancing photocatalytic performance. In photocatalytic processes, the introduction of Cu often serves as a key electronic modulation center, playing a vital role in promoting charge separation, constructing active sites, and regulating reaction pathways.

When used as photocatalysts, the extensive internal surface area of MOFs' porous architecture greatly reduces the transport distance for photogenerated e^- and h^+. This helps to avoid bulk recombination to a certain extent, improving transfer as well utilization efficiency of carriers and, consequently, substantially boosting photocatalytic performance. Electron transfer is a key step in realizing the transfer as well utilization of photoexcited carriers during photocatalysis. Firstly, Cu can act as an electron transfer mediator, accelerating the directional migration of photogenerated e^- toward reaction sites. Lou's research team combined the enzyme laccase with MOF materials (e.g., MIL-53(Fe) and NH_2-MIL-53(Fe)) and employed a Cu-based MOF (Cu-TCPP) to construct a photo-enzyme coupled system [243]. This system achieved efficient degradation of recalcitrant organic pollutants like tetracycline. Using ESR spectroscopy, they found that photogenerated e^- could rapidly transfer from the MOF to the T_1 Cu^{2+} site of laccase (Fig. 13(a)). This resulted in an obvious enhancement towards the degradation rate constant of tetracycline (TC), from 0.0062 min^{-1} to 0.0127 min^{-1} (Fig. 13(b)). This result indicates that the Cu sites act as a bridge for electron transfer, effectively promoting the directional migration of photogenerated e^- and thereby enhancing photocatalytic efficiency.

Secondly, Cu-based MOFs also play a significant role in constructing efficient heterojunctions. Jin's group found that constructing a heterojunction between NH_2-UiO-66 and Cu-TCPP enabled effective separation of photogenerated charge carriers [244]. Using time-resolved photoluminescence (TRPL) and transient absorption spectroscopy (TAS), the researchers observed that the introduction of Cu-TCPP significantly extended the lifetime of the charge carriers. The lifetime increased from a few hundred picoseconds in UIO to 1419.9 ps (for h^+) and 346.3 ps (for e-) in Pt@NH_2-UiO-66@Cu-TCPP (PUC) (Fig. 13(c)). This result suggests that within the heterojunction, Cu not only serves as a channel for electron

transfer but also further optimizes the separation efficiency of photogenerated carriers by modulating the band structure. They constructed a ternary heterojunction, PUC, which achieved efficient photocatalytic CO_2 reduction. PUC displayed decent photoactivity with visible light illumination, with a CO production rate reaching 40.2 $\mu molg^{-1}h^{-1}$. This is an 11.6-fold and 7.0-fold improvement over the conventional UIO and Cu-TCPP, respectively (Fig. 13(d)). This indicates that Cu not only functions as a photosensitizing unit but also synergistically enhances the photocatalytic CO_2 reduction activity through band alignment and interfacial coupling.

Furthermore, Cu can also employ a bimetallic site synergy mechanism to simultaneously regulate charge dynamics and reaction pathway selectivity. Yang et al. designed and synthesized multiple Cu-Fe bimetallic MOFs (Cu-BTB-Fe) for photocatalytic CO_2 reduction [245]. Their study showed that the introduction of iron formed a stable $[Cu_2(COO)_4]$-Fe active unit within the Cu-based framework. This structure not only optimized electron-hole separation efficiency via LMCT but also significantly extended the lifetime of the separated charge state (τ_3 increased from 267.0 ps to 652.0 ps) (Fig. 13(e)). Additionally, the Cu-Fe dual sites exhibited strong affinity for CO_2 and its key intermediates (e.g., *COOH, *CHO), cooperatively promoting the hydrogenation of CO_2 to CH_4. Upon the simulated sunlight, Cu-BTB-2 wt.% Fe achieved a CH_4 production rate of 32.20 $\mu molg^{-1}\ h^{-1}$ with a selectivity of 69.24%, representing a significant improvement over the single Cu-BTB (4.26 $\mu molg^{-1}\ h^{-1}$, 32.80%) (Fig. 13(f)). This work demonstrates that the synergy between Cu and Fe enables dual control over charge separation efficiency and surface reaction pathways, providing a new strategy for highly selective photocatalytic CO_2 conversion.

In summary, Cu-MOF photocatalysts derive their functionality from three distinct Cu integration modes, specifically as framework nodes, encapsulated guests, or postsynthetically installed sites, each offering unique advantages for light absorption, charge transfer, and substrate activation. Across these configurations, common mechanistic features emerge: the porous architecture facilitates charge transport, confinement effects stabilize reactive intermediates, and heterojunction formation with other semiconductors enables efficient charge separation. Key design principles include the choice of organic linkers to tune optical properties and stability, the use of bimetallic combinations to leverage electronic synergy, and the construction of core–shell architectures to suppress photocorrosion. However, significant challenges remain. The low electrical conductivity of most MOFs limits long-range charge transport. The stability of Cu-MOFs in aqueous media under illumination is still a concern due to potential framework degradation. Moreover, achieving atomic-level control over Cu spatial distribution and oxidation state during synthesis remains demanding. Future efforts should prioritize the development of conductive MOF frameworks, the application of operando spectroscopy to probe Cu-MOF dynamics, and the scalable synthesis of Cu-MOFs for practical use.

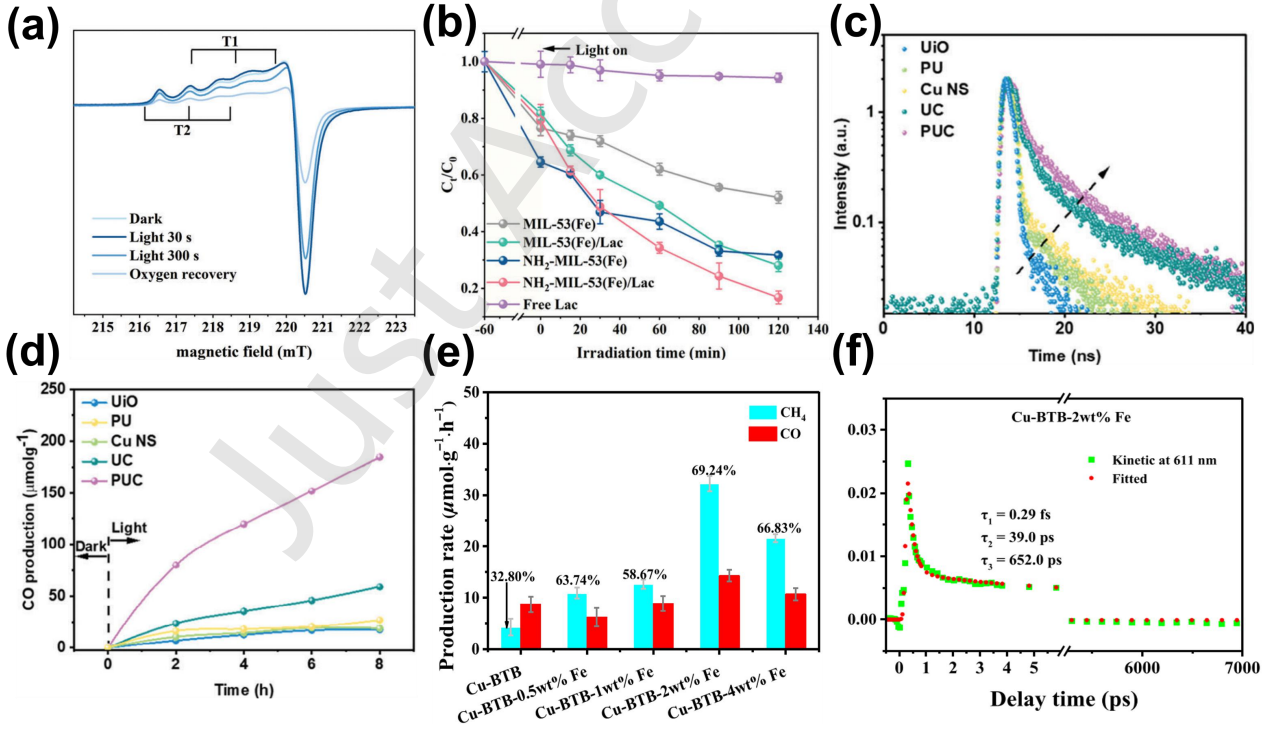

Figure 13 (a) Time-dependent ESR spectra of NH_2-MIL-53(Fe)/Lac under visible light in frozen solution at 120 K and distance between T1 Cu^{2+} and MOF surfaces. (b) Temporal profiles of tetracycline photodegradation efficiency exhibited by various photocatalysts under visible-light exposure. Reproduced with permission from Ref. [243], © Wiley-VCH GmbH 2024. (c) Time-resolved photoluminescence decay of the synthesized samples. (d) Time-dependent CO production of the synthesized materials. Reproduced with permission from Ref. [244], © Wiley-VCH GmbH 2025. (e) UV-Visible absorption spectra of all the photocatalysts; femtosecond transient absorption spectra of Cu-BTB-2 wt.% Fe recorded at 611 nm. (f) Comparative assessment of photocatalytic CO_2 reduction performance of various catalysts. Reproduced with permission from Ref. [245], © Elsevier B.V. 2024.

5.3 Single-Atom catalysts

SACs have attracted significant attention because they maximize the number of active sites, offering a catalytic mode akin to homogeneous catalysis [246–248]. Isolated active metal atoms

anchored on a photocatalyst provide abundant sites for molecular adsorption and reaction [249]. The single atom-support interaction plays a key role to achieve atomically uniform dispersion of Cu. Since it enables the necessary redox cycling and regeneration of the active center in reaction process. Zhang's team developed the renewable and economical pre-embedding technique to stabilize metal single atoms on the surface of titanium dioxide [250].This anchoring of isolated-atom materials provides an ideal route for maximizing performance and reducing costs in photocatalytic hydrogen production. However, due to agglomeration at higher loadings, most reported SACs in the literature have loadings below 0.5 wt.%. Their work achieved high dispersion and a large loading (>1 wt.%) of CuSAs on a TiO_2 photocatalyst. Under simulated sunlight, this catalyst exhibited a hydrogen evolution rate (HER) of 101.7 mmol g^{-1} h^{-1} (Fig. 14(a)), outperforming most reported photocatalysts. It also maintained good stability even after storage for 380 days (Fig. 14(b)). Both experimental and theoretical studies demonstrated that monatomic Cu confined on the support initiated a continuous, invertible, and self-regenerative photocatalysis. The synthesized CuSA-TiO_2 photocatalyst displayed a high HER, featuring an AQE of 56% at 365 nm (Fig. 14(c)). The high activity originates from the MOF-derived structure's large specific surface area, which maximizes CuSA exposure and facilitates photogenerated electron separation on the TiO_2 photocatalyst. Furthermore, the work highlighted the importance of an *in-situ* self-healing effect of the Cu species during photocatalysis. The high dispersion of Cu^{2+} and the substantial incorporation of single atoms enabled the electron transfer from Cu^{2+} to Cu^{+}. Importantly, Zhang et al. employed *in-situ* XPS to track the photoreduction of Cu^{2+} to Cu^{+} under illumination. XPS analysis showed that the as-prepared catalyst predominantly contained Cu^{2+}, with a characteristic Cu $2p_{3/2}$ peak at 933.5 eV and a strong shake-up satellite peak. Under light irradiation, *in-situ* XPS revealed partial reduction of Cu^{2+} to Cu^{+}, providing direct evidence of valence state dynamics during photocatalysis. This atomic-level design strategy for photocatalytic materials (Fig. 14(d)) enables to develop advanced materials with outstanding photoactivity and stability, as well as for competitive commercial hydrogen production.

Cu nanoparticles, with their readily tunable valence states, have emerged as promising candidates for efficient charge separation and transfer. Wang's research team obtained the Z-scheme sample featuring a monoatomic N-Cu1-S electron bridge (Cu-SAEB) (Fig. 14(e)) for modulating the CO_2 RR [251]. Without any sacrificial agent, the Cu-SAEB catalyst achieved CO and O_2 production rates up to 236.0 and 120.1 μmol $g^{-1}h^{-1}$, respectively (Fig. 14(f)), surpassing most previously reported photocatalysts. Kinetic and mechanistic studies of the charge carriers confirmed that, because of the reinforced junction in Cu-SAEB and the influence of the N-Cu1-S atomic framework, the single-atom electron bridge enabled and visibly accelerated a Z-scheme interfacial carrier transfer mode. Notably, Wang et al. used XANES and EXAFS to characterize the local structure of Cu under conditions relevant to catalysis, confirming the N–Cu_1–S coordination geometry. The XANES analysis showed an absorption edge position between Cu^{+} and Cu^{2+} references, indicating a mixed-valence state. This stage maintained photogenerated carriers with strong redox potentials, ultimately leading to a substantial boost in the photoactivity of Cu-SAEB. This study provides an effective avenue for developing strongly active, robust materials with atomic precision, which hold great potential for CO_2 conversion applications.

Shen's experimental group bridged monoatomic Cu into the interlayers of C_3N_4 sheets (Fig. 14(g)) [252]. They achieved this by means of self-organization of the Cu feedstock supramolecule with melamine-cyanuric acid monomers, followed by thermal condensation. This strategy addressed the limitations of bare C_3N_4, whose catalytic efficiency is markedly hampered through weak carrier dynamics. Experiments showed that by introducing nitrogen vacancies via thermal gradient engineering, monoatomic Cu bridges acted as charge routes. This effectively broke the symmetry of pristine C_3N_4, optimized charge distribution, and allowed rich charges to travel via C_3N_4's π-conjugated framework to reach the Cu sites. This facilitated interlamellar electron migration within C_3N_4, leading to abundant efficient carrier separation, favorable carrier arrangement, as well a reduced energy barrier for hydrogen generation (Fig. 14(h)). Experimental results demonstrated that this catalyst exhibited excellent hydrogen evolution performance under visible light (11.23 mmol g^{-1} h^{-1}) (Fig. 14(i)), with an AQE as high as 31.60% at 420 nm. Remarkably, it achieved this high efficiency without requiring any precious metal co-catalysts. This study not only deepens insight into mechanism of variable-valence Cu in photocatalysis but also offers a practical solution to the low charge separation efficiency of traditional C_3N_4.

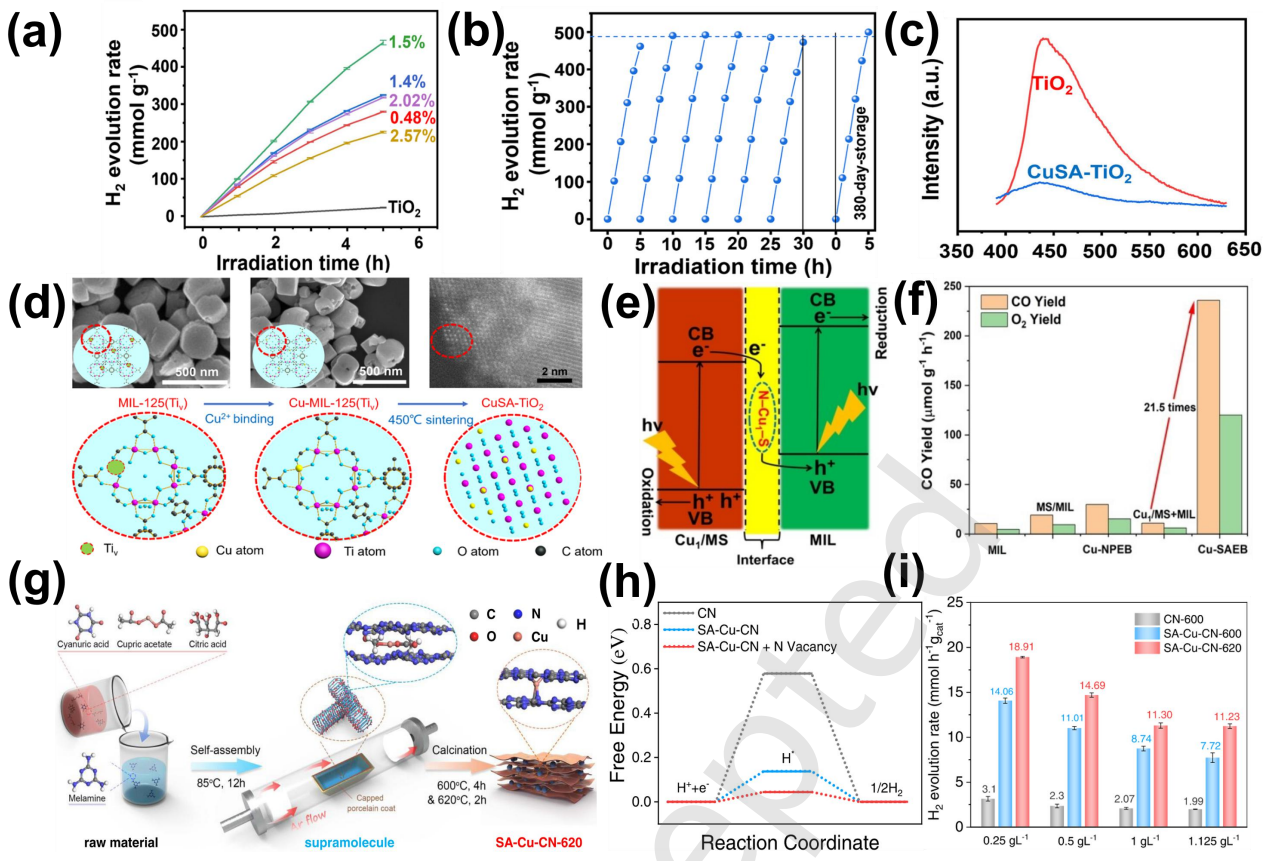

Figure 14 (a) Photocatalytic H_2 evolution performance of TiO_2 as a function of Cu SAC loadings. (b) Long-term performance assessment of ~1.5 wt.% CuSA-TiO_2 photocatalyst: from cyclic water splitting to post-storage activity after 380 days. (c) Photoluminescence quenching behavior of TiO_2 and CuSA-TiO_2 upon 375 nm laser excitation. (d) Atomic-resolution schematic and analytical characterization of the copper single-atom doping mechanism within the TiO_2 lattice. Reproduced with permission from Ref. [250], © Springer Nature 2025. (e) Suggested electron-transport pathway within the Cu-SAEB. (f) Comparative yields of CO and O_2 over different catalysts. Reproduced with permission from Ref. [251], © Wiley-VCH GmbH 2023. (g) Through a supramolecular self-assembly strategy, single-atom Cu was successfully embedded between the layers of carbon nitride (C_3N_4), forming a Cu-N_3C_1 coordination structure, while nitrogen vacancies were introduced via gradient temperature control. (h) Optimization of photocatalyst concentration for H_2 evolution (values and errors are averages from triplicate experiments). (i) Proposed HER pathway and corresponding ΔG profile for the synthesized catalysts. Reproduced with permission from Ref. [252], © American Chemical Society 2023.

The coordination environment-dependent valence states of single-atom Cu catalysts are further summarized in Table 3, which compiles the key characterization results from the studies discussed in this section. This comparison suggests a consistent trend observed in the cited studies: electron-donating coordination environments (e.g., Cu–N_3C_1 with N vacancies) have been reported to stabilize lower valence states (Cu^+), while more electronegative environments (e.g., Cu–O on TiO_2) are associated with Cu^{2+}. Mixed valence states (Cu^+/Cu^{2+}) are observed when the coordination geometry provides moderate electron density, as in the case of N–Cu_1–S. Understanding this structure and valence relationship is essential for the rational design of single-atom Cu photocatalysts with targeted catalytic properties.

Table 3 Valence states and coordination environments of single-atom Cu catalysts discussed in Section 5.3

System	Coordination environment	Dominant valence state	Characterization	Ref.
CuSA-TiO_2	Cu–O (on TiO_2)	Cu^{2+} (initial)→Cu^+ (under light)	XPS, *in-situ* XPS	[250]
Cu-SAEB (N–Cu_1–S)	N–Cu_1–S	Cu^+/Cu^{2+} (mixed)	XANES, EXAFS	[251]
Cu-bridged C_3N_4	Cu–N_3C_1 (with N vacancies)	Cu^+ (dominant)	XPS, XANES	[252]

In summary, single-atom Cu catalysts bridge homogeneous and heterogeneous photocatalysis by combining atom efficiency with well-defined active sites. Their performance is governed by three key factors: the local coordination environment (e.g., Cu–N_4, Cu–N_3C_1, Cu–O_2), which dictates electronic structure and substrate binding; the support material (e.g., TiO_2, C_3N_4), which stabilizes single atoms and facilitates charge transfer; and the reversible $Cu^{2+}/Cu^+/Cu^0$ cycling enabled by single-atom dispersion. Studies reveal that the different Cu observed in some systems is reported to be *in-situ* self-healing, where oxidized or reduced Cu species have been shown to revert to the original single-atom state under specific conditions. Common design principles include strong covalent anchoring (Cu–N, Cu–C), defect engineering to create trapping sites, and MOF-derived precursors to achieve high loading (>1 wt%) without agglomeration. However, critical challenges remain.

Synthesizing Cu SACs with uniform coordination environments at high loadings is still difficult. The dynamic evolution of Cu single atoms during photocatalysis is rarely tracked in situ, and the conditions leading to agglomeration are poorly defined. Moreover, the activity of Cu SACs in multi-electron reactions (e.g., CO_2-to-CH_3OH, N_2-to-NH_3) lags behind nanoparticle catalysts. Future efforts should prioritize high-throughput screening of coordination environments, operando microscopy and spectroscopy to visualize single-atom dynamics, and scalable synthesis from milligram to gram quantities.

Beyond the performance metrics summarized in Tables 1–3, a critical analysis of the field reveals several persistent challenges that are unique to Cu-based photocatalysts arising from their multivalent nature. To provide a systematic overview of these Cu-specific bottlenecks, Table 4 summarizes the four main challenges, uncontrollable valence, instability, poor selectivity, and photocorrosion, along with the affected systems, existing mitigation strategies, and remaining challenges that demand future investigation.

These Cu-specific bottlenecks, rather than generic catalysis challenges, must be the primary focus of future research.

Table 4 Summary of Cu-specific bottlenecks and mitigation strategies

Bottleneck	Description	Affected systems	Mitigation strategies	Remaining challenges
Uncontrollable valence	Difficulty stabilizing target Cu oxidation state	All Cu-based systems	Ligand design, coordination engineering, defect control	Quantitative design rules lacking
Instability	Oxidation of low-valence Cu under ambient conditions	Cu^0 NPs, Cu^+ complexes, Cu_2O	Surface coatings (carbon), antioxidant ligands, inert atmosphere	Long-term ambient stability
Poor selectivity	Mixed products from competing reaction pathways	CO_2 reduction, C–C coupling	Valence gradient heterostructures, single-atom coordination tuning	Product-specific selectivity remains challenging
Photocorrosion	Light-induced degradation of Cu^+ species	Cu_2O, Cu^+-MOFs	Z-scheme/S-scheme heterojunctions, protective shells	Complete suppression not yet achieved

In addition to the bottleneck analysis in Table 4, Table 5 provides a concise cross-system comparison of representative Cu-based photocatalysts, including key performance metrics, advantages, and limitations.

These Cu-specific bottlenecks, rather than generic catalysis challenges, must be the primary focus of future research. The following section discusses these challenges in the context of overall conclusions and outlines promising directions for addressing them.

Table 5 Comparison of representative Cu-based photocatalysts

Catalyst type	Cu valence	Light source	Reaction type	Efficiency metrics	Advantages	Disadvantages
Cu^0 NPs/TiO_2	Cu^0	Simulated sunlight	H_2 evolution	101.7 mmol·g^{-1}·h^{-1} [250]	High activity, good stability (380 days)	Easy oxidation
Cu_2O/TiO_2 heterojunction	Cu^+	Simulated sunlight	VOCs degradation	90.2% degradation [203]	Enhanced charge separation	Photocorrosion
CuSAs@PCN@UiO	Cu^+/Cu^{2+} (mixed)	Visible light ($\lambda \geq 420$ nm)	CO_2→CH_3OH	4.15 mmol·g^{-1}·h^{-1} [116]	High selectivity (>90%)	Complex synthesis
[Cu(dmp)(BINAP)]BF_4	Cu^+	Blue LED (455 nm)	β-chloroacylation	37-99% yield [135]	Long excited-state lifetime (2188 ns)	Homogeneous, difficult recovery
Cu-SAEB (N–Cu_1–S)	Cu^+/Cu^{2+} (mixed)	Simulated sunlight	CO_2→CO	236.0 μmol·g^{-1}·h^{-1} [251]	No sacrificial agent, Z-scheme	Stability under long-term operation
Cu-bridged C_3N_4	Cu^+	Visible light	H_2 evolution	11.23 mmol·g^{-1}·h^{-1} [252]	No noble metal, AQE 31.6%	Moderate activity compared to Pt
Cu-complex (homogeneous)	Cu^+	Blue LED	C–N coupling	45-91% yield [174]	Mild conditions, broad scope	Poor recyclability

6 Conclusion and perspectives

Cu-based photocatalysts are emerging as cost-effective alternatives to traditional noble-metal systems, steering the field of photocatalysis toward a more economical and sustainable path. Their unique physicochemical properties stem from the multivalent nature of Cu (Cu^0, Cu^+, Cu^{2+}). This variable valence not only enables broad-spectrum light absorption and efficient charge separation potential but also facilitates the dynamic switching of redox centers during catalytic cycles. This article systematically reviews the key roles of multivalent Cu in photocatalytic systems, ranging from the long-lived MLCT mechanism of photoexcited Cu^+ in homogeneous catalysis, to the surface plasmon resonance effect of Cu^0 and LMCT pathways involving Cu^{2+} in heterogeneous systems, and further to innovative designs in emerging composite systems such as polymer ligands, metal-organic frameworks, and single-atom Cu catalysts. Studies reveal that the different Cu valence states do not exist in isolation but form a dynamic equilibrium and cooperative network driven by photogenerated charge carriers: Cu^0 acts as an electron reservoir to promote reduction, Cu^+ serves as a charge transport bridge linking homogeneous and heterogeneous regimes, and Cu^{2+} participates in oxidation cycles by trapping h^+. This multivalent synergy constitutes the

structural foundation for high-efficiency photocatalysis. Strategies including ligand engineering to optimize the coordination microenvironment of Cu centers, defect modulation to introduce active sites, interface engineering to construct Z-scheme or S-scheme heterojunctions for directional charge transfer, and single-atom anchoring to achieve atomic-level dispersion for maximizing efficiency, collectively advance Cu-based photocatalysts. These approaches enable synergistic improvements in activity, selectivity, and stability for fine organic synthesis and energy conversion reactions, such as C-C/C-N coupling, alkene/alkyne bifunctionalization, and CO_2 reduction to multi-carbon products. These advances not only deepen our understanding of the structure-activity relationship in Cu-based photocatalytic materials but also provide a theoretical framework and practical paradigm for designing the next generation of non-noble-metal photocatalysts.

Despite significant progress across various fields, Cu-based photocatalysts still face several challenges. First, their stability and resistance to photochemical corrosion require further enhancement, particularly necessitating systematic evaluation and improvement of their durability under complex reaction media or continuous operation. Second, the reaction mechanisms demand deeper investigation, especially the dynamic interconversion mechanisms between different Cu valence states and their impact on photocatalytic performance. Furthermore, their large-scale application is hampered by issues related to cost, recovery, and recyclability. There is a notable lack of comprehensive studies on the synthesis, anti-oxidation strategies, and applications encompassing the full spectrum of Cu valence states. Specifically, the oxidation sensitivity of Cu^0 and Cu^+ under ambient conditions and the photocorrosion of Cu_2O remain major barriers to long-term operation.

Cu-based photocatalysts face four critical bottlenecks specific to their multivalent nature: uncontrollable valence, instability, poor selectivity, and photocorrosion. These challenges must be the primary focus of future research.

Future research on Cu-based photocatalysts can focus on the following directions: 1) Developing precise synthesis and stability strategies. This involves creating novel ligands and support materials for precise control over the microenvironment of Cu active sites, and advancing *in-situ* protection, surface passivation, or self-healing strategies to enhance the structural stability of the catalysts under light irradiation and reactive conditions. 2) Deepening mechanistic investigation and dynamic characterization. Advanced techniques such as time-resolved spectroscopy, *in-situ* X-ray absorption spectroscopy, and surface-enhanced Raman spectroscopy should be integrated to track in real-time the dynamics of photogenerated charge carriers and the transient evolution of Cu valence states. A deep integration of theory and experiment is crucial for establishing a robust structure-electronic state-performance relationship model. Notably, static characterization methods (e.g., ex-situ XPS, conventional XANES) currently dominate the field, capturing only the initial and final states of the catalyst. Direct evidence of valence-state evolution under operando conditions, such as real-time tracking of $Cu^0/Cu^+/Cu^{2+}$ interconversion during photocatalytic turnover, remains scarce. Operando XANES and time-resolved electron paramagnetic resonance (EPR) are powerful techniques to address this gap. Future research should further prioritize the integration of these operando methods to establish causality between electronic structure dynamics and photocatalytic performance. 3) Expanding reaction systems and application scenarios. Exploring the application of Cu-based photocatalysts in emerging fields like nitrogen reduction, plastic upcycling, and biomass conversion is promising. Furthermore, developing multi-field synergistic catalytic systems, such as photo-electro or photo-thermal coupling, can enhance energy utilization efficiency and product selectivity. 4) Promoting material intelligence and system integration. Designing intelligent catalytic materials with light-responsive and self-adaptive regulation capabilities is a key goal. Concurrently, developing modular, continuous-flow photocatalytic reactor systems will facilitate process scale-up and integration. 5) Emphasizing sustainability and circular economy principles. Efforts should focus on developing green, low-energy-consumption methods for catalyst preparation and regeneration. Establishing a complete chain for catalyst recovery, regeneration, and resource recycling is essential to steer Cu-based photocatalysis toward low-carbon, circular industrial applications. 6) Developing multifunctional integrated systems for practical applications. For complex real-world systems like industrial wastewater, mixed exhaust gases, or biomass-derived liquids, it is necessary to design multifunctional Cu-based photocatalytic materials with resistance to poisoning and light shielding, wide pH adaptability, and the capability for synergistic removal of multiple pollutants. Their performance and deactivation mechanisms under realistic illumination conditions, such as natural sunlight, weak light, or intermittent light must be studied to bridge the gap from laboratory "ideal systems" to "real-world scenarios." Simultaneously, exploring technical pathways for seamlessly integrating photocatalytic modules into existing chemical processes or environmental engineering facilities, and evaluating their techno-economic feasibility and full lifecycle environmental impact, will lay the groundwork for large-scale engineering applications. Moreover, improving synthetic reproducibility, particularly for high-loading single-atom catalysts, MOF-based systems and developing standardized protocols for catalyst performance evaluation are essential steps toward industrial translation.

In summary, this article has systematically reviewed the current research status and future challenges of Cu-based photocatalysts. The core advancements and research directions can be encapsulated in the summary and outlook framework presented in (Fig. 15). Cu-based photocatalysts hold broad application prospects in the field of photocatalysis. Future research will continue to drive their widespread use in areas such as organic synthesis, environmental remediation, and energy conversion. Through interdisciplinary collaboration, technological innovation, and engineering practices, Cu-based photocatalytic materials are poised to play an increasingly vital role in green chemical synthesis, clean energy production, and environmental pollution control, thereby providing robust technical support for achieving sustainable development goals.

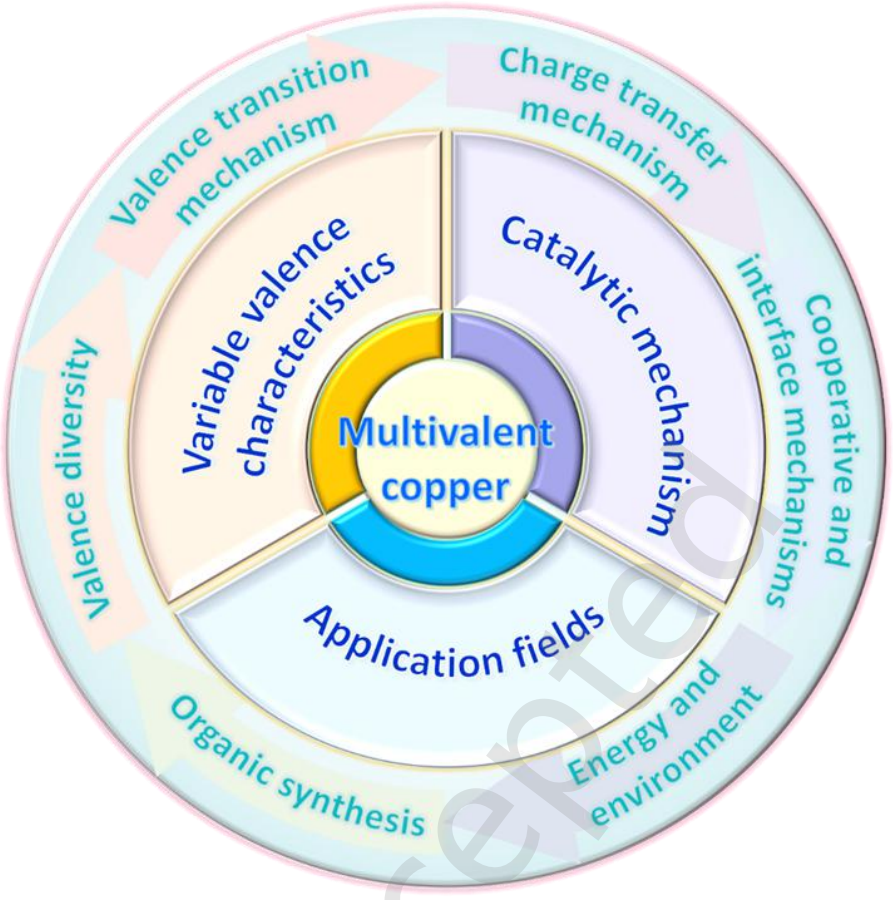

Figure 15 The prospects for unable Cu valence states in next generation photocatalytic systems.

Data availability

Not applicable.

Acknowledgements

This work was financially supported by the National Natural Science Foundation of China (Grant Nos. 52370109 and 52401227), the Natural Science Foundation Project of CQ CSTC (CSTB2025YITP-QCRCX0064, CSTB2025NSCQ-GPX0827 and CSTB2024NSCQ-MSX1045), Science and Technology Research Program of Chongqing Municipal Education Commission of China (KJZD-M202400802) and the Startup Research Grant (No. F1240093) from Chongqing Jiaotong University.

Declaration of competing interest

All the contributing authors report no conflict of interests in this work.

Author contribution statement

S. H. W: Investigation and writing – original draft. H. L.: Data curation, project administration, validation. W. H.: writing manuscript. Y. Y. D.: Project administration, funding acquisition. Y. H. L.: Funding acquisition, supervision, and writing – review & editing. All the authors have approved the final manuscript.

Use of AI statement

None.

References

[1] Lee, B.-H.; Park, S.; Kim, M.; Sinha, A. K.; Lee, S. C.; Jung, E.; Chang, W. J.; Lee, K.-S.; Kim, J. H.; Cho, S.-P. et al. Reversible and cooperative photoactivation of single-atom Cu/TiO_2 photocatalysts. *Nat. Mater.* **2019**, *18*, 620–626.

[2] Cortés, E. Activating plasmonic chemistry. *Science* **2018**, *362*, 28–29.

[3] Hu, Y.; Chao, T.; Dou, Y.; Xiong, Y.; Liu, X.; Wang, D. Isolated metal centers activate small molecule electrooxidation: mechanisms and applications. *Adv. Mater.* **2025**, *37*, 2418504.

[4] Jin, W.; Yang, C.-Y.; Pau, R.; Wang, Q.; Tekelenburg, E. K.; Wu, H.-Y.; Wu, Z.; Jeong, S. Y.; Pitzalis, F.; Liu, T. et al. Photocatalytic doping of organic semiconductors. *Nature* **2024**, *630*, 96–101.

[5] Shen, T.; Lambert, T. H. Electrophotocatalytic diamination of vicinal C–H bonds. *Science* **2021**, *371*, 620–626.

[6] Yang, Q.; Wang, Y.-H.; Qiao, Y.; Gau, M.; Carroll, P. J.; Walsh, P. J.; Schelter, E. J. Photocatalytic C–H activation and the subtle role of chlorine radical complexation in reactivity. *Science* **2021**, *372*, 847–852.

[7] Schultz, D. M.; Yoon, T. P. Solar synthesis: prospects in visible light photocatalysis. *Science* **2014**, *343*, 1239176.

[8] Chen, F.; Huang, H.; Zhang, F.; Wang, R.; Wang, L.; Chang, Z.; Cao, L.; Zhang, W.; Li, L.; Chen, M. et al. Biomimetic chlorosomes: oxygen-independent photocatalytic nanoreactors for efficient combination photoimmunotherapy. *Adv. Mater.* **2025**, *37*, 2413385.

[9] Song, J.-Y.; Huang, J. E.; Ban, H. W.; Chen, Q.-C.; Ji, Y.; Yang, S.; Wang, Y.; Yoo, Y.; Jung, H. S.; Li, J. et al. Copper catalysts inherit and retain precatalyst morphology in extended CO electroreduction to *n* -propanol. *Adv. Mater.* **2025**, *37* ,e08900.

[10] Chan, A. Y.; Ghosh, A.; Yarranton, J. T.; Twilton, J.; Jin, J.; Arias-Rotondo, D. M.; Sakai, H. A.; McCusker, J. K.; MacMillan, D. W. C. Exploiting the marcus inverted region for first-row transition metal–based photoredox catalysis. *Science* **2023**, *382*, 191–197.

[11] Chen, X.; Cai, Y.; Liang, R.; Tao, Y.; Wang, W.; Zhao, J.; Chen, X.; Li, H.; Zhang, D. NH_2-UiO-66(Zr) with fast electron transfer routes for breaking down nitric oxide via photocatalysis. *Appl. Catal. B: Environ.* **2020**, *267*, 118687.

[12] Yadav, R. N.; Srivastava, A. K.; Dey, S.; Das, A.; Banik, B. K.; Hossain, Md. F. Transition metal complexes: a new era of photosensitizers for dearomative photocycloaddition/annulation via energy and electron transfer photocatalysis. *Coord. Chem. Rev.* **2024**, *520*, 216136.

[13] Mo, Y.; Lu, Z.; Rughoobur, G.; Patil, P.; Gershenfeld, N.; Akinwande, A. I.; Buchwald, S. L.; Jensen, K. F. Microfluidic electrochemistry for single-electron transfer redox-neutral reactions. *Science* **2020**, *368*, 1352–1357.

[14] Wang, J.; Liu, D.; Zhu, Y.; Zhou, S.; Guan, S. Supramolecular packing dominant photocatalytic oxidation and anticancer performance of PDI. *Appl. Catal. B: Environ.* **2018**, *231*, 251–261.

[15] Rana, P.; Singh, N.; Majumdar, P.; Prakash Singh, S. Evolution of BODIPY/aza-BODIPY dyes for organic photoredox/energy transfer catalysis. *Coord. Chem. Rev.* **2022**, *470*, 214698.

[16] Witzel, S.; Hashmi, A. S. K.; Xie, J. Light in gold catalysis. *Chem. Rev.* **2021**, *121*, 8868–8925.

[17] Iervolino, G.; Vaiano, V.; Sannino, D.; Rizzo, L.; Palma, V. Enhanced photocatalytic hydrogen production from glucose aqueous matrices on Ru-doped $LaFeO_3$. *Appl. Catal. B: Environ.* **2017**, *207*, 182–194.

[18] Vignolo-González, H. A.; Gouder, A.; Laha, S.; Duppel, V.; Carretero-Palacios, S.; Jiménez-Solano, A.; Oshima, T.; Schützendübe, P.; Lotsch, B. V. Morphology matters: 0D/2D WO_3 nanoparticle-ruthenium oxide nanosheet composites for enhanced photocatalytic oxygen evolution reaction rates. *Adv. Energy Mater.* **2023**, *13*, 2203315.

[19] Jiang, G.; Geng, K.; Wu, Y.; Han, Y.; Shen, X. High photocatalytic performance of ruthenium complexes sensitizing g-C_3N_4/TiO_2 hybrid in visible light irradiation. *Appl. Catal. B: Environ.* **2018**, *227*, 366–375.

[20] Baran, T.; Wojtyła, S.; Dibenedetto, A.; Aresta, M.; Macyk, W. Zinc sulfide functionalized with ruthenium nanoparticles for photocatalytic reduction of CO_2. *Appl. Catal. B: Environ.* **2015**, *178*, 170–176.

[21] Ouyang, W.; Muñoz-Batista, M. J.; Kubacka, A.; Luque, R.; Fernández-García, M. Enhancing photocatalytic performance of TiO_2 in H_2 evolution via Ru co-catalyst deposition. *Appl. Catal. B: Environ.* **2018**, *238*, 434–443.

[22] Zhang, S.; Li, M.; Wu, Q.; Yang, H.; Han, J.; Wang, H.; Liu, X. Photocatalytic hydrogen evolution from formate and aldehyde over molecular iridium complexes stabilized by bipyridine-bridging organosilica nanotubes. *Appl. Catal. B: Environ.* **2018**, *236*, 466–474.

[23] Li, J.; Bhatt, P. M.; Li, J.; Eddaoudi, M.; Liu, Y. Recent progress on microfine design of metal–organic frameworks: structure regulation and gas sorption and separation. *Adv. Mater.* **2020**, *32*, 2002563.

[24] Pham, H. Q.; Pham, H. T. Q.; Huynh, Q.; Huynh, T. T. Single-atom iridium-based catalysts: synthesis strategies and electro(photo)-catalytic applications for renewable energy conversion and storage. *Coord. Chem. Rev.* **2023**, *486*, 215143.

[25] Tritton, D. N.; Tang, F.-K.; Bodedla, G. B.; Lee, F.-W.; Kwan, C.-S.; Leung, K. C.-F.; Zhu, X.; Wong, W.-Y. Development and advancement of iridium(III)-based complexes for photocatalytic hydrogen evolution. *Coord. Chem. Rev.* **2022**, *459*, 214390.

[26] Yamazaki, H.; Shouji, A.; Kajita, M.; Yagi, M. Electrocatalytic and photocatalytic water oxidation to dioxygen based on metal complexes. *Coord. Chem. Rev.* **2010**, *254*, 2483–2491.

[27] Twilton, J.; Le, C.; Zhang, P.; Shaw, M. H.; Evans, R. W.; MacMillan, D. W. C. The merger of transition metal and photocatalysis. *Nat. Rev. Chem.* **2017**, *1*, 0052.

[28] Singh, S.; Kumar, R.; Pant, K. K.; Kumar, S.; Joshi, D.; Biswas, P. Mechanistic exploration in controlling the product selectivity via metals in TiO_2 for photocatalytic carbon dioxide reduction. *Appl. Catal. B Environ. Energy* **2024**, *352*, 124054.

[29] Xiao, L.; Zhang, Q.; Chen, P.; Chen, L.; Ding, F.; Tang, J.; Li, Y.-J.; Au, C.-T.; Yin, S.-F. Copper-mediated metal-organic framework as efficient photocatalyst for the partial oxidation of aromatic alcohols under visible-light irradiation: synergism of plasmonic effect and schottky junction. *Appl. Catal. B: Environ.* **2019**, *248*, 380–387.

[30] Cao, Y.-D.; Yin, D.; Li, S.; Dong, X.-Y.; Feng, Y.; Liu, H.; Fan, L.-L.; Gao, G.-G.; Zang, S.-Q. Substituent effect to fine-tune energy levels of atom-precise $[MoOS_3]^{2-}$ modified copper(I) thiolate clusters boosting

recyclable photocatalysis. *Angew. Chem. Int. Ed.* **2023**, *62*, e202307678.

[31] Zhao, Y.; Zhao, Y.; Shi, R.; Wang, B.; Waterhouse, G. I. N.; Wu, L.-Z.; Tung, C.-H.; Zhang, T. Tuning oxygen vacancies in ultrathin TiO_2 nanosheets to boost photocatalytic nitrogen fixation up to 700 nm. *Adv. Mater.* **2019**, *31*, 1806482.

[32] Iihoshi, T.; Ohwaki, T.; Vequizo, J. J. M.; Yamakata, A. Improvement of photocatalytic activity under visible-light irradiation by heterojunction of Cu ion loaded WO_3 and Cu ion loaded N-TiO_2. *Appl. Catal. B: Environ.* **2019**, *248*, 249–254.

[33] Cheng, Z.; Qi, W.; Pang, C. H.; Thomas, T.; Wu, T.; Liu, S.; Yang, M. Recent advances in transition metal nitride-based materials for photocatalytic applications. *Adv. Funct. Mater.* **2021**, *31*, 2100553.

[34] Xie, S.; Li, Y.; Sheng, B.; Zhang, W.; Wang, W.; Chen, C.; Li, J.; Sheng, H.; Zhao, J. Self-reconstruction of paddle-wheel copper-node to facilitate the photocatalytic CO_2 reduction to ethane. *Appl. Catal. B: Environ.* **2022**, *310*, 121320.

[35] Hernandez-Perez, A. C.; Collins, S. K. Heteroleptic Cu-based sensitizers in photoredox catalysis. *Acc. Chem. Res.* **2016**, *49*, 1557–1565.

[36] Khan, A.; Le Pivert, M.; Ranjbari, A.; Dragoe, D.; Bahena-Uribe, D.; Colbeau-Justin, C.; Herrero, C.; Rutkowska-Zbik, D.; Deschamps, J.; Remita, H. Cu-based MOF/TiO_2 composite nanomaterials for photocatalytic hydrogen generation and the role of copper. *Adv. Funct. Mater.* **2025**, *36*, 2501736.

[37] Dong, C.; Feng, W.; Xu, W.; Yu, L.; Xiang, H.; Chen, Y.; Zhou, J. The coppery age: copper (Cu)-involved nanotheranostics. *Adv. Sci.* **2020**, *7*, 2001549.

[38] Han, D.; Han, Y.; Li, J.; Liu, X.; Yeung, K. W. K.; Zheng, Y.; Cui, Z.; Yang, X.; Liang, Y.; Li, Z. et al. Enhanced photocatalytic activity and photothermal effects of cu-doped metal-organic frameworks for rapid treatment of bacteria-infected wounds. *Appl. Catal. B: Environ.* **2020**, *261*, 118248.

[39] Cao, G.; Deskins, N. A.; Yi, N. Carbon monoxide oxidation over copper and nitrogen modified titanium dioxide⋆. *Appl. Catal. B: Environ.* **2021**, *285*, 119748.

[40] Weng, H.; Zhang, X.; Liu, X.; Tang, Y.; Yuan, H.; Xu, Y.; Li, K.; Huang, X. Enhanced conductivity of multilayer copper–carbon nanofilms via plasma immersion deposition. *Nano Micro Lett.* **2025**, *17*, 130–145.

[41] Zheng, Y.; Niu, J.; Lu, Y.; Xu, S.; Li, Z.; Zhao, H.; La, P. High strength and high conductivity pure copper prepared by ECAP-conform combined with cryogenic rolling and recrystallization annealing. *J. Mater. Res. Technol.* **2025**, *36*, 3192–3204.

[42] Jin, Y.; Jin, K.; Ji, W.; Zhang, Z.; Gan, L.; Han, P.; Yuan, X.; Fu, L.; Wu, Y. Fabrication of a robust zinc powder anode via facile integration of copper nanopowder as a functional conductive medium. *Adv. Funct. Mater.* **2025**, *35*, 2418503.

[43] Liu, N.; Jiang, J.; Chen, Z.; Wu, B.; Zhang, S.; Zhang, Y.-Q.; Cheng, P.; Shi, W. Promoted photocatalytic hydrogen evolution by tuning the electronic state of copper sites in metal-organic supramolecular assemblies. *Angew. Chem. Int. Ed.* **2023**, *62*, e202312306.

[44] Xiao, X.; Gao, Y.; Zhang, L.; Zhang, J.; Zhang, Q.; Li, Q.; Bao, H.; Zhou, J.; Miao, S.; Chen, N. et al. A promoted charge separation/transfer system from Cu single atoms and C_3N_4 layers for efficient photocatalysis. *Adv. Mater.* **2020**, *32*, 2003082.

[45] Zhu, Y.; Deng, N.; Feng, M.; Liu, P. On the comparable activity in plasmonic photocatalytic and thermocatalytic oxidative homocoupling of alkynes over prereduced copper ferrite. *Chin. J. Catal.* **2019**, *40*, 1505–1515.

[46] Su, T.; Tian, H.; Qin, Z.; Ji, H. Preparation and characterization of Cu modified $BiYO_3$ for carbon dioxide reduction to formic acid. *Appl. Catal. B: Environ.* **2017**, *202*, 364–373.

[47] Li, Y.; Liu, Z.; Zhang, L.; Chen, J.; Wang, S.; Ma, M.; Yin, Z.; Man, Z.; Yi, D.; Wang, Z. et al. Boosting photocatalytic hydrogen evolution of 2D multinary copper chalcogenide nanocrystals enabled by tuning metal precursors. *Small* **2025**, *21*, 2501503.

[48] Yang, F.; Feng, C.; Zuo, S.; Wang, Q.; Wei, F.; Hu, M.; Ren, Y.; Liu, D.; Li, W.-L.; Wang, S. et al. Photocatalytic H_2O_2 production with >30% quantum efficiency via monovalent copper dynamics. *J. Am. Chem. Soc.* **2025**, *147*, 17112–17120.

[49] Meng, F.; Zhang, R.; Xu, H.; Shen, L.; Yang, H.; Meng, Q.; Lan, X. Engineering copper single sites in conjugated microporous polymers to enhance selective photocatalytic CO_2 methanation. *Chem. Eng. J.* **2025**, *511*, 162017.

[50] Ebri, G.; Alhashmi, E.; Baghdadi, Y.; Daboczi, M.; Eslava, S.; Hellgardt, K. Simultaneous photocatalytic CO_2 reduction and C-C coupling of benzyl alcohol under high pressure and supercritical conditions. *Chem, Eng, J.* **2025**, *505*, 158356.

[51] Wang, W.; Tao, Y.; Du, L.; Wei, Z.; Yan, Z.; Chan, W. K.; Lian, Z.; Zhu, R.; Phillips, D. L.; Li, G. Femtosecond time-resolved spectroscopic observation of long-lived charge separation in bimetallic sulfide/g-C_3N_4 for boosting photocatalytic H_2 evolution. *Appl. Catal. B: Environ.* **2021**, *282*, 119568.

[52] Zang, Y.; Cheng, Y.-J.; Wang, Z.-D.; Peng, P.; Dong, Q.-G.; Chen, H.; Wang, R.; Zang, S.-Q. Ionic covalent organic nanosheet anchoring discrete copper for efficient quasi-homogeneous photocatalytic proton reduction. *Appl. Catal. B: Environ.* **2022**, *302*, 120817.

[53] Ji, W.; Qu, J.; Li, C.-A.; Wu, J.-W.; Jing, S.; Gao, F.; Lv, Y.-N.; Liu, C.; Zhu, D.-R.; Ren, X.-M. et al. *In-situ* surface assembly of core-shell TiO_2-copper(I) cluster nanocomposites for visible-light photocatalytic reduction of Cr(VI). *Appl. Catal. B: Environ.* **2017**, *205*, 368–375.

[54] Dozzi, M. V.; Chiarello, G. L.; Pedroni, M.; Livraghi, S.; Giamello, E.; Selli, E. High photocatalytic hydrogen production on Cu(II) pre-grafted Pt/TiO_2. *Appl. Catal. B: Environ.* **2017**, *209*, 417–428.

[55] Di Terlizzi, L.; Nicchio, L.; Protti, S.; Fagnoni, M. Visible photons as ideal reagents for the activation of coloured organic compounds. *Chem. Soc. Rev.* **2024**, *53*, 4926–4975.

[56] Lin, F.; Shao, B.; Li, Z.; Zhang, J.; Wang, H.; Zhang, S.; Haruta, M.; Huang, J. Visible light photocatalysis over solid acid: enhanced by gold plasmonic effect. *Appl. Catal. B: Environ.* **2017**, *218*, 480–487.

[57] Li, R.; Luan, J.; Zhang, Y.; Jiang, L.; Yan, H.; Chi, Q.; Yan, Z. A review of efficient photocatalytic water splitting for hydrogen production. *Renew. Sustain. Energy Rev.* **2024**, *206*, 114863.

[58] Cui, Y.; Wang, Y.; Ma, Y.; Su, X.; Tai, R.; Jia, M.; Chen, J.; Liu, A.; Yu, L.; Tian, C. et al. A chiral mesostructured photocatalyst for efficient solar-driven CO_2 reduction to ethanol. *Nat. Synth.* **2025**, *5*, 1–12.

[59] Dong, S.; Feng, J.; Fan, M.; Pi, Y.; Hu, L.; Han, X.; Liu, M.; Sun, J.; Sun, J. Recent developments in heterogeneous photocatalytic water treatment using visible light-responsive photocatalysts: a review. *RSC Adv.* **2015**, *5*, 14610–14630.

[60] Pan, Y.; Yuan, X.; Jiang, L.; Yu, H.; Zhang, J.; Wang, H.; Guan, R.; Zeng, G. Recent advances in synthesis, modification and photocatalytic applications of micro/nano-structured zinc indium sulfide. *Chem. Eng. J.* **2018**, *354*, 407–431.

[61] Liu, Q.; Peng, Y.; Masood, Z.; DuBois, D.; Tressel, J.; Nichols, F.; Ashby, P.; Mercado, R.; Assafa, T.; Pan, D. et al. Stable cuprous hydroxide nanostructures by organic ligand functionalization. *Adv. Mater.* **2023**, *35*, 2208665.

[62] Ran, H.; Wu, D.; Chen, W.; Liu, Y.; Gao, L.; Zhou, J.; Gao, B.; Lai, J.; Luo, H.; Kuang, F. et al. Ligand-engineered Cu-based halide perovskite for highly efficient near-infrared photocatalytic CO_2 reduction. *Appl. Catal. B Environ.* **2024**, *352*, 124048.

[63] Yan, X.; Jia, Z.; Che, H.; Chen, S.; Hu, P.; Wang, J.; Wang, L. A selective ion replacement strategy for the synthesis of copper doped carbon nitride nanotubes with improved photocatalytic hydrogen evolution. *Appl. Catal. B: Environ.* **2018**, *234*, 19–25.

[64] Vaiano, V.; Iervolino, G.; Rizzo, L. Cu-doped ZnO as efficient photocatalyst for the oxidation of arsenite to arsenate under visible light. *Appl. Catal. B: Environ.* **2018**, *238*, 471–479.

[65] Wang, J.; Gao, F.; Wang, D.; Li, Y.; Linping, L.; Zhang, G.; Wang, G.; Tung, C.-H.; Wang, Y. Electronic state modulation of a single-Cu site on a bimetallically doped titanium-oxo cluster to enhance CO_2 storage. *Angew. Chem. Int. Ed.* **2025**, *64*, e202505584.

[66] Yang, Y.; Ma, Z.; Zhang, H.; Sun, S.; Huang, Y.; Liu, Y.; Xu, X.; Liu, Y.; Ding, C.; Li, J. Biomimetic prickly nano purifier with silicified assistor for the treatment of complex wastewater. *Adv. Funct. Mater.* **2025**, *35*, 2506673.

[67] Kumaravel, V.; Mathew, S.; Bartlett, J.; Pillai, S. C.

Photocatalytic hydrogen production using metal doped TiO_2: a review of recent advances. *Appl. Catal. B: Environ.* **2019**, *244*, 1021–1064.

[68] Jiang, D.; Xue, J.; Wu, L.; Zhou, W.; Zhang, Y.; Li, X. Photocatalytic performance enhancement of CuO/Cu_2O heterostructures for photodegradation of organic dyes: effects of CuO morphology. *Appl. Catal. B: Environ.* **2017**, *211*, 199–204.

[69] Sayed, M.; Qi, K.; Wu, X.; Zhang, L.; García, H.; Yu, J. Cu-based S-scheme photocatalysts. *Chem. Soc. Rev.* **2025**, *54*, 4874–4921.

[70] Chen, L.; Yang, X.; He, Z.; Zheng, J.; Zhu, M.; Zeng, Z.; Li, H.; Liu, Y.; Yang, S. Selective photoconversion of CO_2 to C_2H_4 on asymmetrical CeO_2-Cu_2O interfaces driven by oxygen vacancies. *Adv. Funct. Mater.* **2025**, *35*, 2500818.

[71] Huang, F.; Liang, S.; Zhong, R.; Shao, T.; Wu, X.; Liu, S. Interfacial Cu···NH dynamic coordination facilitates S-scheme charge transfer and CO_2 insertion for artificial photosynthesis over CuPc grafted crystalline g-C_3N_4 nanorods. **2025**, *514*, 163128.

[72] Abdelhamid, H. N.; Abdellatif, A. B. A.; El-Bery, H. M. Hydrogen production using noble metal-free metal-organic frameworks (MOFs)-derived CuO@C/TiO_2. *Chem. Eng. J.* **2025**, *514*, 163343.

[73] Li, T.; Zhao, L.; Chen, F.; Cheng, X.; Xu, W.; Liu, Z.; Guan, Q.; Zhou, H.; He, L. Accumulation of long-lived photogenerated holes at copper yolk-shell heterojunctions via heterogeneous contraction and reduction strategies for enhanced photocatalytic oxidation. *Energy Env., Mater,* **2025**, *0*, e70024.

[74] Zhu, K.; Zhang, M.; Feng, X.; Qin, L.; Kang, S.-Z.; Li, X. A novel copper-bridged graphitic carbon nitride/porphyrin nanocomposite with dramatically enhanced photocatalytic hydrogen generation. *Appl. Catal. B: Environ.* **2020**, *268*, 118434.

[75] Wei, Z.; Hu, J.; Zhu, K.; Wei, W.; Ma, X.; Zhu, Y. Self-assembled polymer phenylethnylcopper nanowires for photoelectrochemical and photocatalytic performance under visible light. *Appl. Catal. B: Environ.* **2018**, *226*, 616–623.

[76] Lucchetti, R.; Onotri, L.; Clarizia, L.; Natale, F. D.; Somma, I. D.; Andreozzi, R.; Marotta, R. Removal of nitrate and simultaneous hydrogen generation through photocatalytic reforming of glycerol over "*in-situ*" prepared zero-valent nano copper/P_{25}. *Appl. Catal. B: Environ.* **2017**, *202*, 539–549.

[77] Kumar Tailor, N.; Singh, S.; Afroz, M. A.; Pant, K. K.; Satapathi, S. Unraveling the impact of Cu-doping in lead free halide perovskites for markedly enhancing photocatalytic CO_2 reduction performance. *Appl. Catal. B: Environ.* **2024**, *340*, 123247.

[78] Sun, H.; Lang, Z.; Zhao, Y.; Zhao, X.; Qiu, T.; Hong, Q.; Wei, K.; Tan, H.; Kang, Z.; Li, Y. Copper-bridged tetrakis(4-ethynylphenyl)ethene aggregates with photo-Regulated^1 O_2 and O_2- generation for selective photocatalytic aerobic oxidation. *Angew. Chem. Int. Ed.* **2022**, *61*, e202202914.

[79] Xia, S.; Zhang, X.; Zhou, X.; Meng, Y.; Xue, J.; Ni, Z. The influence of different Cu species onto multi-copper-contained hybrid materials' photocatalytic property and mechanism of chlorophenol degradation. *Appl. Catal. B: Environ.* **2017**, *214*, 78–88.

[80] Chen, J.; Li, M.; Wang, X.; Liu, H.; Jiang, W.; Zhao, B.; Song, W. Putting charge transfer degree as a bridge connecting surface-enhanced raman spectroscopy and photocatalysis. *Angew. Chem. Int. Ed.* **2025**, *64*, e202424986.

[81] Ge, H.; Zhang, B.; Liang, H.; Zhang, M.; Fang, K.; Chen, Y.; Qin, Y. Photocatalytic conversion of CO_2 into light olefins over TiO_2 nanotube confined Cu clusters with high ratio of Cu^+. *Appl. Catal. B: Environ.* **2020**, *263*, 118133.

[82] Zhang, P.; Song, T.; Wang, T.; Zeng, H. Plasmonic Cu nanoparticle on reduced graphene oxide nanosheet support: an efficient photocatalyst for improvement of near-infrared photocatalytic H_2 evolution. *Appl. Catal. B: Environ.* **2018**, *225*, 172–179.

[83] Le, C.; Chen, T. Q.; Liang, T.; Zhang, P.; MacMillan, D. W. C. A radical approach to the copper oxidative addition problem: trifluoromethylation of bromoarenes. *Science* **2018**, *360*, 1010–1014.

[84] Beaudelot, J.; Oger, S.; Peruško, S.; Phan, T.-A.; Teunens, T.; Moucheron, C.; Evano, G. Photoactive copper complexes: properties and applications. *Chem. Rev.* **2022**, *122*, 16365–16609.

[85] Zhu, H.; Chen, D.; Li, N.; Xu, Q.; Li, H.; He, J.; Lu, J. Dual-layer copper mesh for integrated oil-water separation and water purification. *Appl. Catal. B: Environ.* **2017**, *200*, 594–600.

[86] Wang, S.; Zhang, X.; Pan, L.; Zhao, F.-M.; Zou, J.-J.; Zhang, T.; Wang, L. Controllable sonochemical synthesis of Cu_2O/$Cu_2(OH)_3NO_3$ composites toward synergy of adsorption and photocatalysis. *Appl. Catal. B: Environ.* **2015**, *164*, 234–240.

[87] Cheng, Y.-J.; Zhao, J.-Q.; Ma, X.-F.; Zheng, H.-L.; He, L.; Zhang, J.; Lin, Q. Simultaneously tailoring hydrostability and photoelectroactivity in heterocluster metal–organic frameworks for efficient photocatalytic hydrogen production. *Adv. Mater.* **2025**, *37*, 2503756.

[88] Zhang, Z.; Liu, K.; Bao, Y.; Dong, B. Photo-assisted self-optimizing of charge-carriers transport channel in the recrystallized multi-heterojunction nanofibers for highly efficient photocatalytic H_2 generation. *Appl. Catal. B: Environ.* **2017**, *203*, 599–606.

[89] Wang, Z.-D.; Zang, Y.; Liu, Z.-J.; Peng, P.; Wang, R.; Zang, S.-Q. Opening catalytic sites in the copper-triazoles framework via defect chemistry for switching on the proton reduction. *Appl. Catal. B: Environ.* **2021**, *288*, 119941.

[90] Xin, X.; Song, Y.; Guo, S.; Zhang, Y.; Wang, B.; Yu, J.; Li, X. *In-situ* growth of high-content 1T phase MoS_2 confined in the CuS nanoframe for efficient photocatalytic hydrogen evolution. *Appl. Catal. B: Environ.* **2020**, *269*, 118773.

[91] Liu, X.; Zhang, Y.; Mao, C.; Jin, X.; Yang, J.; Xiao, Z.; Huang, L.; Zhao, Z.; Peng, F. Self-amplifying cuprophoric nanocatalyst reprograms mitochondrial copper homeostasis to drive tumor-selective cuproptosis in oral squamous cell carcinoma. *Chem. Eng. J.* **2025**, *522*, 167450.

[92] Xiong, R.-Z.; Xu, H.-M.; Zhu, H.-R.; Zhang, Z.-J.; Li, G.-R. Recent progress in Cu-based electrocatalysts for CO_2 reduction. *Chem. Eng. J.* **2025**, *505*, 159210.

[93] Albadr, R. J.; Taher, W. M.; Alwan, M.; Jawad, M. J.; Mushtaq, H.; Saadi, B. M.; Smerat, A.; Kazemi, M.; Javahershenas, R. Copper catalyzed formation of carbon–silicon bond: a review. *J. Inorg. Organomet. Polym. Mater.* **2025**, *35*, 3197–3221.

[94] Zhang, X.; Zeng, X.; Sun, S.-P.; Zhao, H.-Y. Copper difluorocarbene involved catalytic gem-difluoropropargylation. *Nat. Commun.* **2024**, *16*, 4547.

[95] Li, M.; Jiang, Y.; Chen, W.; Huang, Y.; Lu, Y.; Xu, L.; Li, S.; Wu, Y.; Xia, Z.; Wang, R. et al. Internal lattice oxygen sites invert product selectivity in electrocatalytic alkyne hydrogenation over copper catalysts. *Nat. Commun.* **2025**, *16*, 3884.

[96] Wang, S.; Wang, L.; Zhou, X.; Fang, J.; Deng, C.; Wang, D. Design principles of single-atom catalysts anchored over porous materials for green catalysis and conversion. *Nano Res.* **2025**, *18*, 94907137.

[97] Song, L.; Cai, L.; Van Der Eycken, E. V.; Gong, L. Recent advances in copper-catalyzed multicomponent reactions with photoinduction. *Coord. Chem. Rev.* **2025**, *528*, 216428.

[98] Li, F.; Han, G.-F.; Noh, H.-J.; Kim, S.-J.; Lu, Y.; Jeong, H. Y.; Fu, Z.; Baek, J.-B. Boosting oxygen reduction catalysis with abundant copper single atom active sites. *Energy Environ. Sci.* **2018**, *11*, 2263–2269.

[99] Ali, S.; Ali, S.; Ismail, A.; Zahid, M.; Raziq, F.; Qiao, L. Cu-based metal oxide catalysts for NH_3-SCR of NO: from fundamentals to mechanistic insights. *Coord. Chem. Rev.* **2025**, *536*, 216676.

[100] Guo, X.; Wu, Y.; Shao, Y.; Zhou, S.; Song, H.; Izumi, Y.; Deng, L.; Wang, W.; He, J.; Zhang, H. Dual active sites of embedded Ni and surface frustrated lewis pairs on CeO_2 (110) for efficient photocatalytic CO_2 methanation. *ACS Nano* **2025**, *19*, 38004–38015.

[101] Li, R.; Wang, D. Understanding the structure-performance relationship of active sites at atomic scale. *Nano Res.* **2022**, *15*, 6888–6923.

[102] Sardana, S.; Pattanaik, A.; Rehbein, J.; Reiser, O. Copper(II)-photocatalyzed radical anellation of nitroalkanes with alkenes or alkynes for the synthesis of isoxazolines and isoxazoles. *Angew. Chem. Int. Ed.* **2025**, *64*, e202509658.

[103] Wang, Y.; Chen, Y.; Nan, C.; Li, L.; Wang, D.; Peng, Q.; Li, Y. Phase-transfer interface promoted corrosion from $PtNi_{10}$ nanoctahedra to Pt_4Ni nanoframes. *Nano Res.* **2015**, *8*, 140–155.

[104] Luo, H.; Yang, Y.; Ma, Y.; Yu, F.; Gao, M.; Xu, S.; Ju, H.; Li, Y.;

Wu, K.; Lin, L. Light-driven radical copper-catalyzed allylic amination via allylic copper intermediates. *Nat. Commun.* **2025**, *16*, 10425.

[105] Zhang, M.; Song, X.; Qin, Y.; Peng, Y.; Zhang, S.; Feng, W.; Huang, H.; Chen, Y.; Zhou, J. Single-atom–doped piezocatalyst induces copper-free cuproptosis in tumor therapy. *Sci. Adv.* **2025**, *11*, eadt8451.

[106] Zheng, X.; Li, B.; Wang, Q.; Wang, D.; Li, Y. Emerging low-nuclearity supported metal catalysts with atomic level precision for efficient heterogeneous catalysis. *Nano Res.* **2022**, *15*, 7806–7839.

[107] Zhao, H.; Yu, R.; Ma, S.; Xu, K.; Chen, Y.; Jiang, K.; Fang, Y.; Zhu, C.; Liu, X.; Tang, Y. et al. The role of Cu_1–O_3 species in single-atom Cu/ZrO_2 catalyst for CO_2 hydrogenation. *Nat. Catal.* **2022**, *5*, 818–831.

[108] Jiang, Z.; Sun, W.; Shang, H.; Chen, W.; Sun, T.; Li, H.; Dong, J.; Zhou, J.; Li, Z.; Wang, Y. et al. Atomic interface effect of a single atom copper catalyst for enhanced oxygen reduction reactions. *Energy Environ. Sci.* **2019**, *12*, 3508–3514.

[109] Liu, J.; Wen, Y.; Yan, W.; Huang, Z.; Liu, X.; Huang, X.; Zhan, C.; Zhang, Y.; Huang, W.-H.; Pao, C.-W. et al. Single-atom mediated crystal facet engineering for the exceptional production of acetate in CO electrolysis. *Energy Environ. Sci.* **2025**, *18*, 4396–4404.

[110] Du, X.; Fu, N.; Zhang, S.; Chen, C.; Wang, D.; Li, Y. $Au/CuSiO_3$ nanotubes: high-performance robust catalysts for selective oxidation of ethanol to acetaldehyde. *Nano Res.* **2016**, *9*, 2681–2686.

[111] Chen, Z.-X.; Song, Y.-J.; Li, R.-Z.; Guo, S.-J.; Shi, L.; Yang, Z.-R.; Xue, X.-M.; Zhang, T. Advances in copper nanocrystals: synthesis, anti-oxidation strategies, and multiple applications. *Coord. Chem. Rev.* **2025**, *529*, 216455.

[112] Hao, Z.; Wang, M.; Cheng, L.; Si, M.; Feng, Z.; Feng, Z. Synergistic antibacterial mechanism of silver-copper bimetallic nanoparticles. *Front. Bioeng. Biotechnol.* **2024**, *11*, 1337543.

[113] Zhan, E.; Liang, Z.; Wang, Y.; Zhang, L.; Zhuang, G. Self-assembly of Cu-glutathione nanoparticles on WO_3 nanorods: amelioration of charge transfer and photocatalytic performance. *CrystEngComm* **2024**, *26*, 5734–5745.

[114] Cui, T.; Li, L.; Ye, C.; Li, X.; Liu, C.; Zhu, S.; Chen, W.; Wang, D. Heterogeneous single atom environmental catalysis: fundamentals, applications, and opportunities. *Adv. Funct. Mater.* **2022**, *32*, 2108381.

[115] Lu, D.; Wu, F.; Chen, K.; Li, W.; Zhang, P.; Hou, Y.; Su, Y.; Liu, W.; Wang, T.; Liu, Y. et al. NIR-photocatalytic LDHB-mimetic CuS@ZnS nanoenzyme regulates arthritis microenvironment through lactate oxidation and hydrogen evolution. *Chem, Eng, J.* **2024**, *490*, 151772.

[116] Liu, X.; Zhu, C.; Li, M.; Xing, H.; Zhu, S.; Liu, X.; Zhu, G. Confinement synthesis of atomic copper-anchored polymeric carbon nitride in crystalline $UiO\text{-}66\text{-}NH_2$ for high-performance CO_2-to-CH_3OH photocatalysis. *Angew. Chem.* **2024**, *136*, e202412408.

[117] Woldu, A. R.; Yohannes, A. G.; Huang, Z.; Kennepohl, P.; Astruc, D.; Hu, L.; Huang, X.-C. Experimental and theoretical insights into single atoms, dual atoms, and sub-nanocluster catalysts for electrochemical CO_2 reduction (CO_2RR) to high-value products. *Adv. Mater.* **2024**, *36*, 2414169.

[118] Zhou, K.; Fu, N. Asymmetric cyanoesterification of vinylarenes by electrochemical copper catalysis. *Nat. Commun.* **2025**, *16*, 6767.

[119] Naher, M.; Gonzálvez, M. A.; Williams, C. M.; Bernhardt, P. V. Emerging applications and mechanistic insights of copper mediated electrocatalysts in organic transformations. *Chem. Soc. Rev.* **2025**, *54*, 7304–7338.

[120] Gorai, M.; Franzen, J. H.; Rotering, P.; Rüffer, T.; Dielmann, F.; Teichert, J. F. Broadly applicable copper(I)-catalyzed alkyne semihydrogenation and hydrogenation of α,β-unsaturated amides enabled by bifunctional iminopyridine ligands. *J. Am. Chem. Soc.* **2025**, *147*, 14481–14490.

[121] Tzaras, D.-I.; Gorai, M.; Jacquemin, T.; Arndt, T.; Zimmermann, B. M.; Breugst, M.; Teichert, J. F. Site-selective copper(I)-catalyzed hydrogenation of amides. *J. Am. Chem. Soc.* **2025**, *147*, 1867–1874.

[122] Zhong, F.; Anderson, R. L.; Oyala, P. H.; Fu, G. C. Photoinduced, copper-catalyzed enantioconvergent azidation of alkyl halides. *J. Am. Chem. Soc.* **2025**, *147*, 32963-32970.

[123] Zhuang, Z.; Kang, Q.; Wang, D.; Li, Y. Single-atom catalysis enables long-life, high-energy lithium-sulfur batteries. *Nano Res.* **2020**, *13*, 1856–1866.

[124] Zhang, H.-M.; Liu, Z.-C.; Xiao, J.-Z.; Yin, L. Copper(I)-catalyzed asymmetric alkylation of α-sulfanyl acetamides. *ACS Catal.* **2025**, *15*, 4953–4962.

[125] Liu, M.; Zhang, C.; Ying, Y.; Zhao, Y.; Zhao, Z.; Jia, Y.; Chen, Y.; Shi, J.; Li, Y. Optimization strategies for enhancing the stability of Cu-based catalysts. *Mater. Rep.: Energy* **2025**, *5*, 100355.

[126] Ou-Ichen, Z.; Boussetta, A.; Kassab, Z.; Ihammi, A.; Ait Benhamou, A.; Ouchetto, K.; Moubarik, A.; Hafid, A.; Ouchetto, H.; Khouili, M. Sustainable catalysis with cellulose-copper: a review of click reaction applications. *Carbohydr, Polym,* **2025**, *364*, 123746.

[127] McMillin, D. R.; Buckner, M. T.; Ahn, B. Tae. A light-induced redox reaction of bis(2,9-dimethyl^{-1},10-phenanthroline) copper(I). *Inorg. Chem.* **1977**, *16*, 943–945.

[128] Kern, J.-M.; Sauvageb, J.-P. PhotoassistedG C coupling via electron transfer to benzylic halides by a bis(di-imine) copper(i) complex. *Chem. Commun.* **1987**, *8* ,546.

[129] Sagadevan, A.; Hwang, K. C. Photo-induced sonogashira C-C coupling reaction catalyzed by simple copper(I) chloride salt at room temperature. *Adv. Synth. Catal.* **2012**, *354*, 3421–3427.

[130] Hernandez-Perez, A. C.; Collins, S. K. A visible-light-mediated synthesis of carbazoles. *Angew. Chem. Int. Ed.* **2013**, *52*, 12696–12700.

[131] Alkan-Zambada, M.; Hu, X. Cu photoredox catalysts supported by a 4,6-disubstituted 2,2′-bipyridine ligand: application in chlorotrifluoromethylation of alkenes. *Organometallics* **2018**, *37*, 3928−3935.

[132] Zhu, X.; Jian, W.; Huang, M.; Li, D.; Li, Y.; Zhang, X.; Bao, H. Asymmetric radical carboesterification of dienes. *Nat. Commun.* **2021**, *12*, 6670.

[133] Liu, X.-M.; Li, F.; Wang, T.; Dai, L.; Yang, Y.; Jiang, N.-Q.; Xue, L.-Y.; Liu, J.-Y.; Xue, X.-S.; Xiao, L.-J. et al. Catalytic asymmetric oxidative coupling between $C(sp^3)$–H bonds and carboxylic acids. *J. Am. Chem. Soc.* **2025**, *147*, 627–635.

[134] Chen, H.; Yang, W.; Zhang, J.; Lu, B.; Wang, X. Divergent geminal alkynylation–allylation and acylation–allylation of carbenes: evolution and roles of two transition-metal catalysts. *J. Am. Chem. Soc.* **2024**, *146*, 4727–4740.

[135] Mandal, T.; Ghosh, M.; Paps, H.; Mandal, T.; Reiser, O. A general photocatalytic platform for the regio- and stereoselective β-chloroacylation of alkenes and alkynes using a heteroleptic copper(I) complex. *Nat. Catal.* **2025**, *8*, 607-622.

[136] Li, Z.-L.; Fang, G.-C.; Gu, Q.-S.; Liu, X.-Y. Recent advances in copper-catalysed radical-involved asymmetric 1,2-difunctionalization of alkenes. *Chem. Soc. Rev.* **2020**, *49*, 32–48.

[137] Hossain, A.; Bhattacharyya, A.; Reiser, O. Copper's rapid ascent in visible-light photoredox catalysis. *Science* **2019**, *364*, eaav9713.

[138] Bach, T.; Hehn, J. P. Photochemical reactions as key steps in natural product synthesis. *Angew. Chem. Int. Ed.* **2011**, *50*, 1000–1045.

[139] Roth, H. D. The beginnings of organic photochemistry. *Angew. Chem., Int. Ed. Engl.* **1989**, *28*, 1193–1207.

[140] Trommsdorff, H. Ueber santonin. *Ann. Pharm.* **1834**, *11*, 190–207.

[141] Narayanam, J. M. R.; Stephenson, C. R. J. Visible light photoredox catalysis: applications in organic synthesis. *Chem. Soc. Rev.* **2011**, *40*, 102–113.

[142] Xuan, J.; Xiao, W.-J. Visible-light photoredox catalysis. *Angew. Chem. Int. Ed.* **2012**, *51*, 6828–6838.

[143] Wang, L.; Wu, J.; Wang, S.; Liu, H.; Wang, Y.; Wang, D. The reformation of catalyst: from a trial-and-error synthesis to rational design. *Nano Res.* **2024**, *17*, 3261–3301.

[144] Melchiorre, P. Introduction: photochemical catalytic processes. *Chem. Rev.* **2022**, *122*, 1483–1484.

[145] Bhuyan, R.; Mony, J.; Kotov, O.; Castellanos, G. W.; Gómez Rivas, J.; Shegai, T. O.; Börjesson, K. The rise and current status of polaritonic photochemistry and photophysics. *Chem. Rev.* **2023**, *123*, 10877–10919.

[146] Zhang, Y.; He, S.; Guo, W.; Hu, Y.; Huang, J.; Mulcahy, J. R.; Wei, W. D. Surface-plasmon-driven hot electron photochemistry. *Chem. Rev.* **2018**, *118*, 2927–2954.

[147] Kainz, Q. M.; Matier, C. D.; Bartoszewicz, A.; Zultanski, S. L.; Peters, J. C.; Fu, G. C. Asymmetric copper-catalyzed C-N cross-couplings induced by visible light. *ACS Nano* **2025**, *19*, 42589-42598.

[148] Mo, F.; Qiu, D.; Zhang, L.; Wang, J. Recent development of aryl diazonium chemistry for the derivatization of aromatic compounds. *Chem. Rev.* **2021**, *121*, 5741–5829.

[149] Bunescu, A.; Abdelhamid, Y.; Gaunt, M. J. Multicomponent alkene azidoarylation by anion-mediated dual catalysis. *Nature* **2021**, *598*, 597–603.

[150] Cai, Y.; Chatterjee, S.; Ritter, T. Photoinduced copper-catalyzed late-stage azidoarylation of alkenes via arylthianthrenium salts. *J. Am. Chem. Soc.* **2023**, *145*, 13542–13548.

[151] Zhu, P.; Xiong, X.; Wang, D. Regulations of active moiety in single atom catalysts for electrochemical hydrogen evolution reaction. *Nano Res.* **2022**, *15*, 5792–5815.

[152] Wang, Y.; Ma, F.; Zhang, G.; Zhang, J.; Zhao, H.; Dong, Y.; Wang, D. Precise synthesis of dual atom sites for electrocatalysis. *Nano Res.* **2024**, *17*, 9397–9427.

[153] Engl, S.; Reiser, O. Copper-photocatalyzed ATRA reactions: concepts, applications, and opportunities. *Chem. Soc. Rev.* **2022**, *51*, 5287–5299.

[154] Bagal, D. B.; Kachkovskyi, G.; Knorn, M.; Rawner, T.; Bhanage, B. M.; Reiser, O. Trifluoromethylchlorosulfonylation of alkenes: evidence for an inner-sphere mechanism by a copper phenanthroline photoredox catalyst. *Angew. Chem. Int. Ed.* **2015**, *54*, 6999–7002.

[155] Chen, J.; Wei, W.-T.; Li, Z.; Lu, Z. Metal-catalyzed markovnikov-type selective hydrofunctionalization of terminal alkynes. *Chem. Soc. Rev.* **2024**, *53*, 7566–7589.

[156] Han, B.-L.; Zhao, L.-C.; Yuan, Z.-R.; Wang, Z.; Yu, Q.; Luo, G.-G.; Wang, L.-K.; Tung, C.-H.; Sun, D. Dipropyne-modified N-heterocyclic carbene stabilized atomically precise copper(I) nanocluster catalysts for CO_2 electroreduction. *Adv. Funct. Mater.* **2025**, *35*, 2500149.

[157] Ren, R.; Guo, K.; Gu, Y.; Li, G.; Zhang, L.; Wang, Y.; Zhang, Q.; Wang, Q.; Zhang, J. Advanced spectroscopic, microscopic, and compositional techniques in catalytic material characterization: applications and progress. Nano Res. 2026, 19, 94907814.

[158] Engl, S.; Reiser, O. Copper makes the difference: visible light-mediated atom transfer radical addition reactions of iodoform with olefins. *ACS Catal.* **2020**, *10*, 9899–9906.

[159] Tang, Y.; Tsui, G. C. Copper-catalyzed pentafluoroethylation of aryl/alkenyl iodides with pentafluoroethylsilane. *Org. Chem. Front.* **2024**, *11*, 4366–4370.

[160] Olding, A.; Cameron, L.; Pham, L. N.; Shephard, J. P.; Lucas, N. T.; Moggach, S. A.; Massi, M.; Connell, T. U.; Ho, C. C.; Coote, M. L. et al. Copper(I) photoredox catalysts bearing tetradentate phenanthroline-based ligands: understanding the interplay between structure and function. *ACS Catal.* **2025**, *15*, 3731–3740.

[161] Wang, S.; Chen, K.; Niu, J.; Guo, X.; Yuan, X.; Yin, J.; Zhu, B.; Shi, D.; Guan, W.; Xiong, T. et al. Copper-catalyzed regiodivergent asymmetric difunctionalization of terminal alkynes. *Angew. Chem. Int. Ed.* **2024**, *63*, e202410833.

[162] Ren, Y.; Yu, J.; Zhang, J.; Lv, L.; Zhang, W. An *in-situ* strategy to analyze multi-effect catalysis in iron-copper bimetals catalyzed fenton-like processes. *Appl. Catal. B: Environ.* **2021**, *299*, 120697.

[163] Lv, Y.; Cao, X.; Jiang, H.; Song, W.; Chen, C.; Zhao, J. Rapid photocatalytic debromination on TiO_2 with *in-situ* formed copper co-catalyst: enhanced adsorption and visible light activity. *Appl. Catal. B: Environ.* **2016**, *194*, 150–156.

[164] Yang, Y.; Feijóo, J.; Figueras-Valls, M.; Chen, C.; Shi, C.; Fonseca Guzman, M. V.; Murhabazi Maombi, Y.; Liu, S.; Jain, P.; Briega-Martos, V. et al. Operando probing dynamic migration of copper carbonyl during electrocatalytic CO_2 reduction. *Nat. Catal.* **2025**, *8*, 579–594.

[165] Huang, X.; Bao, L.; Bao, R.; Liu, L.; Tao, J.; Wang, J.; Zhang, Z.; Ge, Z.; Tan, S.; Yi, J. et al. Reinforced copper matrix composites with highly dispersed nano size TiC *in-situ* generated from the carbon polymer dots. Adv. Powder Mater. **2023**, *2*, 100090.

[166] Xie, J.-Q.; Ji, Y.-Q.; Kang, J.-H.; Sheng, J.-L.; Mao, D.-S.; Fu, X.-Z.; Sun, R.; Wong, C.-P. *In-situ* growth of $Cu(OH)_2$@FeOOH nanotube arrays on catalytically deposited Cu current collector patterns for high-performance flexible in-plane micro-sized energy storage devices. *Energy Environ. Sci.* **2019**, *12*, 194–205.

[167] Matsunaga, P. T.; Hillhouse, G. L.; Rheingold, A. L. Oxygen-atom transfer from nitrous oxide to a nickel metallacycle. Synthesis, structure, and reactions of [cyclic](2,2'-bipyridine)Ni($OCH_2CH_2CH_2CH_2$). *J. Am. Chem. Soc.* **1993**, *115*, 2075–2077.

[168] Han, R.; Hillhouse, G. L. Carbon-oxygen reductive-elimination from nickel(II) oxametallacycles and factors that control formation of ether, aldehyde, alcohol, or ester products. *J. Am. Chem. Soc.* **1997**, *119*, 8135–8136.

[169] Camasso, N. M.; Sanford, M. S. Design, synthesis, and carbon-heteroatom coupling reactions of organometallic nickel(IV) complexes. *Science* **2015**, *347*, 1218–1220.

[170] Evans, D. A.; Katz, J. L.; West, T. R. Synthesis of diaryl ethers through the copper-promoted arylation of phenols with arylboronic acids. An expedient synthesis of thyroxine. *Tetrahedron Lett.* **1998**, *39*, 2937–2940.

[171] Chan, D. M. T.; Monaco, K. L.; Wang, R.-P.; Winters, M. P. New N- and O-arylations with phenylboronic acids and cupric acetatet. *Tetrahedron Lett.* **1998**, *39*, 2933–2936.

[172] Lam, P. Y. S.; Clark, C. G.; Saubern, S.; Adams, J.; Winters, M. P.; Chan, D. M. T.; Combs, A. New aryl/heteroaryl C-N bond cross-coupling reactions via arylboronic acid/cupric acetate arylation. *Tetrahedron Lett.* **1998**, *39*, 2941–2944.

[173] Wang, C.; Ge, Q.; Xu, C.; Xing, Z.; Xiong, J.; Zheng, Y.; Duan, W.-L. Photoinduced copper-catalyzed C(sp^3)–P bond formation by coupling of secondary phosphines with N-(acyloxy)phthalimides and N-fluorocarboxamides. *Org. Lett.* **2023**, *25*, 1583–1588.

[174] Shi, P.; Tu, Y.; Ma, D.; Bolm, C. Copper-catalyzed *N*-alkylations of *N*H-sulfoximines under visible light. *Adv. Synth. Catal.* **2023**, *365*, 1613–1617.

[175] Roland, G.; Hurdal, K. N.; Bouchouicha, A.; Dowe, N.; Davis, R. L.; Collins, S. K. [2 + 2] photocycloadditions to form cyclobutanes and bicyclo[2.1.1]hexanes employing copper-based photocatalysis. *ACS Catal.* **2024**, *14*, 11490–11497.

[176] Abderrazak, Y.; Reiser, O. Copper photocatalyzed divergent access to organic thio- and isothiocyanates. *ACS Catal.* **2024**, *14*, 4847–4855.

[177] Goldberg, I. Ueber phenylirungen bei gegenwart von kupfer als katalysator. *Ber. Dtsch. Chem. Ges.* **1906**, *39*, 1691–1692.

[178] Ullmann, F.; Sponagel, P. Ueber die phenylirung von phenolen. *Ber. Dtsch. Chem. Ges.* **1905**, *38*, 2211–2212.

[179] Zheng, A.; Zhang, Q.; Yin, K.; Sun, L. Film-based liquid cell TEM: Advances and applications in atomic-scale dynamics of metal nanocrystals. *Nano Res.* **2026**, *19*, 94908203.

[180] Johansson Seechurn, C. C. C.; Kitching, M. O.; Colacot, T. J.; Snieckus, V. Palladium-catalyzed cross-coupling: a historical contextual perspective to the 2010 nobel prize. *Angew. Chem. Int. Ed.* **2012**, *51*, 5062–5085.

[181] Bhunia, S.; Pawar, G. G.; Kumar, S. V.; Jiang, Y.; Ma, D. Selected copper-based reactions for C-N, C-O, C-S, and C-C bond formation. *Angew. Chem. Int. Ed.* **2017**, *56*, 16136–16179.

[182] Hein, J. E.; Fokin, V. V. Copper-catalyzed azide–alkyne cycloaddition (CuAAC) and beyond: new reactivity of copper(I) acetylides. *Chem. Soc. Rev.* **2010**, *39*, 1302.

[183] Sambiagio, C.; Marsden, S. P.; Blacker, A. J.; McGowan, P. C. Copper catalysed ullmann type chemistry: from mechanistic aspects to modern development. *Chem. Soc. Rev.* **2014**, *43*, 3525–3550.

[184] Lo, Q. A.; Sale, D.; Braddock, D. C.; Davies, R. P. Mechanistic and performance studies on the ligand-promoted ullmann amination reaction. *ACS Catal.* **2018**, *8*, 101–109.

[185] Giri, R.; Brusoe, A.; Troshin, K.; Wang, J. Y.; Font, M.; Hartwig, J. F. Mechanism of the ullmann biaryl ether synthesis catalyzed by complexes of anionic ligands: evidence for the reaction of iodoarenes with

ligated anionic Cu^{I} intermediates. *J. Am. Chem. Soc.* **2018**, *140*, 793–806.

[186] Delaney, C. P.; Lin, E.; Huang, Q.; Yu, I. F.; Rao, G.; Tao, L.; Jed, A.; Fantasia, S. M.; Püntener, K. A.; Britt, R. D. et al. Cross-coupling by a noncanonical mechanism involving the addition of aryl halide to Cu(II). *Science* **2023**, *381*, 1079–1085.

[187] Chen, C.; Peters, J. C.; Fu, G. C. Photoinduced copper-catalysed asymmetric amidation via ligand cooperativity. *Nature* **2021**, *596*, 250–256.

[188] Zhang, J.; Wu, K.; Xiong, J.; Ren, Q.; Zhong, J.; Cai, H.; Huang, H.; Chen, P.; Wu, J.; Chen, L. et al. Static and dynamic quantification tracking of asymmetric oxygen vacancies in copper-ceria catalysts with superior catalytic activity. *Appl. Catal. B: Environ.* **2022**, *316*, 121620.

[189] Li, X.; Rong, H.; Zhang, J.; Wang, D.; Li, Y. Modulating the local coordination environment of single-atom catalysts for enhanced catalytic performance. *Nano Res.* **2020**, *13*, 1842–1855.

[190] Rong, H.; Mao, J.; Xin, P.; He, D.; Chen, Y.; Wang, D.; Niu, Z.; Wu, Y.; Li, Y. Kinetically controlling surface structure to construct defect-rich intermetallic nanocrystals: effective and stable catalysts. *Adv. Mater.* **2016**, *28*, 2540–2546.

[191] Song, L.; Cai, L.; Gong, L.; Van Der Eycken, E. V. Photoinduced copper-catalyzed enantioselective coupling reactions. *Chem. Soc. Rev.* **2023**, *52*, 2358–2376.

[192] Wang, P.-Z.; Zhang, B.; Xiao, W.-J.; Chen, J.-R. Photocatalysis meets copper catalysis: a new opportunity for asymmetric multicomponent radical cross-coupling reactions. *Acc. Chem. Res.* **2024**, *57*, 3433–3448.

[193] Feng, J.; Xi, L.-L.; Lu, C.-J.; Liu, R.-R. Transition-metal-catalyzed enantioselective C–N cross-coupling. *Chem. Soc. Rev.* **2024**, *53*, 9560–9581.

[194] Yang, F.; Chi, L.; Ye, Z.; Gong, L. Photoinduced regiodivergent and enantioselective cross-coupling of glycine derivatives with hydrocarbon feedstocks. *J. Am. Chem. Soc.* **2025**, *147*, 1767–1780.

[195] Chen, Y.-Z.; Li, W.-H.; Li, L.; Wang, L.-N. Progress in organic photocatalysts. *Rare Met.* **2018**, *37*, 1–12.

[196] Luo, Y.; Wang, X.; Gao, F.; Jiang, L.; Wang, D.; Pan, H. From single atom photocatalysts to synergistic photocatalysts: design principles and applications. *Adv. Funct. Mater.* **2025**, *35*, 2418427.

[197] Chakraborty, A.; Roy, M.; Alam, A.; Adhikari, D.; Pachfule, P. Covalent organic frameworks as heterogeneous photocatalysts for cross-coupling reactions. *Green Chem.* **2024**, *26*, 9619–9651.

[198] Alam, A.; Roy, M.; Maji, S.; Chakraborty, A.; Singh, V.; Kumar, A.; Mondal, S.; Banerjee, A.; Kailasam, K.; Adhikari, D. et al. Xantphos–Cu-decorated covalent organic frameworks for C-H arylation through sensitized electron transfer. *Adv. Mater.* **2025**, *37*, 2416100.

[199] Zhao, Z.; Wang, H.; Yu, Q.; Roy, S.; Yu, X. Photo-/electrocatalytic approaches to CO_2 conversion on Cu_2O-based catalysts. *Appl. Catal., A* **2023**, *667*, 119445.

[200] Wang, D.; Peng, Q.; Li, Y. Nanocrystalline intermetallics and alloys. *Nano Res.* **2010**, *3*, 574–580.

[201] Budi, S.; Sutrisno, M. G.; Pratiwi, Y.; Yusmaniar Enhanced photocatalytic activity of CoNi-decorated Zn-doped Cu_2O synthesized by electrodeposition technique. *Mater. Adv.* **2023**, *4*, 1081–1088.

[202] Tai, Y.; Yang, B.; Li, J.; Meng, L.; Xing, P.; Wang, S. Design and preparation of heterostructured Cu_2O/TiO_2 materials for photocatalytic applications. *Molecules* **2024**, *29*, 5028.

[203] Chen, S.; Zhang, L.; Melhi, S.; Alshammari, D. A.; Amin, M. A.; Dai, L.; Li, S.; Yu, W.; Cui, L. Photocatalytic degradation of toluene by three-dimensional monolithic titanium dioxide / cuprous oxide foams with Z-schemed heterojunction. *Adv. Compos. Hybrid Mater.***2024**, *7*, 250–263.

[204] Yan, X.; Xu, T.; Zhan, W.; Yang, Y.; Yu, Y.; Yi, J.; He, X.; Yang, L.; Zhao, J.; Sun, L. et al. Engineering Cu_2O/Cu/N-C interface to induce directional migration of charge for driving photocatalytic homo-coupling of terminal alkynes. *Nano Res.* **2024**, *17*, 6895–6902.

[205] Staniuk, M.; Zindel, D.; Van Beek, W.; Hirsch, O.; Kränzlin, N.; Niederberger, M.; Koziej, D. Matching the organic and inorganic counterparts during nucleation and growth of copper-based nanoparticles – *in-situ* spectroscopic studies. *CrystEngComm* **2015**, *17*, 6962–6971.

[206] Ebri, G.; Hellgardt, K. Flow synthesis development and photocatalytic activity optimization of copper oxide nanoparticles using design of experiments. *Chem. Eng. J.* **2024**, *486*, 150131.

[207] Greiner, M. T.; Jones, T. E.; Beeg, S.; Zwiener, L.; Scherzer, M.; Girgsdies, F.; Piccinin, S.; Armbrüster, M.; Knop-Gericke, A.; Schlögl, R. Free-atom-like d states in single-atom alloy catalysts. *Nat. Chem.* **2018**, *10*, 1008–1015.

[208] Cho, H.; Tong, X.; Zuccarello, G.; Anderson, R. L.; Fu, G. C. Synthesis of tertiary alkyl amines via photoinduced copper-catalysed nucleophilic substitution. *Nat. Chem.* **2025**, *17*, 271–278.

[209] Della-Felice, F.; Roelfes, G. A copper enzyme for lewis acid biocatalysis. *Nat. Catal.* **2025**, *8*, 633–634.

[210] Song, J.; Xiao, D.; He, J.; Zhang, C.; Zhang, Q.; Wang, Z.; Liu, Y.; Zheng, Z.; Cheng, H.; Wu, Y. et al. Revealing the electrochemical-autocatalytic coupling mechanism of Cu-based catalysts for high-potential formaldehyde oxidation. *Energy Environ. Sci.* **2025**, *18*, 6106–6116.

[211] Xiao, X.; Wang, L.; Wang, D.; He, X.; Peng, Q.; Li, Y. Hydrothermal synthesis of orthorhombic $LiMnO_2$ nano-particles and $LiMnO_2$ nanorods and comparison of their electrochemical performances. *Nano Res.* **2009**, *2*, 923–930.

[212] Minakata, D.; Kamath, D.; Maetzold, S. Mechanistic insight into the reactivity of chlorine-derived radicals in the aqueous-phase UV–chlorine advanced oxidation process: quantum mechanical calculations. *Environ. Sci. Technol.* **2017**, *51*, 6918–6926.

[213] Wang, P.-S.; Wang, Z.-T.; Tan, Y.-Y.; Chen, P.; Zhang, X.-C.; Zhang, L.-N.; Wei, Y.-G.; Ni, L.-B. Structural transformation from waugh-type to keggin-type polyoxomolybdate-based crystalline material for photo/electrocatalysis. *Rare Met.* **2024**, *43*, 2241–2250.

[214] Reichle, A.; Koch, M.; Sterzel, H.; Großkopf, L.-J.; Floss, J.; Rehbein, J.; Reiser, O. Copper(I) photocatalyzed bromonitroalkylation of olefins: evidence for highly efficient inner-sphere pathways. *Angew. Chem. Int. Ed.* **2023**, *62*, e202219086.

[215] Zhou, M.; Xu, S.; Zhang, W.; Shi, G.; He, Y.; Qiao, X.; Pang, X. How luminescence performances of silicon-doped carbon dots contribute to copper-catalyzed photoATRP? *ACS Catal.* **2024**, *14*, 10418–10426.

[216] Zheng, X.; Song, Y.; Wang, C.; Gao, Q.; Shao, Z.; Lin, J.; Zhai, J.; Li, J.; Shi, X.; Wu, D. et al. Properties, applications, and challenges of copper- and zinc-based multinary metal sulfide photocatalysts for photocatalytic hydrogen evolution. *Chin. J. Catal.* **2025**, *74*, 22–70.

[217] Xia, Z.; Lin, L.; Chen, X.; Zhai, J.; Xue, C.; Jia, S.; Jiao, J.; Dong, M.; Han, W.; Zheng, X. et al. Solar-driven upcycling of polylactic acid to alanine over Pt/CdS–TiO_2 heterojunction single-atom photocatalyst. *J. Am. Chem. Soc.* **2025**, *147*, 45357–45365.

[218] Deng, D.; Wu, J.; Feng, Q.; Zhao, X.; Liu, M.; Bai, Y.; Wang, J.; Zheng, X.; Jiang, J.; Zhuang, Z. et al. Highly reversible zinc-air batteries at -40°C enabled by anion-mediated biomimetic fat. *Adv. Funct. Mater.* **2024**, *34*, 2308762.

[219] Zhu, H.-L.; Liao, P.-Q.; Chen, X.-M. Precise engineering of multimetal sites in metal–organic frameworks for efficient and selective electrochemical reduction of CO_2 to C_2 and urea products. *Acc. Chem. Res.* **2025**, *58*, 3530–3542

[220] Wang, Y.; Zheng, X.; Wang, D. Design concept for electrocatalysts. *Nano Res.* **2022**, *15*, 1730–1752.

[221] She, H.; Hua, R.; Zhao, J.; Xia, Y.; Wang, L.; Huang, J.; Wang, Q. Synergetic regulation of interfacial electronic structure of Cu, N co-doped carbon modified TiO_2 for efficient photocatalytic CO_2 reduction. *Chem. Eng. J.* **2024**, *496*, 153799.

[222] Shi, W.; Ge, B.; Jiang, P.; Wang, Q.; He, L.; Huang, C. SiQDs-mediated highly efficient hole transfer for photocatalytic overall water splitting over Cu-doped $ZnIn_2S_4$. *Appl. Catal. B: Environ.* **2024**, *354*, 124121.

[223] Xu, F.; Ge, B.; Jiang, P.; Cai, X.; Xing, F.; Huang, C. Amphiphilic heterojunctions with atomically dispersed copper–alkynyl active units for highly efficient CO_2 photoreduction. *Appl. Catal. B: Environ.* **2025**, *360*, 124518.

[224] Xu, Y.; Dong, J.-P.; Wang, L.; Geng, R.-L.; Wang, R.; Si, Y.-N.; Zang, S.-Q.; Mak, T. C. W. 3D cluster-based covalent organic framework for efficient CO_2 photoreduction. *Angew. Chem. Int, Ed,* **2025**, *64*, e202501391.

[225] Gan, T.; Wang, D. Atomically dispersed materials: ideal catalysts in atomic era. *Nano Res.* **2024**, *17*, 18–38.

[226] Sun, T.; Xu, L.; Wang, D.; Li, Y. Metal organic frameworks derived single atom catalysts for electrocatalytic energy conversion. *Nano Res.* **2019**, *12*, 2067–2080.

[227] Zhang, L.; Zhu, J.; Li, X.; Mu, S.; Verpoort, F.; Xue, J.; Kou, Z.; Wang, J. Nurturing the marriages of single atoms with atomic clusters and nanoparticles for better heterogeneous electrocatalysis. *Interdiscip. Mater.* **2022**, *1*, 51–87.

[228] Wang, J.; Liu, C.; Li, J.; Luo, R.; Hu, X.; Sun, X.; Shen, J.; Han, W.; Wang, L. *In-situ* incorporation of iron-copper bimetallic particles in electrospun carbon nanofibers as an efficient fenton catalyst. *Appl. Catal. B: Environ.* **2017**, *207*, 316–325.

[229] Wang, P.-Z.; Liang, Y.-J.; Wu, X.; Guan, W.; Xiao, W.-J.; Chen, J.-R. Copper-catalyzed three-component photo-ATRA-type reaction for asymmetric intermolecular C–O coupling. *ACS Catal.* **2022**, *12*, 10925–10937.

[230] Zoric, M. R.; Basera, P.; Palmer, L. D.; Aitbekova, A.; Powers-Riggs, N.; Lim, H.; Hu, W.; Garcia-Esparza, A. T.; Sarker, H.; Abild-Pedersen, F. et al. Oxidizing role of Cu cocatalysts in unassisted photocatalytic CO_2 reduction using p-GaN/Al_2O_3/Au/Cu heterostructures. *ACS Nano* **2024**, *18*, 19538–19548

[231] Li, M.; Hu, Z.; Liu, D.; Liang, Y.; Liu, S.; Wang, B.; Niu, C.; Xu, D.; Li, J.; Han, B. Efficient antibacterial and microbial corrosion resistant photocatalytic coating: enhancing performance with S-type heterojunction and Cu synergy. *Chem, Eng, J.* **2024**, *495*, 153519.

[232] De Almeida, J. C.; Wang, Y.; Rodrigues, T. A.; Nunes, P. H. H.; De Mendonça, V. R.; Falsetti, P. H. E.; Savazi, L. V.; He, T.; Bardakova, A. V.; Rudakova, A. V. et al. Copper-based materials for photo and electrocatalytic process: advancing renewable energy and environmental applications. *Adv. Funct. Mater.* **2025**, *36* ,2502901.

[233] Cai, Q.; Meng, Y.; Wu, C.; Qu, W.; Wang, Q.; Li, T.; Liu, C.; Chen, J.; Lin, H.; He, Q. et al. De-saturation of single-atom copper catalysts for accelerating propargylic substitution reactions. *Adv. Mater.* **2025**, *37*, e09221.

[234] Wang, Z.; Wang, W.; Wang, J.; Wang, D.; Liu, M.; Wu, Q.; Hu, H. Single-atom catalysts with ultrahigh catalase-like activity through electron filling and orbital energy regulation. *Adv. Funct. Mater.* **2023**, *33*, 2209560.

[235] Soleiman-Beigi, M.; Mohammadi, M.; Kohzadi, H. An overview on copper in industrial chemistry: from ancient pigment to modern catalysis. *Coord. Chem. Rev.* **2025**, *529*, 216438.

[236] Ma, Q.; Mu, S. Acidic oxygen evolution reaction: mechanism, catalyst classification, and enhancement strategies. *Interdiscip, Mater,* **2023**, *2*, 53–90.

[237] Wan, S.; Xu, J.; Cao, S.; Yu, J. Promoting intramolecular charge transfer of graphitic carbon nitride by donor–acceptor modulation for visible-light photocatalytic H_2 evolution. *Interdiscip, Mater,* **2022**, *1*, 294–308.

[238] Shi, Y.; Zhang, T.; Jiang, X.-M.; Xu, G.; He, C.; Duan, C. Synergistic photoredox and copper catalysis by diode-like coordination polymer with twisted and polar copper–dye conjugation. *Nat. Commun.* **2020**, *11*, 5384.

[239] Rana, P.; Saini, K. M.; Kaushik, B.; Solanki, K.; Dixit, R.; Sharma, R. K. Unleashing the photocatalytic potential of a noble-metal-free heteroleptic copper complex-based nanomaterial for an enhanced aza-henry reaction. *Nanoscale* **2023**, *15*, 14007–14017.

[240] Ma, B.; Xia, Q.; Wang, D.; Jin, J.-K.; Li, Z.; Liang, Q.-J.; Sun, M.-Y.; Liu, D.; Liu, L.-J.; Shu, H.-X. et al. Metal-organic framework suppor copper photoredox catalysts for iminyl radical-mediated reactions. *Angew. Chem. Int. Ed.* **2023**, *62*, e202300233.

[241] Zhang, Q.; Yang, H.; Zhou, T.; Chen, X.; Li, W.; Pang, H. Metal–organic frameworks and their composites for environmental applications. *Adv. Sci.* **2022**, *9*, 2204141.

[242] Liu, Z.; Hong, T.; Xu, L.; Wang, S.; Gao, X.; Chang, C.; Ding, X.; Xiao, Y.; Zhao, L.-D. Lattice expansion enables interstitial doping to achieve a high average *ZT* in *n* -type PbS. *Interdiscip. Mater.* **2023**, *2*, 161–170.

[243] Lou, X.; Zhang, C.; Xu, Z.; Ge, S.; Zhou, J.; Qin, D.; Qin, F.; Zhang, X.; Guo, Z.; Wang, C. Enhanced interfacial electron transfer in photocatalyst-natural enzyme coupled artificial photosynthesis system: tuning strategies and molecular simulations. *Small* **2024**, *20*, 2404055.

[244] Jin, R.; Li, R.; Ma, M.-L.; Chen, D.-Y.; Zhang, J.-Y.; Xie, Z.-H.; Ding, L.-F.; Xie, Y.; Li, J.-R. Beyond tradition: a MOF-on-MOF cascade Z-scheme heterostructure for augmented CO_2 photoreduction. *Small* **2025**, 2409759.

[245] Yang, H.; Liu, G.; Zheng, L.; Zhang, M.; Guan, Z.; Liu, T.; Yang, J. Cu-Fe bimetallic MOFs with long lifetime separated-state charge for enhancing selectivity for CO_2 photoreduction to CH_4. *Appl. Catal. B: Environ.* **2024**, *359*, 124491.

[246] Liu, L.; Corma, A. Metal catalysts for heterogeneous catalysis: from single atoms to nanoclusters and nanoparticles. *Chem. Rev.* **2018**, *118*, 4981–5079.

[247] Qiao, B.; Wang, A.; Yang, X.; Allard, L. F.; Jiang, Z.; Cui, Y.; Liu, J.; Li, J.; Zhang, T. Single-atom catalysis of CO oxidation using Pt1/FeOx. *Nat. Chem.* **2011**, *3*, 634–641.

[248] Zhu, C.; Yang, J.; Zhang, J.; Wang, X.; Gao, Y.; Wang, D.; Pan, H. Single-atom materials: the application in energy conversion. *Interdiscip. Mater.* **2024**, *3*, 74–86.

[249] Zhu, Y.; Sun, W.; Chen, W.; Cao, T.; Xiong, Y.; Luo, J.; Dong, J.; Zheng, L.; Zhang, J.; Wang, X. et al. Scale-up biomass pathway to cobalt single-site catalysts anchored on N-doped porous carbon nanobelt with ultrahigh surface area. *Adv. Funct. Mater.* **2018**, *28*, 1802167.

[250] Zhang, Y.; Zhao, J.; Wang, H.; Xiao, B.; Zhang, W.; Zhao, X.; Lv, T.; Thangamuthu, M.; Zhang, J.; Guo, Y. et al. Single-atom Cu anchored catalysts for photocatalytic renewable H_2 production with a quantum efficiency of 56%. *Nat. Commun.* **2022**, *13*, 58–67.

[251] Wang, G.; Wu, Y.; Li, Z.; Lou, Z.; Chen, Q.; Li, Y.; Wang, D.; Mao, J. Engineering a copper single-atom electron bridge to achieve efficient photocatalytic CO_2 conversion. *Angew. Chem.* **2023**, *135*, e202218460.

[252] Shen, J.; Luo, C.; Qiao, S.; Chen, Y.; Tang, Y.; Xu, J.; Fu, K.; Yuan, D.; Tang, H.; Zhang, H. et al. Single-atom Cu channel and N-vacancy engineering enables efficient charge separation and transfer between C_3N_4 interlayers for boosting photocatalytic hydrogen production. *ACS Catal.* **2023**, *13*, 6280–6288.